Agenzia nazionale per le nuove tecnologie,
l'energia e lo sviluppo economico sostenibile

MINISTERO DELLO SVILUPPO ECONOMICO

Ricerca di Sistema elettrico

Validazione di codici e qualifica modelli per problematiche di scambio termico in generatori di vapore innovativi

Marco Santinello, Antonio Cammi, Marco E. Ricotti

CIRTEN - CONSORZIO INTERUNIVERSITARIO PER LA RICERCA TECNOLOGICA NUCLEARE

Report RdS/2013/075

VALIDAZIONE DI CODICI E QUALIFICA MODELLI PER PROBLEMATICHE DI SCAMBIO TERMICO IN GENERATORI DI VAPORE INNOVATIVI

Marco Santinello, Antonio Cammi, Marco E. Ricotti (POLIMI)

Settembre 2013

Report Ricerca di Sistema Elettrico

Accordo di Programma Ministero dello Sviluppo Economico - ENEA
Piano Annuale di Realizzazione 2012
Area: Produzione di energia elettrica e protezione dell'ambiente
Progetto: Sviluppo competenze scientifiche nel campo della sicurezza nucleare e collaborazione ai programmi internazionali per il nucleare di IV Generazione
Obiettivo: Sviluppo competenze scientifiche nel campo della sicurezza nucleare
Responsabile del Progetto: Felice De Rosa, ENEA

Il presente documento descrive le attività di ricerca svolte all’interno dell’Accordo di collaborazione “Sviluppo competenze scientifiche nel campo della sicurezza nucleare e collaborazione ai programmi internazionali per il nucleare di IV generazione”
Responsabile scientifico ENEA: Felice De Rosa.
Responsabile scientifico CIRTEN: Giuseppe Forasassi

CIRTEN

<u>C</u>onsorzio <u>I</u>nteruniversitario per la <u>R</u>icerca <u>TE</u>cnologica <u>N</u>ucleare

POLITECNICO DI MILANO

Department of Energy

Nuclear Reactors Group

Validazione di codici e qualifica modelli per problematiche di scambio termico in generatori di vapore innovativi

EXPERIMENTAL AND CFD INVESTIGATIONS OF SINGLE-PHASE AND TWO-PHASE STEAM-WATER FLOW IN HELICALLY COILED TUBES

Autori

Marco Santinello

Antonio Cammi

Marco E. Ricotti

CERSE-POLIMI RL 1491/2013

Milano, Settembre 2013

Lavoro svolto in esecuzione dell'Attività LP1.C2c
AdP MSE-ENEA sulla Ricerca di Sistema Elettrico - Piano Annuale di Realizzazione 2012
Progetto B.3.1 "Sviluppo competenze scientifiche nel campo della sicurezza nucleare e collaborazione ai programmi internazionali per il nucleare di IV generazione

Indice

Sommario

Three important issues concerning the flow in helically coiled tubes are investigated in this work. Firstly, an approach based on the analysis of experimental friction factor profiles of liquid water single phase-flow in thirteen different geometries is undertaken, in order to examine the laminar to turbulent flow transition. The strong influence of the curvature ratio D_{coil} / d_{tube} *on the shape of friction factor profiles is evidenced and then correlations are provided for the beginning and the end of transition zone. Secondly, experimental data of steam-water two-phase pressure drop are analyzed, with the purpose to understand the effects of power input on the frictional component of pressure drop. The results reveal the influence of mass flux on this phenomenon, but do not allow carrying out any quantitative conclusion. Lastly, a CFD investigation of steam-water two-phase flow under adiabatic conditions is performed using commercial software ANSYS FLUENT 14.0, with the intention of defining a code able to predict experimental pressure drop data. A good accordance between numerical and experimental pressure drop values has been found, thus letting visualize and discuss also void fraction profiles. Thanks to these results, it has been possible to conduce also an analysis of wall shear stress, providing a physical explanation for the presence of a maximum in the "frictional pressure drop vs. quality" curve.*

1 Laminar to turbulent flow transition in helically coiled tubes

1.1 Generalities

Several authors studied the consequences of curvature and torsion in helical tubes and showed that they have a strong influence on flow conditions. In literature it is well known that the curved shape of the tube causes the appearance of a centrifugal force which generates important deviations in the local axial velocity of fluid particles. The existence of a secondary flow induced by centrifugal forces due to curvature was demonstrated for the first time in 1910 by J. Eustice [1], by injecting ink into water flowing through a coiled pipe: this flow consists in slower-moving fluid in the boundary layer on the wall moving inward and faster-moving fluid in the core moving outward [2]. This phenomenon happens because the effect of a centrifugal force is greater as the velocity increases, thus the fluid particles close to the boundary layer, which are characterized by a lower axial velocity than the particles flowing near the center line, are subjected to a lower centrifugal action than the others. The described motion generates a pair of recirculating counter-rotating vortices, which are symmetrical if the shape of the tube is toroidal. In presence of an increase of height, a torsional force arises, causing a rotation on the flowing fluid: the vortex rotating in the same direction of the torsion enlarges while the other shrinks, thus the symmetry is broken. The problem was analyzed theoretically by W. R. Dean in 1927 – 1928 [3] [4]: he succeeded in obtaining an analytical solution for fully developed laminar flow in a curved tube of circular cross section, finding that the reduction in flow rate due to the secondary flow is functionally dependent only on a single variable $K = 2Re^2(d_{tube}/D_{coil})$. In the following decades this work has been widely used in theoretical as well as experimental studies.

It is simple to deduce that, because of the presence of these motions, the laminar to turbulent flow transition in helical tubes results strongly different from that in straight ones: other factors come into play, like the coil diameter and the coil pitch. Authors usually define three dimensionless parameters which summarize the geometry of the test section.

$$coil\ curvature\ \delta = \frac{\pi^2 d_{tube} D_{coil}}{p^2 + \pi^2 D_{coil}^2} \tag{1.1}$$

$$coil\ torsion\ \tau = \frac{\pi d p}{p^2 + \pi^2 D_{coil}^2} \tag{1.2}$$

$$torsion\ parameter\ \beta = \tau\sqrt{2\delta} \qquad (1.3)$$

Many experimental studies in literature proved that coil curvature has a stabilizing effect on turbulent fluctuations arising in the flow: when coil diameter is dominant in respect to coil pitch and tube inner diameter, turbulence is significantly inhibited and the turbulent kinetic energy shows much lower levels than in straight pipe flow; hence the critical Reynolds number at which laminar to turbulent flow transition occurs is higher than in straight tubes [5]. On the other hand, the impact of torsion on fluid flow is believed to be destabilizing: Yamamoto et al. [6] found that the critical Reynolds number at the onset of turbulence decreases from the value of the toroidal tube as β increases at fixed value of δ, has a minimum and then increases with further large β; the minimum critical Reynolds number is far below that of a straight pipe. Destabilization has thus a maximum for a specific value of coil pitch. From equations (1.2) and (1.3) it is easy to see that, if $D_{coil} >> p$, coil torsion τ and, in consequence, torsion parameter β tend to zero; therefore the geometry of the test section is uniquely described by coil curvature δ, which becomes:

$$\delta \cong \frac{d_{tube}}{D_{coil}} \qquad (1.4)$$

Whenever the above condition is verified, the approximation (1.4) allows to neglect the effects of torsion and to consider a helical tube as toroidal. Manlapaz and Churchill [7] found that toroidal assumption is reasonable provided that the coil pitch is lower than the coil radius; Yamamoto et al. proposed the condition $\beta < 0.5$; Srinivasan et al. concluded that the torsion effect on friction factor can be ignored.

1.2 Review of correlations for laminar to turbulent flow transition in coiled pipes

It is well accepted that, in straight circular tubes with fully developed flow, the onset of turbulence corresponds to critical Reynolds number $Re_c \approx 2300$, although much larger Reynolds numbers ($Re_c \approx 10000$) are required to achieve fully turbulent conditions [8]. Conditions in helical tubes are strongly different and a more exhaustive analysis is needed. The first method used to find the location of critical Reynolds number in curved pipes was proposed by White (1929) [9]: this consists of plotting f_c and f_s vs. Re, where f_c and f_s are the friction factors at the same Reynolds number in a coil and a straight tube, respectively, of equal length and cross-sectional diameter. In this plot the functional form of f_s presents a well known interruption in its continuity in correspondence of laminar to turbulent flow transition, while f_c does not; however, there appears to be a change of law at a certain value of Reynolds number. White thus concluded that at this point the flow becomes turbulent. An example of White's method is presented in Figure 1.1. In the following decades this approach, based on the analysis of pressure drops, has been principally used. Ali (1999) [10] subdivided the flow into four different regimes (low-laminar, laminar, mixed and turbulent), defining three critical Reynolds number from experimental pressure drops data:

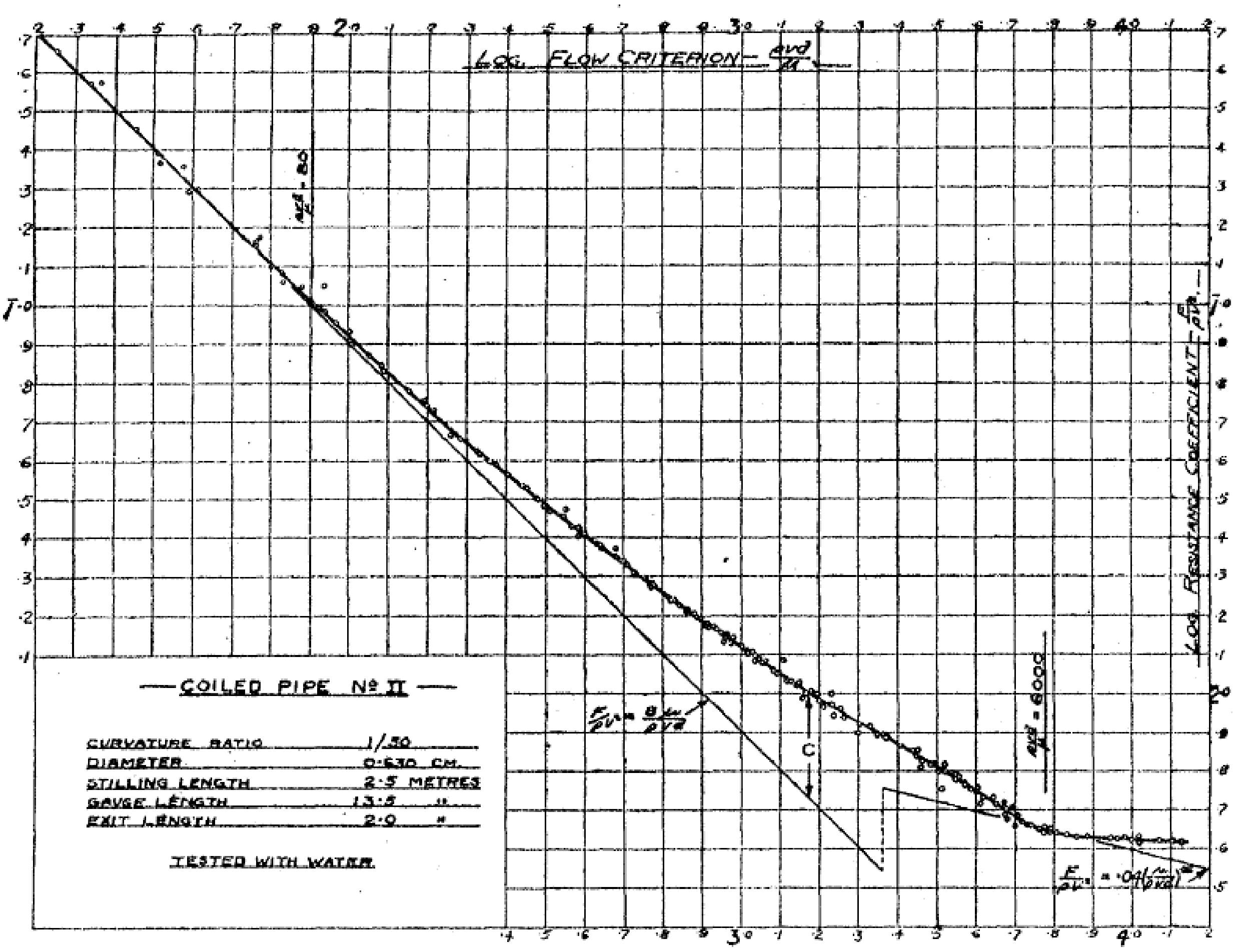

***Figure 1.1**: Example of White's method for the determination of critical Reynolds [9]*

$$Re_{crit_{low\ laminar-laminar}} = 500 \quad (1.5)$$

$$Re_{crit_{laminar-mixed}} = 6000 \quad (1.6)$$

$$Re_{crit_{mixed-turbulent}} = 10000 \quad (1.7)$$

These values show a good agreement with White's method. Many researchers correlated the critical Reynolds number as a function of curvature ratio D_{coil}/d_{tube} : this value is retained to summarize the geometry of the tube when toroidal assumption is made and it was used as characteristic dimensionless group in numerous correlations. Ito (1959) [11] derived a correlation to calculate the critical Reynolds number at which transition occurs, given by:

$$Re_{crit} = 2000\left[1 + 13.2\left(\frac{D_{coil}}{d_{tube}}\right)^{-0.6}\right] \tag{1.8}$$

and valid in the range of $5 < D_{coil}/d_{tube} < 2000$. Srinivasan et al [12] proposed the following correction to Ito's formula in the range of $7.5 < D_{coil}/d_{tube} < 100$:

$$Re_{crit} = 2100\left[1 + 12\left(\frac{D_{coil}}{d_{tube}}\right)^{-0.5}\right] \tag{1.9}$$

More recently, Cioncolini and Santini (2005) [13] proposed a distinction among three different types of curvature: strong ($D_{coil}/d_{tube} < 24$), medium ($30 < D_{coil}/d_{tube} < 110$) and mild ($D_{coil}/d_{tube} > 150$). They analyzed the behavior of Fanning friction factor in these zones and then provided correlations for the beginning of the transition:

$$Re_{crit_{strong}} = 30{,}000\left(\frac{D_{coil}}{d_{tube}}\right)^{-0.47} \tag{1.10}$$

$$Re_{crit_{medium-1}} = 12{,}500\left(\frac{D_{coil}}{d_{tube}}\right)^{-0.31} \tag{1.11}$$

$$Re_{crit_{mild}} = 2300\left[1 + 210\left(\frac{D_{coil}}{d_{tube}}\right)^{-1.12}\right] \tag{1.12}$$

These authors also stated that in the regions of strong and mild curvature the laminar to turbulent transition is defined by only one discontinuity in the range of friction factor, identified by equations (1.10) and (1.12), whereas in the region of medium curvature a large zone of mixed flow is recognized; the onset of transition is given by equation (1.11), while for the end a second correlation is provided:

$$Re_{crit_{medium-2}} = 120{,}000\left(\frac{D_{coil}}{d_{tube}}\right)^{-0.57} \tag{1.13}$$

1.3 Purpose of present work

In this chapter the influence of the ratio of inner tube diameter to coil diameter in turbulence emergence is investigated, with the purpose to find simple correlations which can easily express the laminar to turbulent flow transition in helically coiled tubes. In order to do this, an experimental approach based on the Darcy friction factor has been employed. The relative error between experimental data and two empirical correlations for laminar and turbulent flow was analyzed; for this purpose Ito equations for laminar [14] and turbulent [11] friction factor were chosen. A detailed study analyzing the profile of friction factor and its dependence with the ratio of coil diameter to tube inner diameter is carried out: actually the geometric parameters play an important role in determining the beginning, the ending and the amplitude of the transition zone.

Thirteen coils have been tested, using liquid water as fluid and measuring pressure drops in a wide range of Reynolds number. The composition of the data set is the following:

(a) 963 pressure drop measures performed by Cioncolini and Santini in their experimental study [13] on twelve different test sections at Politecnico di Milano, with ratios of coil diameter to tube inner diameter ranging from 6.9 to 369;

(b) 73 pressure drop measures performed on SIET facility settled in Piacenza, with ratio of coil diameter to tube inner diameter equal to 79.80.

All the twelve coils in (a) satisfy the above mentioned Manlapaz and Churchill's conditions for toroidal assumption, while the test section in (b) does not. Nevertheless, the results of this study will show that torsional effects are not visible in the experimental friction factor profile of SIET facility.

1.4 Experimental facilities description

1.4.1 SIET forced flow experiences test section

The SIET test section, built and operated at SIET labs (Piacenza, Italy), is an helically coiled AISI 316 SS steam generator tube, framed into an open loop facility built inside the boiler building of the "Emilia" power station in Piacenza.

Figure 1.2 *Global view of the SIET facility test section*

A sketch of the experimental structure is reported in Figure 1.3: the whole facility is made by a supply section and a test section. The supply section feeds demineralized water from a tank to the test section, by means of a centrifugal booster pump and a feed water pump, i.e. a volumetric three cylindrical pump with a maximum head of about 200 bar. The flow rate is controlled by a throttling valve (V3) positioned downwards the feed water pump and after a bypass line. System pressure control is accomplished by acting on a throttling valve (V4) placed at the end of the steam generator. An electrically heated pre-heater is located before the test section, and allows creating the desired temperature at the inlet of the test section. The test section equipped with two helical tubes, even though only one was employed for the purpose of the present work. The heating along the tubes is guaranteed via Joule effect by DC current; two distinct,

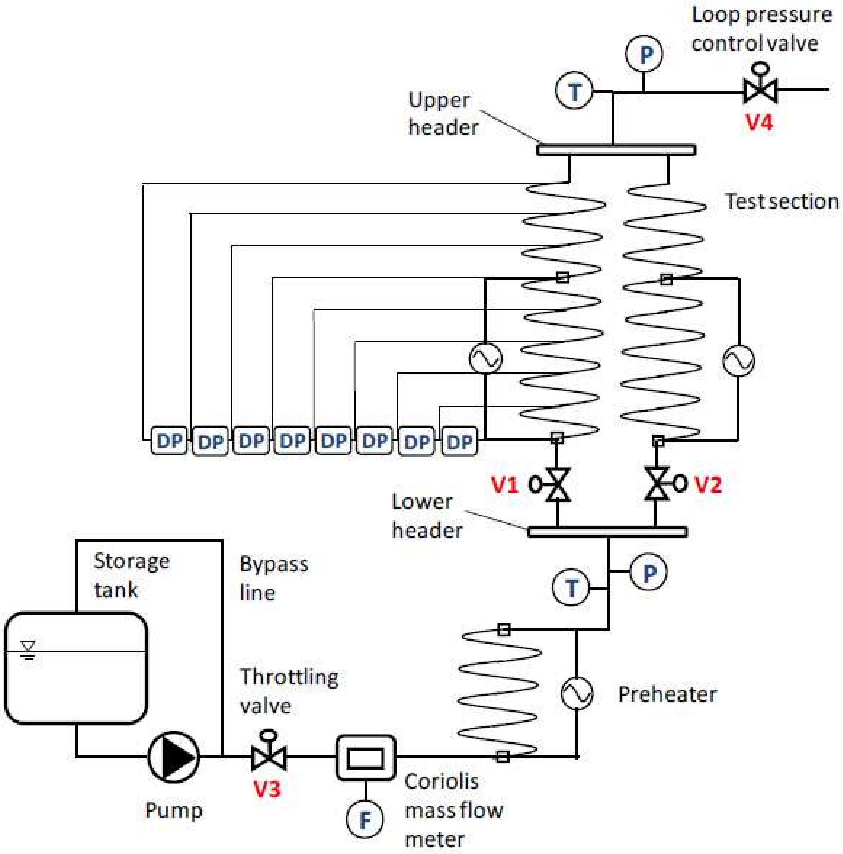

Figure 1.3 *Sketch of the experimental facility installed at SIET labs*

independently controllable and contiguous sections are provided, in order to be able to vary the thermal fluxes: the first one, from tube inlet to 24 meters, intends to simulate the subcooling zone and the two-phase saturated zone of the steam generator, while the second, from 24 meters to the tube outlet, reproduces the post dryout and superheating zones. Although the tube is accurately insulated with wool rock, thermal losses are not negligible. In the present work pressure drops measured in three different conditions are used: single-phase adiabatic, two-phase adiabatic and two-phase with power input. No heat was supplied in the second section in a large number of measures during the two-phase diabatic experience, considering as adiabatic the data there measured; in the two-phase adiabatic experience steam was generated at the desired quality in the pre-heater and then sent into the test section.

Since this facility has been widely used for IRIS (International Reactor Innovative and Secure) project, geometric parameters are representative of IRIS steam generator [16]. Test section tube is composed by five verges of 6 meters and one tube of 2 meters preventively coiled and welded together: the total length results 32 meters; the tube has an inner nominal diameter of 12.53 mm (near to IRIS real value 13.24 mm) and an outer nominal one of 17.15 mm; the coil diameter, 1000 mm, is a mean value of the dimension in IRIS steam generator tube bundle, in which coil diameter varies in the range 610 mm – 1620 mm; the coil is composed by 10 shells with a coil pitch of 800 mm, therefore the total height of the tube results 8 meters. Test section main data are summarized in Table 1.1.

Tube material	SS AISI 316L
Tube inner diameter [mm]	12.53
Tube outer diameter [mm]	17.24
Coil diameter [mm]	1000
Coil pitch [mm]	800
Tube length [m]	32
Test section height [m]	8
D_{coil}/d_{tube}	79.81
$\delta \times 10^3$	11.76
$\tau \times 10^3$	2.996
$\beta \times 10^3$	14.52

Table 1.1 *Test section main data*

Notice that β parameter satisfy Yamamoto et al.'s condition (β<0.5), while Manlapaz and Churchill's approximation is not verified. Nine pressure taps are disposed nearly every four meters along the coiled tube used in present work, and eight differential pressure transducers connect the pressure taps; the detailed distances between the taps and the tube inlet are reported in Table 1.2. Measures made with digital caliber with an accuracy of 1/100 mm on tube inner and outer diameters, made on a sample straight tube of the same verges used for the test section, showed a maximum difference between measured values and nominal ones of 0.44% and an ovalization (defined as the ratio of the difference between two measured tube orthogonal diameter and diameter nominal value) of tube outer diameter that never exceeds 1.22%. Thanks to these small values, the nominal straight values of tube inner and outer diameters were considered in all the calculations regarding the test section. Tube inner surface roughness measures gave a mean value of 3.08 μm.

Tap 1	*Tap 2*	*Tap 3*	*Tap 4*	*Tap 5*	*Tap 6*	*Tap 7*	*Tap 8*	*Tap 9*
200	5173	9186	13148	17141	21643	25586	29088	32059

Table 1.2 *Pressure taps distribution along the test section [mm]*

All the measurement devices have been tested and calibrated at the certified SIET labs. The water absolute pressure at heating section inlet is measured by an absolute pressure transducer with a 100 bar range and a maximum error of about 0.1%, while the eight differential pressure transducers have a maximum error of about 0.4%. An accurate measurement of the flow rate is obtained by a Coriolis flow-meter, having a 1% maximum uncertainty in the range of the explored flow rates. A K-class thermocouple drowned in a small well provides bulk temperature with an accuracy of 0.6 °C; wall temperatures are measured with a set of 128 K-class thermocouples either brazed in tube wall or manually attached on tube external, for which a reasonable uncertainty value is 1.5 °C (no tests were made due to time and costs limitation). The thermal power given to the fluid is intended to be the difference between the electrical power supplied to the tube, whose uncertainty is retained to be lower than 2.5%, and the thermal losses; these are evaluated by means of a specific process, including single-phase runs through the helical tube with temperature jumps varying between 8 and 19 °C, whose result is the following formula:

$$Q_{loss} = 0.8674 e^{0.0076(T_{wall} - T_{air})} \tag{1.14}$$

the uncertainty on this procedure, and consequentially the error on thermal losses is estimated to be approximately 15%; by applying the rules of error propagation (see Appendix I) it is possible to obtain the error on thermal power. A summary of uncertainties of physical quantities is given in Table 1.3.

Water flow rate	± 1%
Fluid bulk temperature	± 0.6 K
Fluid wall temperature	± 1.5 K
Absolute pressure	± 0.1%
Differential pressure	± 0.4%
Supplied electrical power	± 2.5%
Evaluated thermal losses	± 15%

Table 1.3 *List of the uncertainties of physical quantities referred to measurement values.*

1.4.2 Twelve coils forced flow experiences test sections[1]

Twelve coils have been tested in order to investigate the influence of coil diameter on turbulence emergence. The experiments were performed with water at ambient temperature as the testing fluid in an open loop flow system of which a schematic representation is shown in Figure 1.4. In Figure 1.5 a schematic representation of the test section is showed.

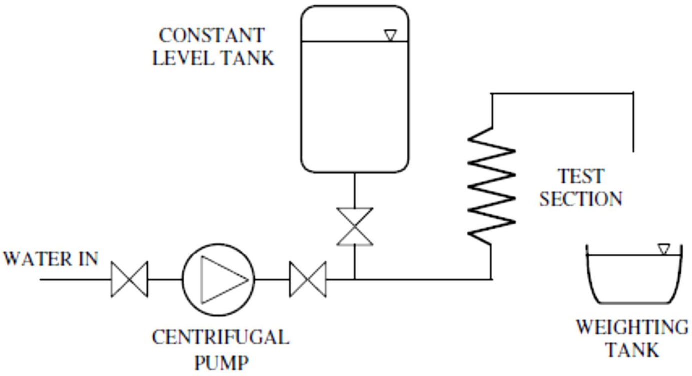

Figure 1.4 *Schematic representation of the open loop flow system.*

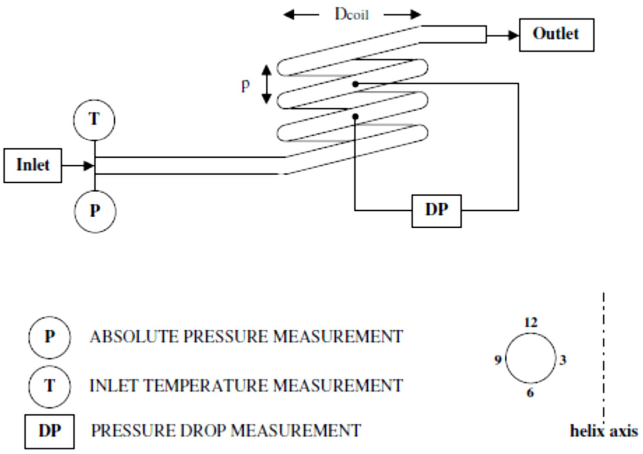

Figure 1.5 *Schematic representation of the test section*

---

[1] Only a brief explanation is here presented; further information concerning test sections description and measurement procedures are available on "Cioncolini A., Santini L. (2005) An experimental investigation regarding the laminar to turbulent flow transition in helically coiled pipes, *Experimental Thermal and Fluid Science 30 (2006)* 367-380." [13]

Coil no.	d_{tube} [mm]	D_{coil} [mm]	pitch [mm]	D_{coil}/d_{tube}	$\delta \times 10^3$	$\tau \times 10^3$	$\beta \times 10^3$
Coil 01	4.04*	28.0	7.0	6.9	143.4	11.41	21.31
Coil 02	6.79*	114.3	18.0	16.8	59.26	2.970	8.628
Coil 03	6.80*	163.0	23.0	24.0	41.63	1.870	6.480
Coil 04	10.44	368.9	20.0	35.3	28.29	0.488	2.053
Coil 05	8.59	368.6	22.0	42.9	23.30	0.453	2.097
Coil 06	6.81	362.9	20.0	53.3	18.76	0.329	1.699
Coil 07	7.98	520.0	20.0	65.2	15.34	0.188	1.072
Coil 08	8.59	729.5	22.0	84.9	11.77	0.113	0.737
Coil 09	6.82	707.3	25.0	103.7	9.641	0.108	0.781
Coil 10	4.05	619.7	19.0	153.0	6.535	0.064	0.558
Coil 11	4.05	721.5	15.0	178.1	5.613	0.037	0.351
Coil 12	4.05	1495.3	15.0	369	2.708	0.009	0.118

***Table 1.4** Dimensions of the coils tested (*equivalent diameter)*

The coils were constructed of smooth copper tube, completely filled with water before bending to minimize ovalization; despite this, deformation occurred in bending for the most tightly packed coils manufactured, i.e. coil 01, coil 02 and coil 03, resulting an elliptical flow section; hence, an equivalent diameter (four times the flow area divided by the wetted perimeter) was assumed in calculations. No appreciable deformation was detected for coils other than Coil 01, Coil 02 and Coil 03: the tube inner diameter experimental uncertainty was estimated to be within 0.25%. Geometric data of the twelve coils are listed in Table 1.4. The quite large range of the ratio D_{coil}/d_{tube} explored in this experience allows identifying three different types of curvature: strong ($D_{coil}/d_{tube} < 24$), medium ($30 < D_{coil}/d_{tube} < 110$) and mild ($D_{coil}/d_{tube} > 150$); this distinction is due to different behaviors of the curve "friction factor versus Reynolds number". For all the test sections the pitch is smaller than the coil radius and the parameter β result small: thus torsion effects can be neglected in accordance with Yamamoto's et al. condition (β< 0.5) and Manlapaz and Churchill's approximation. A list of the experimental instrumentation employed to measure physical quantities and the respective uncertainties is reported in Table 1.5.

Quantity	Instrument / Method	Uncertainty

Mass flow rate	*"Weighting technique" (weighting the amount of fluid collected in steady state operation in a given time interval)*	*1%*
Absolute pressure	*Manometer*	*5%*
Pressure drop	*Piezometer*	*2.5%*
	Water manometer	*2.5%*
	Mercury manometer	*1.5%*
	Differential pressure transducer	*2.5%*
Temperature	*Pt100 thermo-resistor*	*0.3 K*

Table 1.5 *Experimental instrumentation and uncertainty*

1.5 Review of pressure drops correlations for single-phase fluid in helical tubes

The first attempt in order to predict pressure drops single phase flow through helically coiled tubes was carried out by Dean in 1928 [4]: in his investigation he discovered that the friction factor for coil pipes with slight curvature depends approximately on a one dimensionless group called "Dean number", obtained from the simplified Navier–Stokes equations for developed flow:

$$De = Re\sqrt{\frac{d_{tube}}{D_{coil}}} \tag{1.15}$$

For single-phase laminar flow in a toroidal duct with small value of the ratio d_{tube}/D_{coil} and $De < 20$, he suggested the following analytical correlation:

$$\frac{f_{c\_Dean}}{f_s} = 1.03058\left(\frac{De^2}{288}\right)^2 + 0.01195\left(\frac{De^2}{288}\right)^4 \tag{1.16}$$

where f_c represents Darcy friction factor for coiled tubes while and f_s is the analogous for straight ones; the same geometric (tube diameter, flow direction) and operative conditions are supposed. Since this, various experimental as well as theoretical studies have been done to obtain correlations for pressure drop in regular helical coiled tubes with single-phase fluid, both for laminar and turbulent flow conditions.

1.5.1 Single-phase laminar flow

Despite few industrial applications of laminar flow in helical tubes, a quite large amount of researches with the aim of achieving reliable predictions for friction factor have been carried out. Following Dean's theoretical work, White (1929) [9] and Adler (1934) [17] proposed two simple experimental formulas depending even them only on Dean number:

$$\frac{f_{c\_White}}{f_s} = 1 - \left[1 - \left(\frac{11.6}{De}\right)^{0.45}\right]^{1/0.45} \tag{1.17}$$

$$\frac{f_{c\_Adler}}{f_s} = 0.1064\sqrt{De} \tag{1.18}$$

Later, Prandtl (1949) [18], Hasson (1955) [19] and Ito (1959) [14] conducted empirical studies finding out correlations which provide very similar predictions:

$$\frac{f_{c\_Prandtl}}{f_s} = 0.37(0.5De)^{0.36} \tag{1.19}$$

$$\frac{f_{c\_Hasson}}{f_s} = 0.556 + 0.0969\sqrt{De} \tag{1.20}$$

$$\frac{f_{c\_Ito}}{f_s} = \frac{21.5De}{[1.56 + \log_{10} De]^{5.73}} \tag{1.21}$$

Prandtl's equation validity range is 40 < De < 2000, while Ito's formula is valid in the range 13.5 < De < 2000. Other correlations are due to Collins and Dennis (1975), Van Dyke (1978), Yanase et al. (1989).

It is worth mentioning Schmidt (1964) [20] and Mishra & Gupta (1979) [21] correlations, in which the friction factor does not depend only on the Dean number, but the characterizing dimensionless groups are Reynolds number and the ratio of tube diameter and coil diameter:

$$\frac{f_{c\_Schmidt}}{f_s} = \left[1 + 0,14\left(\frac{d_{tube}}{D_{coil}}\right)^{0.97} Re\right]^{i} \tag{1.22}$$

$$\frac{f_{c\_Mishra\_\&\_Gupta}}{f_s} = 1 + 0.033[\log_{10} He]^4 \tag{1.23}$$

where $i = 1 - 0.664(d_{tube}/D_{coil})^{0.312}$ and the helical number He is defined as:

$$He = Re\sqrt{\frac{\frac{d_{tube}}{D_{coil}}}{1 + \left(\frac{p}{\pi D_{coil}}\right)^2}}$$

Equation (1.22) is not specific for laminar flow: as it will be shown in next paragraph, the predictions provided by this correlation are better in turbulent regime. Equation (1.23) takes into account torsional effects by including the coil pitch p in Helical number and it is suitable for 1 < He < 3000; further similar correlations have been proposed by Manlapaz and Churchill (1980), Liu and Masliyah (1993).

An important difference between f_c and f_s should be remarked: it is well known in fact that the friction factor in straight tubes has a discontinuity in correspondence of the critical Reynolds number, i.e. $Re_{crit\_straight} \approx 2300$ [8], while such behavior is not visible in coiled pipes and the laminar to turbulent flow transition is settled at a higher value of Reynolds number because of the stabilizing effect of curvature. Thus, the curve f_c /f_s versus Reynolds is quite complex when the flow in straight tubes become turbulent; since all the above mentioned equations contains this ratio, various authors sustain that their validity should be limited at $Re < 2300$ and recommend other formulas which do not include f_s for the entire range of coil flow. Nevertheless, many of these correlations show good agreement with experimental data also at higher Reynolds number.

1.5.2 Single-phase turbulent flow

Numerous industrial applications of single-phase turbulent flow in helical tubes have justified lots of efforts in order to predict pressure drops. The first research in this region was presented by White in 1932 [22]: White extended his laminar flow study (equation (15)) and developed the following correlation to determine Darcy friction factor:

$$f_{c\_White} = 0.32Re^{-0.25} + 0.048\left(\frac{d_{tube}}{D_{coil}}\right)^{0.5} \tag{1.24}$$

In the following decades many authors recommended various correlations: the most popular one is Ito’s equation (1959) [11], obtained from an experimental test of smooth tubes and suitable for $Re < 150000$:

$$f_{c\_Ito} = 0.304Re^{-0.25} + 0.029\left(\frac{d_{tube}}{D_{coil}}\right)^{0.5} \tag{1.25}$$

Several other correlations have been developed for different geometries of holding tubes. Kubar and Varrier (1961-1962) [23] suggested a correlation applicable for a limited range of geometries and Reynolds:

$$f_{c\_Kubar\_\&\_Varrier} = 0.013152Re^{0.09}exp\left(1.887\frac{d_{tube}}{D_{coil}}\right) \qquad (1.26)$$

$$10 < \frac{d_{tube}}{D_{coil}} < 27, \qquad 9000 < Re < 25000$$

Srinivasan et al. (1968) [24] and Mishra and Gupta (1979) [21] proposed the following equations respectively:

$$f_{c\_Srinivasan} = 4.336\left(Re\sqrt{\frac{D_{coil}}{d_{tube}}}\right)^{-0.2} \qquad (1.27)$$

$$f_{c\_Mishra\_\&\_Gupta} = 0.3164Re^{-0.25} + 0.03\sqrt{\frac{d_{tube}}{D_{coil}}} \qquad (1.28)$$

Further correlations are due to Mori and Nakayama (1967), Tarbell and Samuels (1973).

The research results of various authors [25] for curved pipes or helical tubes show that Ito's equation (1.25) is of elevated accuracy and it is recommended as the standard formula for turbulent region. Despite this, none of these equations try to quantify the effects of roughness, which is believed to play a significant role on single-phase pressure drop at high Reynolds numbers; Ito's experience was conducted using smooth drawn-copper tubes, therefore his formula is suitable only for $Re < 150000$. During AGR (Advanced Gas Reactor) tests, Ruffel (1974) [26] developed a correlation to calculate the turbulent flow frictional pressure drop in a stainless steel coarse pipe (even thought roughness was not quantified in the paper):

$$f_{c\_Ruffel} = 0.014 + 2.54\left(\frac{D_{coil}}{d_{tube}}\right)^{-0.275} Re^{-0.4} \qquad (1.29)$$

The validity of this correlation can be extended up to $Re < 600000$. Comparing Ito's and Ruffel's equations (Figure 1.6) on SIET facility geometry, a considerable difference arises between the two curves: roughness causes an increase in the friction factor when Reynolds number exceeds the value 100000.

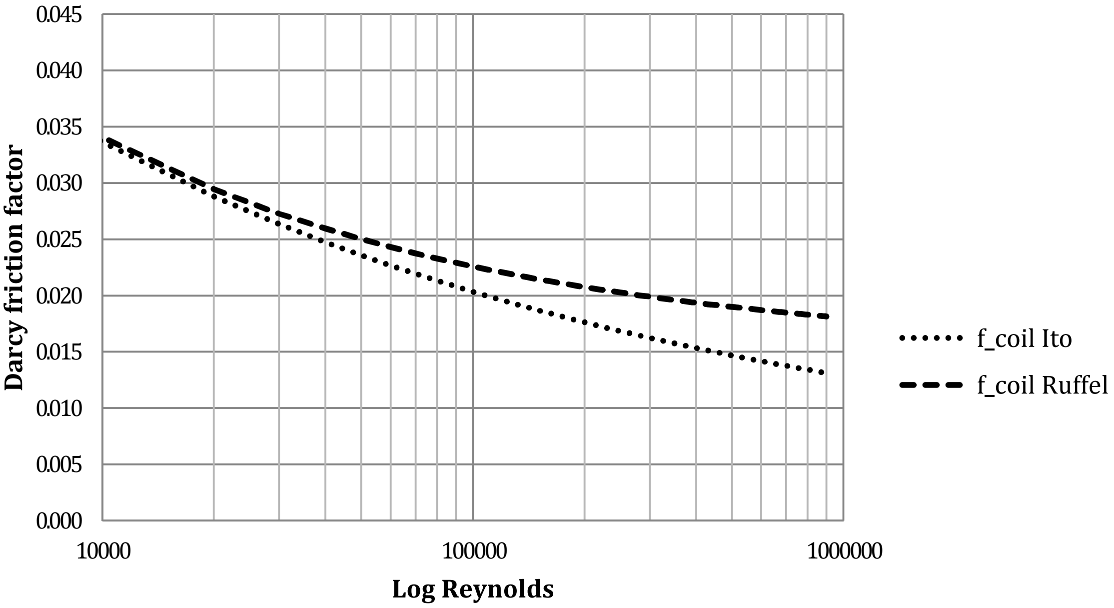

Figure 1.6: *Ito's and Ruffel's equations versus Reynolds (Log scale)*

1.6 Friction factor profile in helically coiled tubes

1.6.1 Friction factor in straight cylindrical tubes

Darcy friction factor for internal flow in cylindrical tubes is defined as:

$$f \equiv \frac{-\left(\frac{dp}{dz}\right) D}{\rho \frac{\overline{u_z}^2}{2}} \tag{1.30}$$

where *-dp/dz* indicates the frictional pressure drop along the tube, *D* is the tube inner diameter, *ρ* is the fluid density and $\overline{u_z}$ denotes the average axial velocity of the flow on the tube section; it is a mean value of the axial velocity, which, for a viscous fluid, is maximum in the center of the tube and minimum on the wall. This term can be calculated theoretically only for laminar symmetrical flow: the radial dependence of the axial velocity can be found by imposing the momentum conservation, which reduces, for fully developed laminar flow, to a balance between shear and pressure forces. The result, obtained under the conditions of zero slip at the tube surface and radial symmetry, i.e. $u_z(r_0) = 0$ and $\left.\frac{\partial u_z}{\partial r}\right|_{r=0} = 0$, is a parabolic profile:

$$u_z(r) = -\frac{1}{4\mu}\left(\frac{dp}{dz}\right)r_0^2\left[1-\left(\frac{r}{r_0}\right)^2\right] \tag{1.31}$$

Computing the average surface integral of the profile (eq. 1.31), the mean velocity u_m is:

$$\overline{u_z} = -\frac{r_0^2}{8\mu}\left(\frac{dp}{dz}\right) \tag{1.32}$$

Substituting this result in eq. (1.30), the well known Hagen-Poiseuille theoretic resistance formula for Darcy friction factor is achieved [8]:

$$f = \frac{64}{\frac{\rho\overline{u_z}d}{\mu}} = \frac{64}{Re} \tag{1.33}$$

As turbulent flow is concerned, no analytical formulas can be obtained, therefore experimental approach is required in order to carry out correlations for friction factor; moreover, roughness effect becomes more important as Reynolds number increases. Various correlations are available in literature; in this work, Selander formula is used:

$$f_{straight\_Selander} = \left[3.8\log\left(\frac{10}{Re}+0.2\frac{e}{d}\right)\right]^{-2} \tag{1.34}$$

Moody diagram (Figure 1.7) provides friction factors profiles for a wide range of Reynolds number: in the chart it is clear that laminar and turbulent zone are not connected, but the curve presents a discontinuity in correspondence of the critical zone; this phenomenon is clearly visible also with experimental data. An example is shown in Log-Log plot of Figure 1.8 (smooth copper tube, inner diameter = 6.06 mm): in this case, the curve changes abruptly its slope in correspondence of Re≈2300 and Re≈2700; thus the discontinuity can be located in this zone. Eq. (1.33) and eq. (1.34) are also drawn: in Selander's correlation roughness has been neglected, i.e. $e = 0$.

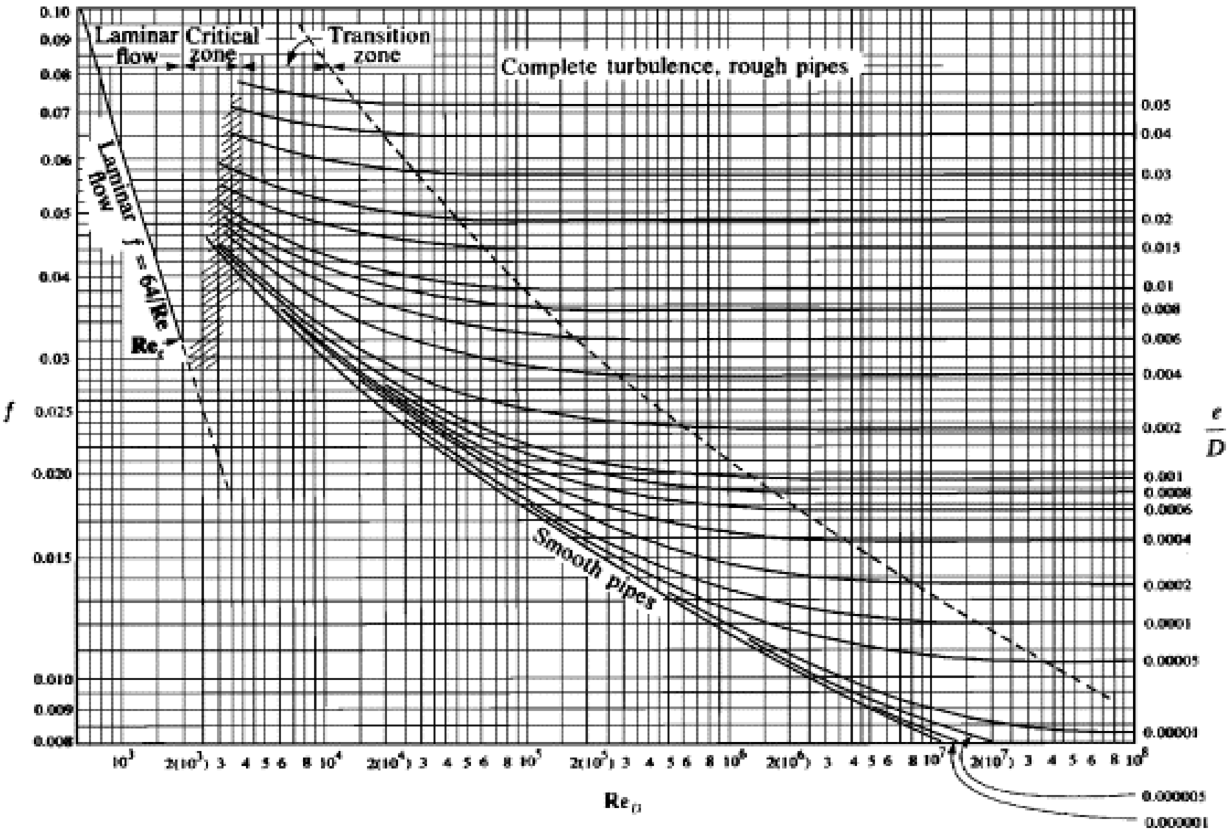

Figure 1.7 *Moody diagram for Darcy friction factor*

Since the behavior of friction factor is strongly influenced by flow regime, many authors in literature suggested the possibility to study laminar to turbulent flow transition empirically from direct observation of experimental profiles; in this way, the analysis becomes less complicated, as only pressure drop measures are required. Even though this approach does not allow the accurate determination of the transition zone, it often exhibits a good agreement with specific studies made with dedicated techniques; the results presented by Cioncolini and Santini [13] are in accordance with Webster and Humphrey's work [27], in which laminar to turbulent flow transition is investigated by means of laser-Doppler instantaneous velocity measurement in a helical tube.

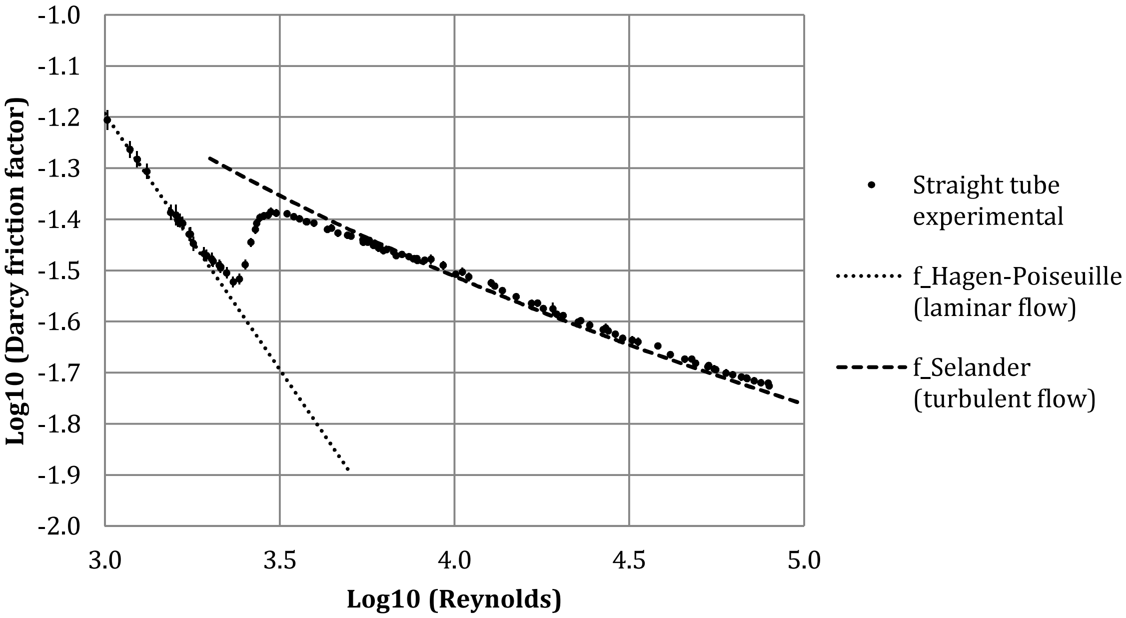

Figure 1.8 *Experimental friction factor profile in a straight smooth tube*

1.6.2 Comparison between empirical correlations and experimental data

Thermal-hydraulic conditions for single-phase pressure drop measurements are listed in Table 1.6. The experiments were performed with water at ambient temperature and pressure, varying the flow rate by changing the inlet velocity. Both laminar and turbulent regimes have been explored, with particular attention to the transition zone; no data are available in the zone of Re < 1000.

The experimental uncertainty of friction factor values is calculated with standard error propagating techniques: it turns out to be lower than 3.6% for coils other than SIET facility and coil 01, while for SIET facility and coil 01 it is lower than 7%; uncertainty of Reynolds number is always lower than 1%, thus it has not been reported. Generally, experimental uncertainty of friction factor is higher in laminar zone than in turbulent one, especially for SIET facility data. The examples which follow (Figures 1.9 – 1.16) are referred to SIET facility (D_{coil}/d_{tube} = 79.80), Coil 02 (strong curvature, D_{coil}/d_{tube} = 16.83), Coil 06 (medium curvature, D_{coil}/d_{tube} = 53.28) and Coil 10 (mild curvature, D_{coil}/d_{tube} = 153.01). Since the position and the amplitude of critical zone vary in the 13 coils tested, in graphics for both laminar and turbulent flow general values for, respectively, maximum and minimum Reynolds number on the abscissa axis are taken. The friction factor profile in transition region is distorted and cannot be predicted by any standard equation, therefore only fully developed laminar and turbulent flow conditions should be considered in the comparison between experimental data and correlations.

As far as laminar flow is concerned, most of equations listed in paragraph 1.3 give quite similar predictions: the relative difference[2] among Ito's (eq. 1.21), Prandtl's (eq. 1.19), White's (eq. 1.17), Hasson's (eq. 1.20), and Mishra & Gupta's (eq. 1.23) laminar flow correlations never exceeds 4% in the range $800 < Re < 3000$ for all the geometries explored, and, excluding Prandtl's equations, never exceeds 10% in the range $400 < Re < 800$. The measured data in laminar zone with the above mentioned correlations: the relative error on friction factor is always lower than 5% for all the geometries tested in the range $1000 < Re < 3000$ (189 experimental points). Beyond $Re = 3000$ the flow in straight tubes is in general believed to be definitely not laminar because of the beginning of the transition, thus the validity of the correlations is not guaranteed: the friction factor f_s included in these correlations cannot be calculated with the Hagen-Poseuille resistance formula. Best predictions of experimental data are given by Ito's equation, whose relative error hardly ever exceeds 2% for all the types of curvature.

Coil No.	Velocity [m/s]	Reynolds x 10^{-3}
01	0.8 – 12.0	2.8 - 43
02	0.3 – 10.0	1.7 - 60
03	0.3 – 10.0	2.3 - 60
04	0.2 - 6.5	2.2 - 60
05	0.2 - 7.5	2.0 - 59
06	0.2 - 8.5	1.1 - 51
07	0.2 - 7.5	1.1 - 53
08	0.2 - 7.0	1.2 - 53
09	0.2 - 7.5	1.3 - 45
10	0.3 - 6.5	1.1 - 24
11	0.5 - 5.5	1-7 - 20
12	0.5 - 4.5	1.6 - 16
SIET	0.2 – 2.3	2.5 - 28

Table 1.6 *Explored range for pressure drop measurements*

---

[2] Once fixed Reynolds number and geometric parameters, the relative difference among a group of friction factor f was calculated in the following way:

$$difference = \frac{\max_f f_i - \min_f f_i}{average\ f_i}$$

In the field of turbulent regime, Ito's (eq. 1.25) and Mishra & Gupta's (eq. 1.28) turbulent flow equations give close predictions for all the investigated type of geometry: the relative difference remains near 4% for all the validity range of the correlations. Schmidt's equation (eq. 1.22) is particularly interesting as it is not specific for laminar or turbulent regime: despite this, turbulent flow predictions result to be much more in accordance with other existing correlations; one possible explanation could be the more sensitive dependence on f_s in comparison to other correlations in laminar regime, rendering unreliable the predictions in this region. In general, Schmidt's formula shows a quite good agreement with Ito's and Mishra & Gupta's equations: the relative difference with Ito's equations always lower than 8% in the range $10{,}000 < Re < 100{,}000$ for mild and medium curvature, while for strong curvature this difference tends to be a little bit higher. The predictions of Ruffel's equation (eq. 1.29) in case of strong curvature are quite different from those of the above mentioned correlations: the reason could be the fact that this formula was carried out for a particular type of facility used in AGR reactor. Even in case of turbulent flow the correlation made by Ito shows the best accordance with experimental data: the relative error in fully developed turbulent conditions never exceeds 2% for coils other than SIET facility and coil 10, while for those it remains under 4%.

In light of this, Ito' laminar and turbulent regime equations have been chosen as standard formulas during the development of this work.

Laminar flow	***Turbulent flow***
● f_experimental	● f_experimental
— f_straight Hagen-Poiseuille	— f_straight Selander
— f_Ito	— f_Ito
— f_Adler	— f_Ruffel
— f_White	— f_White
— f_Prandtl	— f_Mishra-Gupta
— f_Hasson	— f_Schmidt
— f_Mishra and Gupta	
— f_Van Dyke	

Table 1.7 *Legend for graphics in Figures 1.9 – 1.16*

LAMINAR FLOW

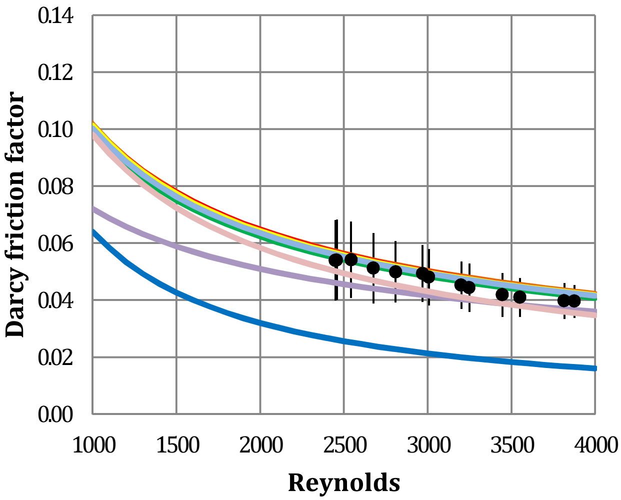

Figure 1.9 *Correlations for friction factor compared with* ***SIETfacility*** *experimental data*

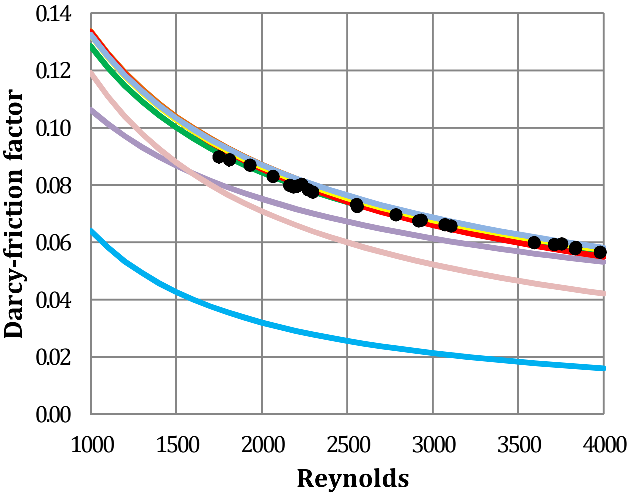

Figure 1.10 *Correlations for friction factor compared with* ***Coil 02*** *experimental data*

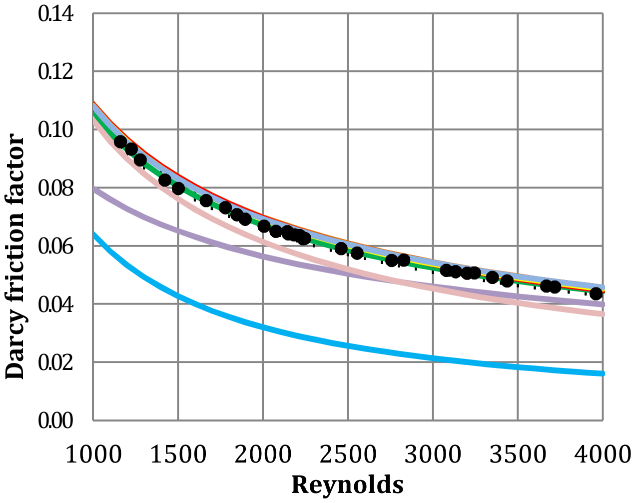

FIgure 1.11 *Correlations for friction factor compared with* ***Coil 06*** *experimental data*

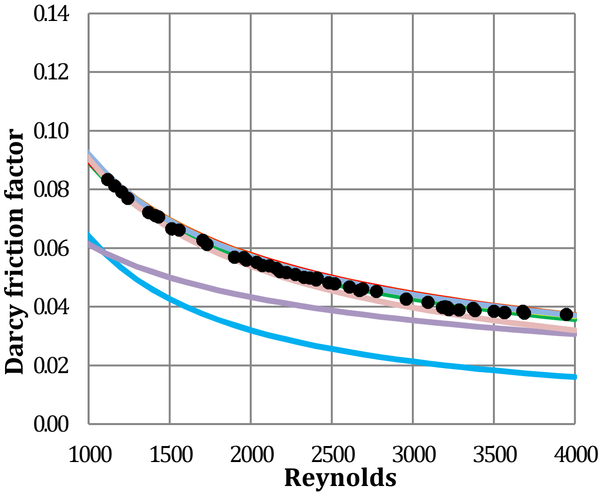

Figure 1.12 *Correlations for friction factor compared with* ***Coil 10*** *experimental data*

TURBULENT FLOW

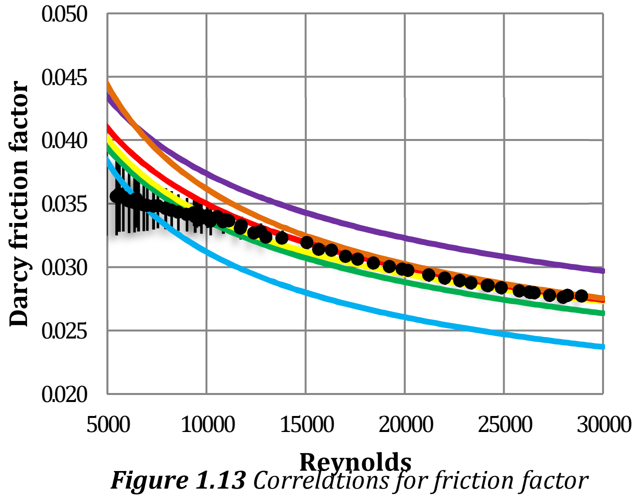

***Figure 1.13** Correlations for friction factor compared with **SIET facility** experimental data*

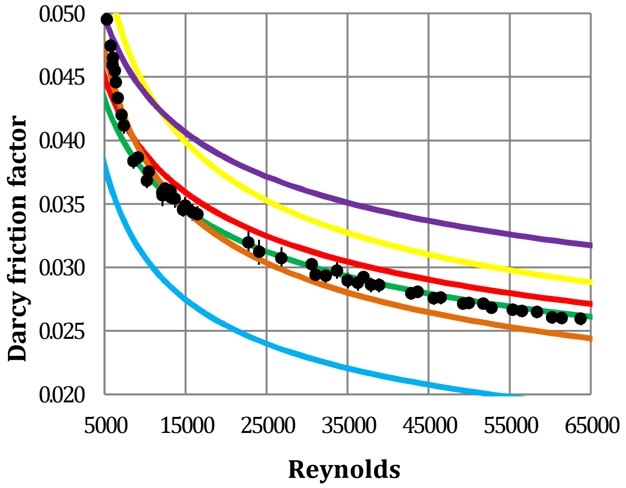

***Figure 1.14** Correlations for friction factor compared with **Coil 02** experimental data*

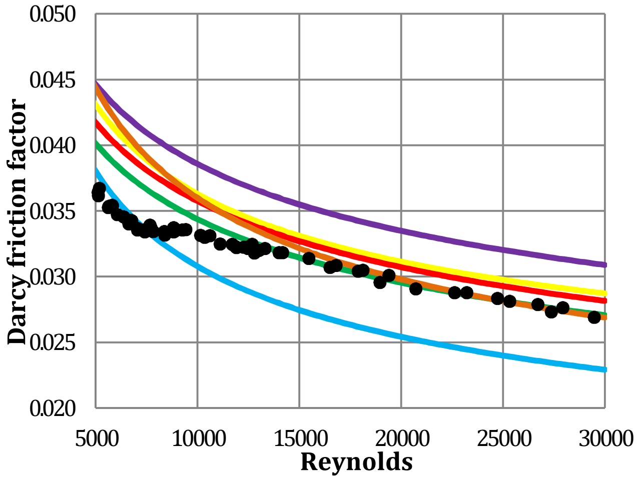

***Figure 1.15** Correlations for friction factor compared with **Coil 06** experimental data*

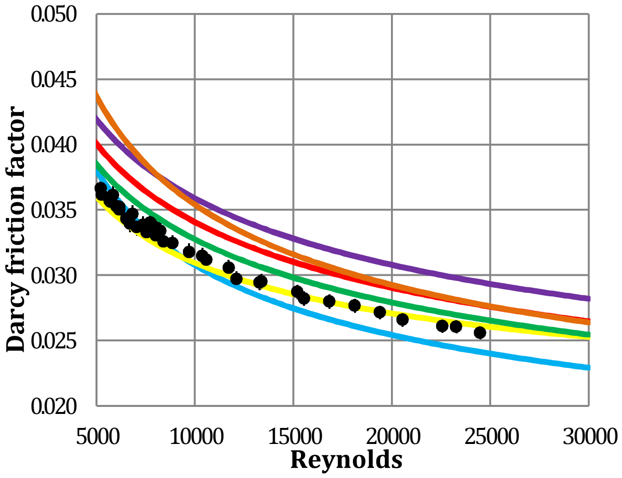

***Figure 1.16** Correlations for friction factor compared with **Coil 10** experimental data*

1.6.3 Friction factor analysis in transition zone

It well known that the presence of curvature has a strong influence on the laminar to turbulent flow transition. Supposed that the flow regime can be studied by observing the frictional component of pressure drop, Cioncolini and Santini's work [13] reveals some interesting features about friction factor profile in helically coiled tubes, that suggest that the behavior of the flow in the critical region is much more complicated compared to what happens in straight tubes: the coil diameter plays a very important role, so that the amplitude and the position of the critical zone is function not only of Reynolds number, but also of the curvature ratio D_{coil} / d_{tube}.

The experimental data (Figures 1.17 through Figure 1.29, [13] Log-Log plots) show an unstable behavior of friction factor profile included between two points, in correspondence of which the curve present a change in its law; the result is that the profile exhibits a depression. This could be interpreted as an instability in flowing fluid and therefore the two discontinuities in the slope would mark the beginning and the end of the laminar to turbulent flow transition. The extent of this zone appears very wide in the range of medium curvature, i.e. $30 < D_{coil}/d_{tube} < 110$ (Coil 04 through Coil 09 and SIET facility), while it becomes more narrow at higher values of the ratio (Coil 10 through Coil 12). The accurate determination of the Reynolds number values which include this zone is quite complicated. Eq. (1.11), eq. (1.12) and eq. (1.13) are Cioncolini and Santini's correlations for medium and mild[3] curvature; other formulas will be provided in present work. It is worth to underline an interesting phenomenon that is visible in coils with mild curvature, especially in Coil 12: besides the alteration in its law, the profiles present also a change in the sign of the slope; in other words, in a small zone the slope becomes positive, the friction factor increases with increasing Reynolds number. Since this feature is typical of rectilinear channels in correspondence of the departure from laminar zone, it is possible to deduce that in the range of very high values of the ratio D_{coil} / d_{tube} the behavior of the flow tends to become similar to that of straight tubes. On the other hand, when the curvature is particularly strong, i.e. $D_{coil}/d_{tube} < 20$ (Coil 01 and Coil 02), this two points collapse and only one discontinuity in the slope is visible, without modification in the sign: since this detail represents the unique instability observable in friction factor profile, in this range of curvature ratios it is accepted that the laminar to turbulent flow transition can be identified as point-wise; the Reynolds number value at which this point is located varies in the range $8000 < Re < 12000$ and decreases with increasing curvature ratio (eq. 1.10). The curvature ratio of Coil 03 can be placed halfway between the conditions of point-wise and large transition zone: a small depression in the profile is actually visible, even thought the change in slope can be well approximated as punctual; this characteristic anticipates the above explained behavior of the coils with medium curvature. It is interesting to notice that, although the profile in the region of strong and medium curvature is highly dissimilar, the curvature ratios of Coil 03 and Coil 04 are not very different; this fact could signifies that in the range $24 < D_{coil}/d_{tube} < 35$ the flow is strongly sensitive to the curvature ratio. The available data are not sufficient to determine what

---

[3] In eq. (1.12) for mild curvature the transition zone is approximated as point-wise

happens to the flowing fluid in this zone; more detailed experiences should be carried out in order to investigate this phenomenon.

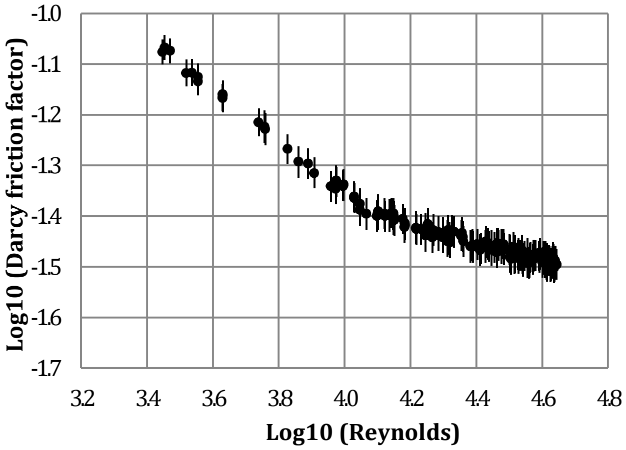

Figure 1.17 *Experimental friction factor profile for* ***Coil 01***

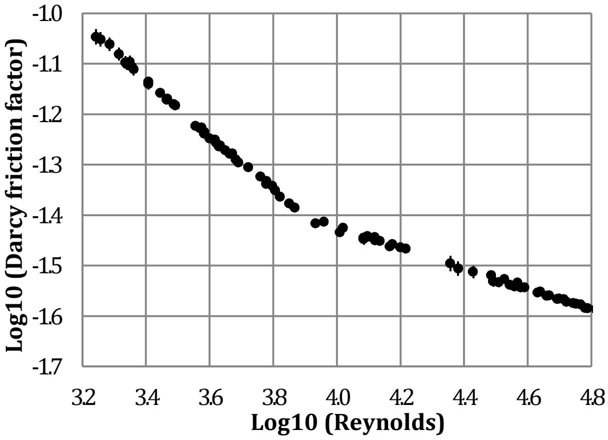

Figure 1.18 *Experimental friction factor profile for* ***Coil 02***

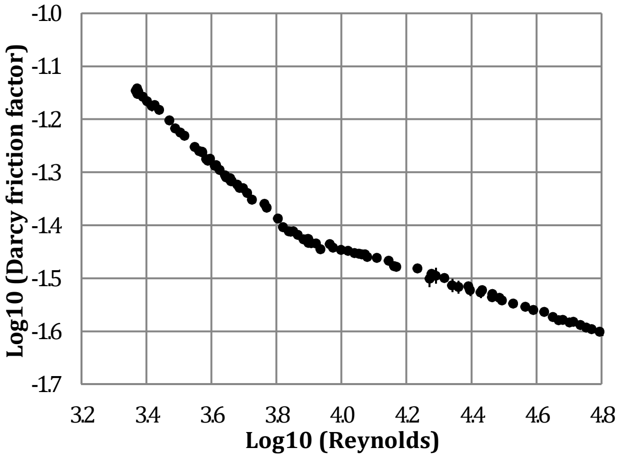

Figure 1.19 *Experimental friction factor profile for* ***Coil 03***

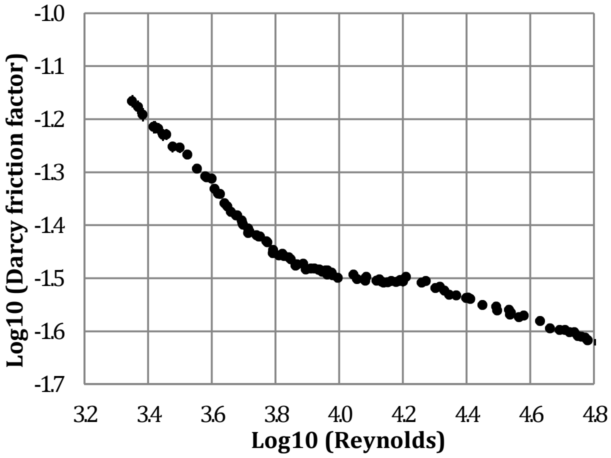

Figure 1.20 *Experimental friction factor profile for* ***Coil 04***

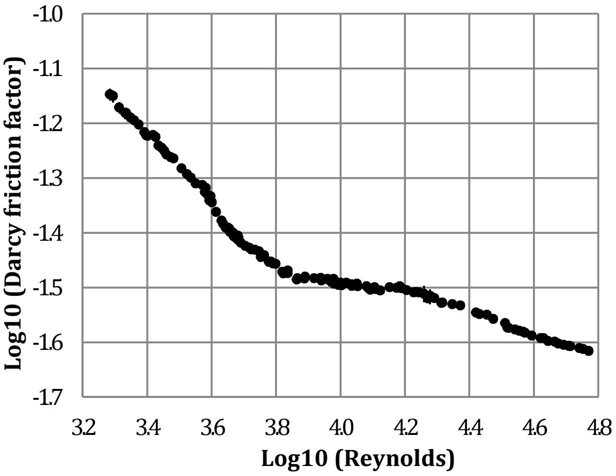

Figure 1.21 Experimental friction factor profile for **Coil 05**

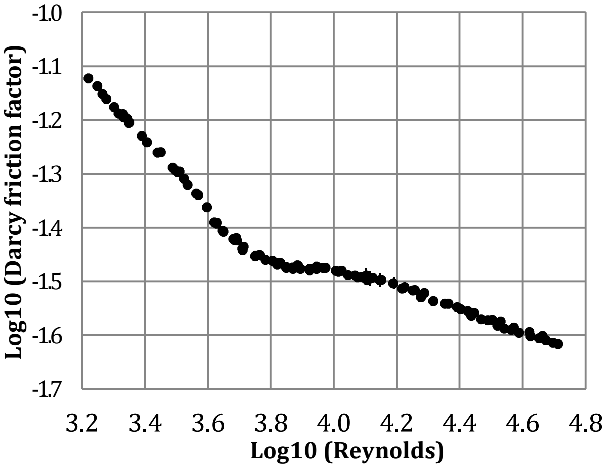

Figure 1.22 Experimental friction factor profile for **Coil 06**

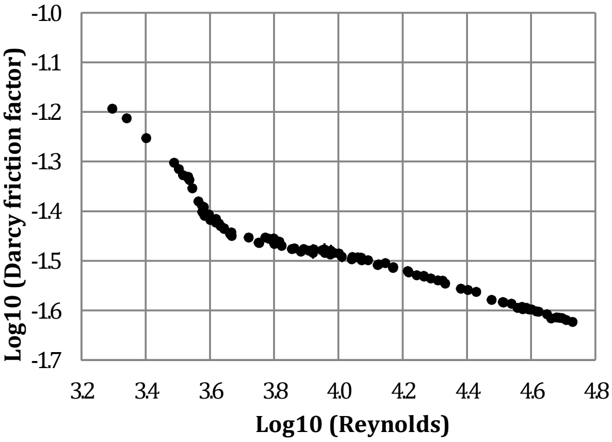

Figure 1.23 Experimental friction factor profile for **Coil 07**

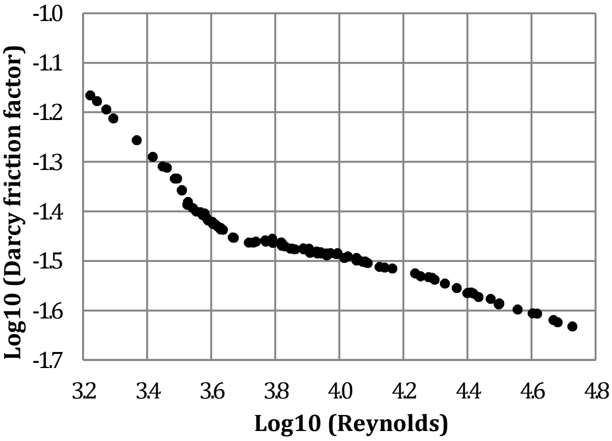

Figure 1.24 Experimental friction factor profile for **Coil 08**

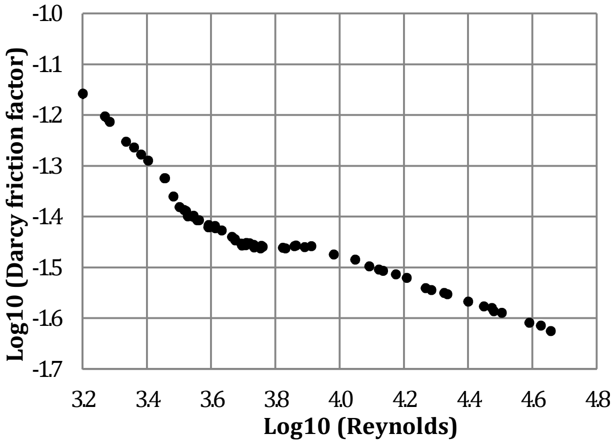

Figure 1.25 *Experimental friction factor profile for* ***Coil 09***

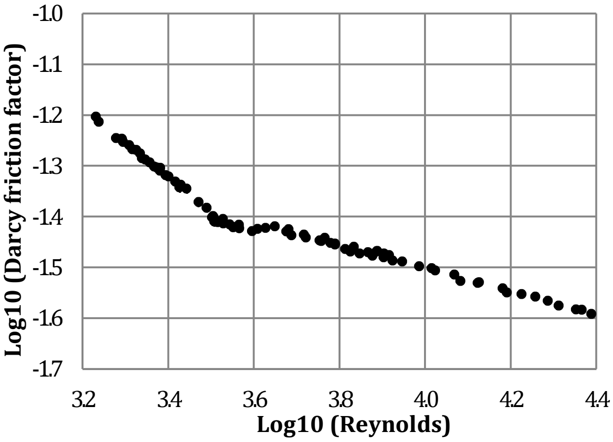

Figure 1.26 *Experimental friction factor profile for* ***Coil 10***

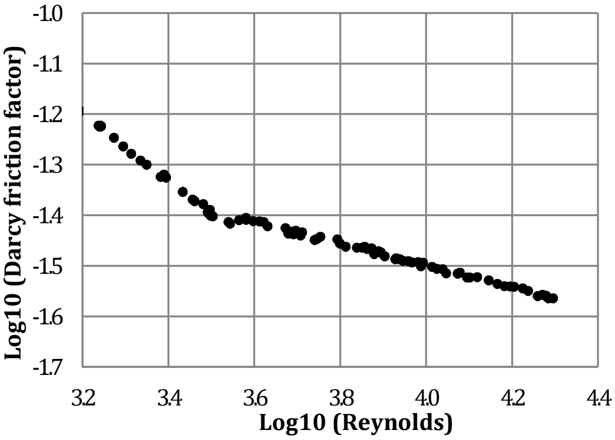

Figure 1.27 *Experimental friction factor profile for* ***Coil 11***

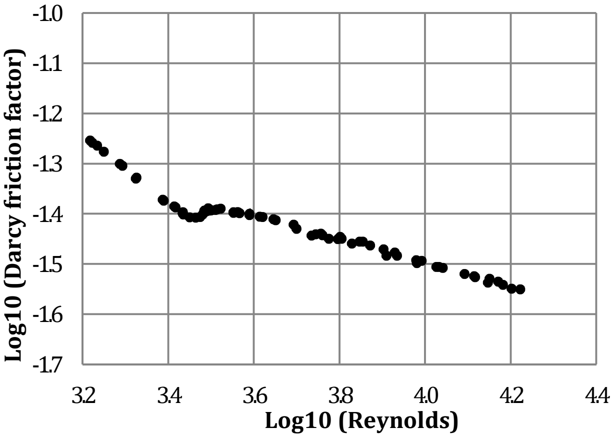

Figure 1.28 *Experimental friction factor profile for* ***Coil 12***

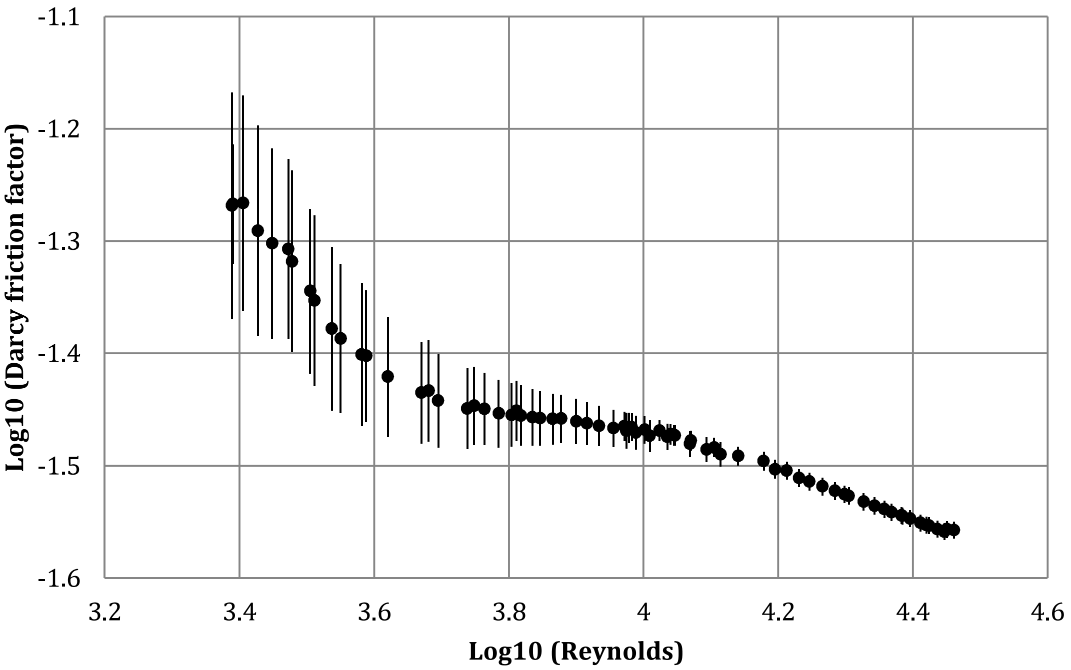

Figure 1.29 *Experimental friction factor profile for* ***SIET facility***

Even thought SIET facility does not satisfy Manlapaz and Churchill [7] toroidal assumption, having a pitch greater than the coil radius, in the experimental friction factor profile no appreciable effect due to the increase in height are visible: the curve is quite similar to those for Coil 07 and Coil 08, whose curvature ratios are the closest to the value of SIET facility; this result seems to allow to neglect the influence of torsion. Hence the empirical correlations proposed in this work can be considered suitable also for geometries with values of coil pitch larger than coil radius.

1.6.4 Pressure drop in circular straight and coiled tubes

It is ascertained that, compared to rectilinear channels, in coiled tubes the distortion of axial velocity profiles due to curvature and the presence of a secondary flow cause a greater shear within the fluid (internal friction) as well as friction with the confining wall: this phenomenon is visible in experimental data as an increase in the measured values of pressure drop; consequently, for equal Reynolds number and tube inner diameter, the frictional component dp_{frict}/dz, and therefore the Darcy friction factor (eq. 1.30), turns out to be larger in helically coiled tubes than in straight ones, the higher the difference the stronger the coil curvature. In Figures 1.30 – 1.31 this behavior is observable in case of smooth tubes (f_c and f_s are expressed using appropriate correlations). Furthermore, this difference is greater in laminar regime: it increases with increasing Reynolds number, and for strong curvature f_c can be sometimes the triple of f_s in the range $1500 < Re < 3000$. As far as turbulent flow is concerned, the difference is less visible, the ratio f_c / f_s never exceeds the value 2 and does not show large growth with increasing Reynolds number when fully turbulent regime is achieved; for high curvature ratios the conditions become progressively similar to those of straight tubes, thus the value of the ratio f_c / f_s tends to the unity.

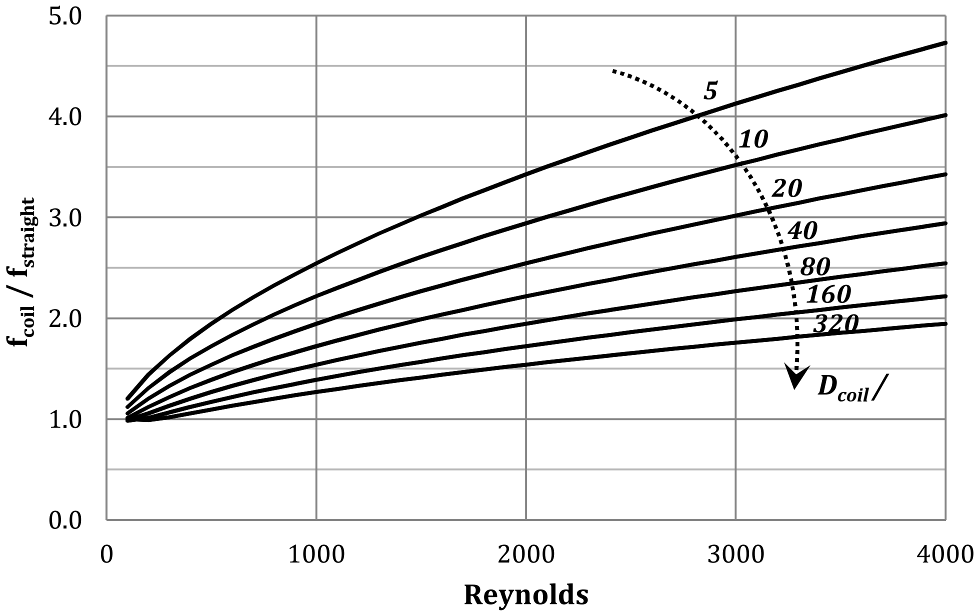

Figure 1.30 *f_{coil} / $f_{straight}$ vs Reynolds number at various curvature ratios for laminar flow, using Ito's equation (eq. 1.21) for the ratio f_{coil} / $f_{straight}$*

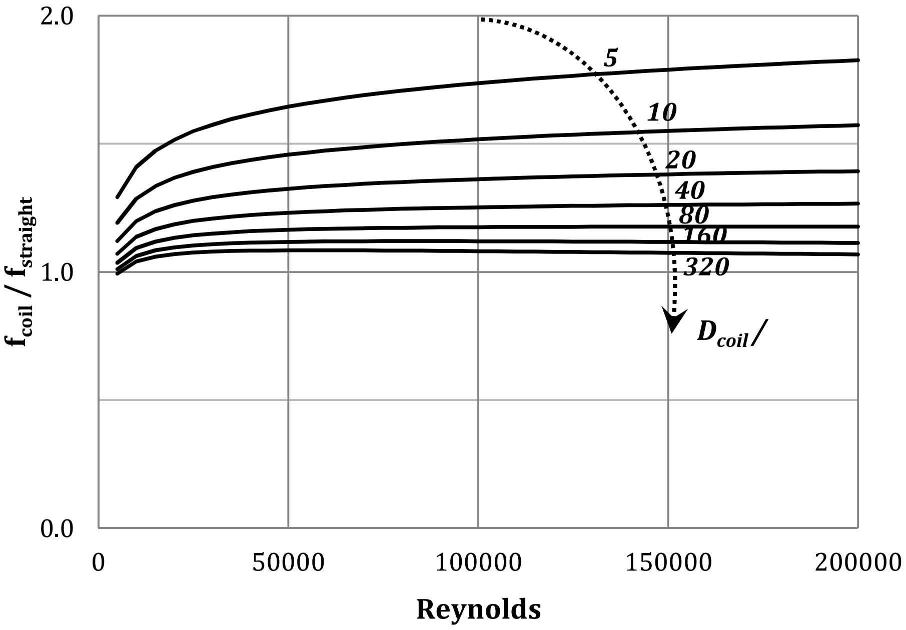

Figure 1.31 *f_{coil} / $f_{straight}$ vs. Reynolds number at various curvature ratios for turbulent flow, using Ito's equation (eq. 1.25) for f_{coil} and Selander's equation (eq. 1.34) for $f_{straight}$ (roughness value set to zero)*

In order to understand the reasons of this phenomenon, it is worth analyzing the axial velocity profiles in straight and coiled tubes, for laminar and turbulent flow. As already explained in sub-paragraph 1.4.1, a viscous fluid, under the condition of zero slip at the tube wall, flowing in laminar regime in a straight circular tube, presents a parabolic profile of axial velocity; actually this case can be studied theoretically by solving the momentum balance and the form in eq. (1.31) is obtained. Turbulent flow in straight tubes cannot be investigated analytically because of the complexity of governing equations; despite this, a general profile is obtained with the time averaged Navier-stokes equations due to Reynolds. In Figure 1.32 these profiles are shown: it is important to underline the symmetry of the axial velocity distribution.

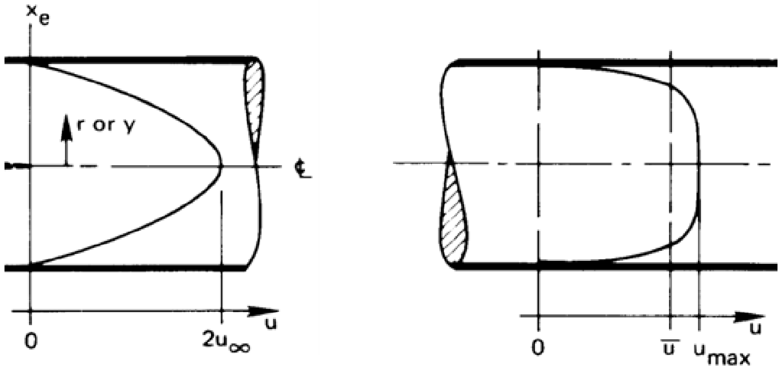

LAMINAR FLOW *TURBULENT FLOW*

Figure 1.32 *Axial velocity profiles in a straight tube [28]*

As far as curved tubes are concerned, the presence of a centrifugal force breaks this symmetry, thus, compared to the straight case, the velocity gradient near the outer wall increases while that near the inner wall decreases. This situation is shown in Figure 1.33 with a graphic made by Huttl and Friedrich [29], carried out by means of numerical methods.

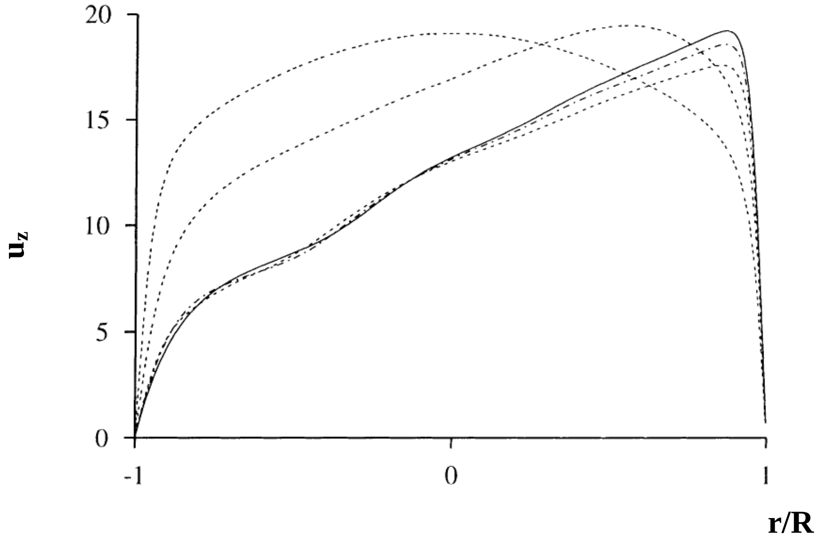

Figure 1.33 *Axial velocity profile in a straight tube (---), in two toroidal tubes with different geometries and flow conditions (--) (—), and in two helical tubes with different geometries and flow conditions (-) (-.-.-.)*

In literature, it is not unusual to find the definition of the frictional coefficient, a dimensionless parameter also called Fanning friction factor:

$$f_{Fanning} = \frac{2\tau_w}{\rho \overline{u_z}^2} \tag{1.35}$$

τ_w represents the surface shear stress for a Newtonian fluid, and it may be evaluated from knowledge of the velocity gradient at the surface:

$$\tau_w = -\mu \frac{du_z}{dr}\bigg|_{r=r_0} \tag{1.36}$$

The frictional coefficient expresses the importance of wall effects referred to the kinetic energy of the flowing fluid. By combining eq. (1.36) with eq. (1.30) and eq. (1.32), the well known relation between Darcy and Fanning friction factor is obtained:

$$f_{Darcy} = 4 f_{Fanning} \tag{1.37}$$

It is therefore evident that the frictional component of pressure drop is directly dependent on the axial velocity gradient near the wall. As far as laminar flow is concerned, the term $\frac{du_z}{dr}$ at the outer wall is particularly high when the fluid is subjected to a great centrifugal force, i.e. for strongly curved tubes; in general, the lower the curvature ratio the higher the average axial velocity gradient at the tube surface, and then the higher the frictional component of pressure drop. The same situation is verified for turbulent flow, but in this case the weight of the kinetic component is greater, a lower the distortion of the velocity profile due to centrifugal force appears and the increasing of the frictional coefficient is less important.

These results and those illustrated in sub-paragraph 1.4.3 contribute to justify the necessity to have correlations at our disposal, in order to be able to predict friction factor and laminar to turbulent flow transition in the design phase of a heat exchanger in which a helical tube is employed. The influence of the curvature on helically coiled tube is very strong and needs to be studied accurately, especially for those applications, like steam generators for nuclear reactors, in which the arising of natural convection is required in case of emergency.

1.7 An engineering approach to the study of laminar to turbulent flow transition

1.7.1 The relative error based approach

A first rough approach to the study of flow transition is here proposed. Even thought the amplitude and the position of the critical zone are strongly variable with the curvature ratio, in the very first phases of the design of a helically coiled tube a simple general correlation, valid in the entire range of curvature ratio, can be useful; this formula should be able to estimate, within an acceptable uncertainty, a value for critical Reynolds number representative of the laminar to turbulent flow transition. By observing the profiles of friction factor for all the 13 coils tested, it is possible to notice that the Reynolds number in correspondence of which the depression begins decreases with increasing value of curvature ratio; this happens as a consequence of the stabilizing effect due to curvature on the flowing fluid, the higher the stabilization, and thus Reynolds number that mark the departure from laminar flow, the stronger the coil curvature; furthermore, also the ending point of the depression shows the same behavior, although the two variables are linked with a different law[4]. In view of this, one can try to multiply the critical Reynolds number and the curvature ratio in order to obtain a series of linked values; two type of dependence between this product and the curvature ratio will be tested: a linear and a decreasing power model. However, the crucial part of this approach remains the method for the determination of the critical Reynolds number.

Once established that Ito's laminar and turbulent resistance equations yield very reliable predictions, they have been used as standard formulas: hence, the relative error committed by

---

[4] Obviously, the point-wise discontinuities in the slope of friction factor profile observable in Coil 01 and Coil 02 are excluded from this remark.

these correlations predicting the experimentally measured friction factors has been chosen as the key parameter. Looking at the graphics in Figure 1.34 through Figure 1.46, the accuracy of the above mentioned correlations is observable. In the region of fully laminar and fully turbulent flow the difference between Ito’s correlations, in their respective field of applicability, and experimental values is constant with varying Reynolds number and it is in general very close to zero. As far as the transition region is concerned, when leaving the appropriate range of pertinence the extrapolated values of Ito’s equations tend to intersect the depression characteristic of experimental data obtained in coils other than Coil 01 and Coil 02: thus in this zone there is a Reynolds number value for which the relative error is almost zero; this is just a mathematical effect, no physical meanings can be recognized. Beyond this point the theoretic resistance formulas present a rapid growth of the relative error.

● Ito’s equation for laminar flow ● Ito’s equation for turbulent flow

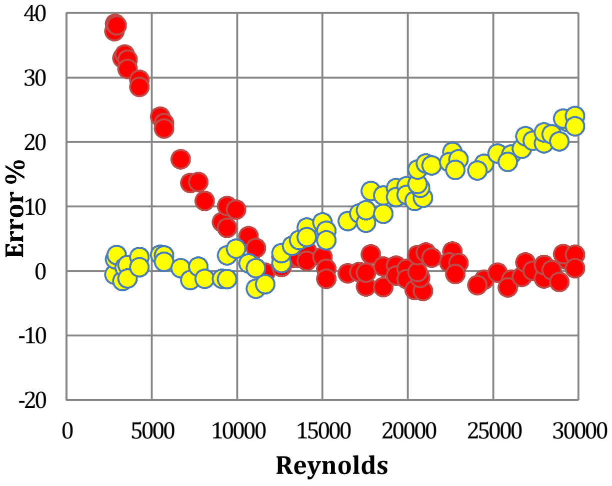

Figure 1.34Relative error between Ito’s formulas and experimental data of ***Coil 01***

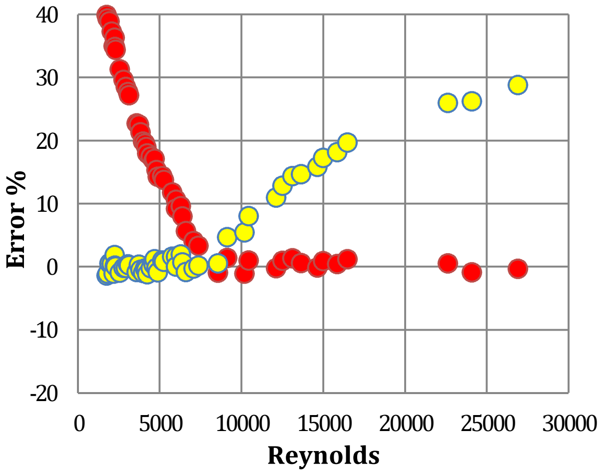

Figure 1.35 *Relative error between Ito’s formulas and experimental data of* ***Coil 02***

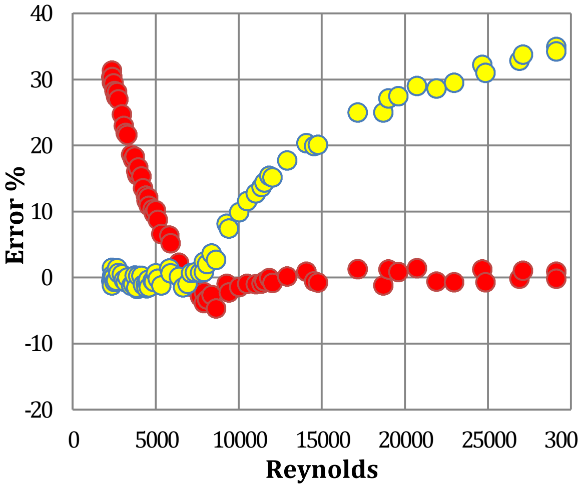

Figure 1.36 *Relative error between Ito's formulas and experimental data of* ***Coil 03***

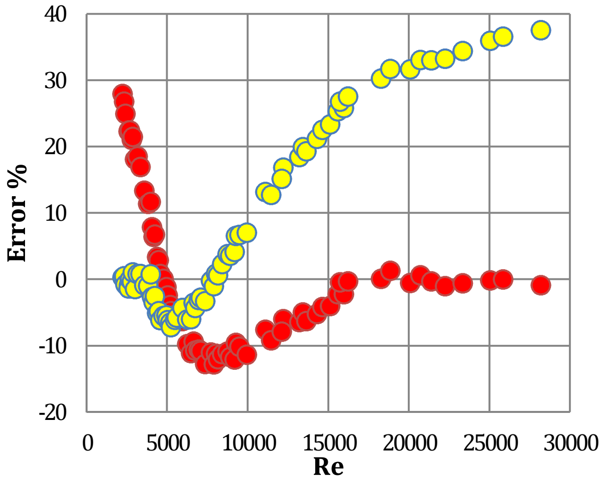

Figure 1.37 *Relative error between Ito's formulas and experimental data of* ***Coil 04***

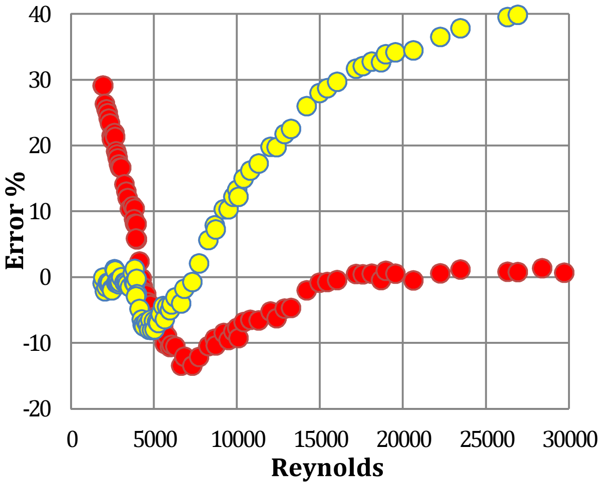

Figure 1.38 *Relative error between Ito's formulas and experimental data of* ***Coil 05***

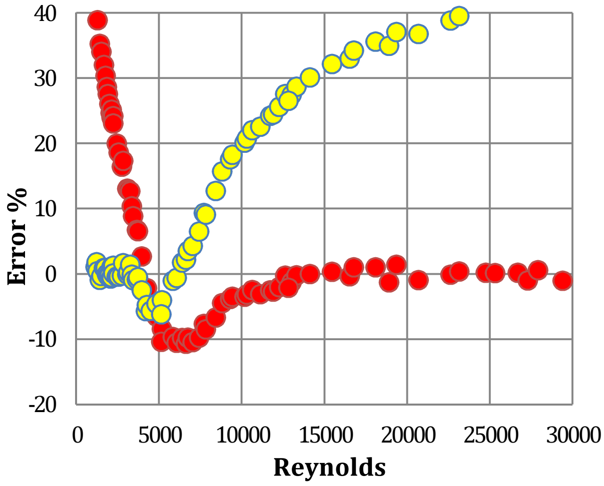

Figure 1.39 *Relative error between Ito's formulas and experimental data of* ***Coil 06***

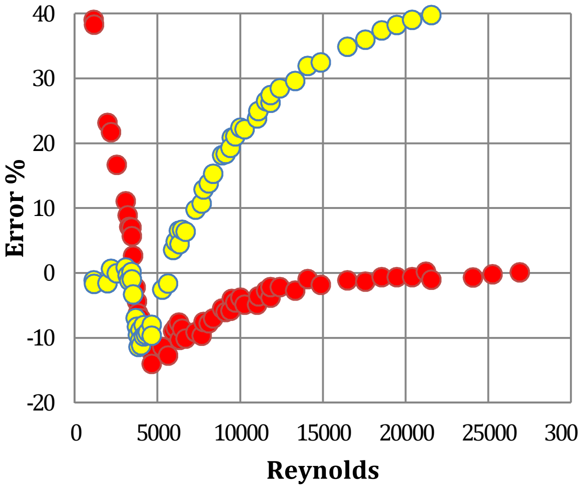

Figure 1.40 *Relative error between Ito's formulas and experimental data of* ***Coil 07***

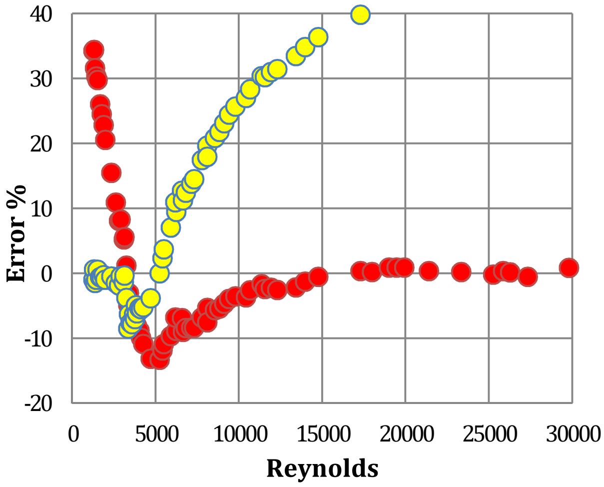

Figure 1.41 *Relative error between Ito's formulas and experimental data of* ***Coil 08***

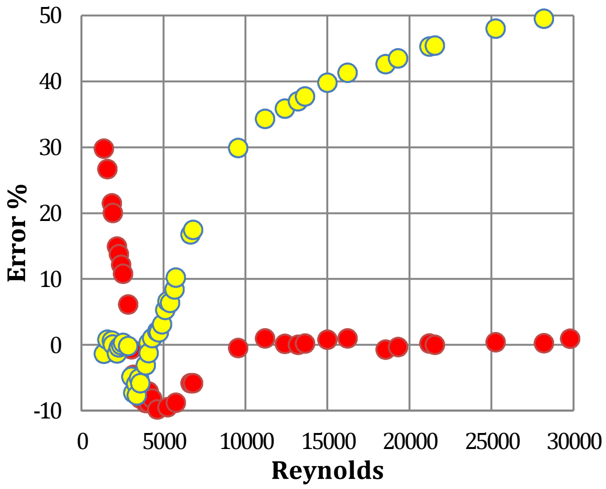

Figure 1.42 *Relative error between Ito's formulas and experimental data of* ***Coil 09***

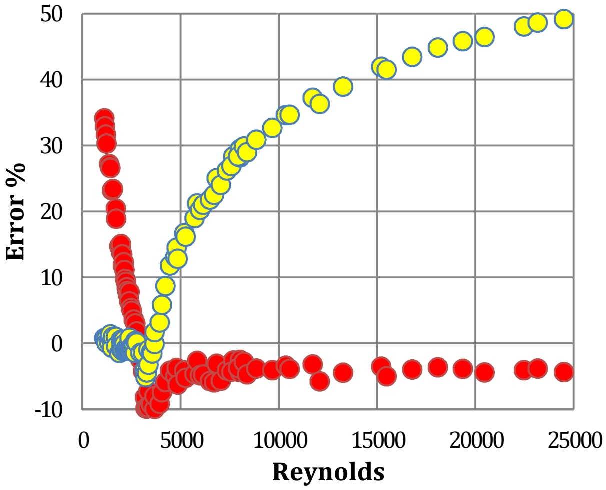

Figure 1.43 *Relative error between Ito's formulas and experimental data of* ***Coil 10***

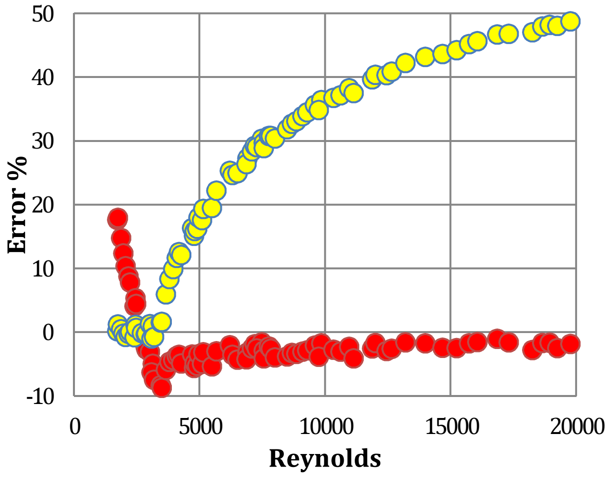

Figure 1.44 *Relative error between Ito's formulas and experimental data of* ***Coil 11***

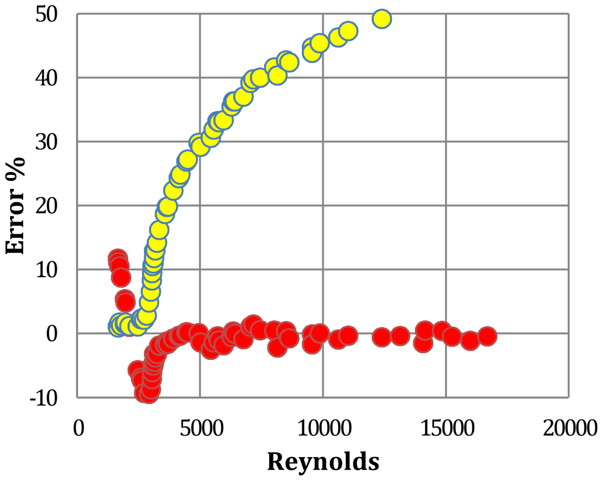

Figure 1.45 *Relative error between Ito's formulas and experimental data of* ***Coil 12***

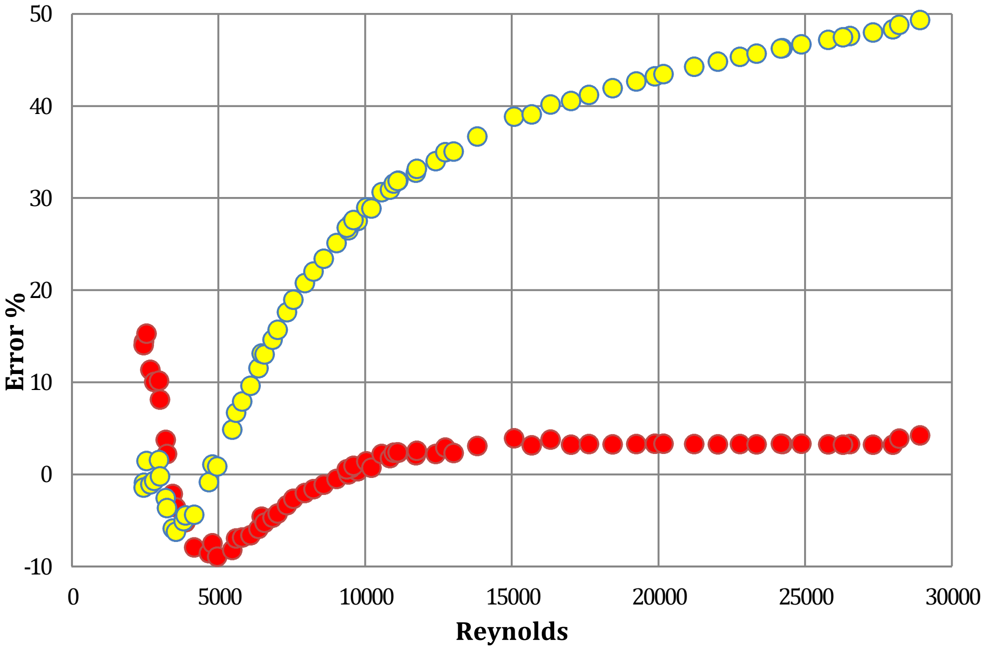

Figure 1.46 *Relative error between Ito's formulas and experimental data of* ***SIET facility***

The beginning of the critical zone can be located indicatively at the Reynolds number for which the yellow profile leaves from a near zero constant value; on the contrary the stabilization of the red curve identify the ending of turbulence region. The discontinuities in the slope observed in friction factor profiles are also visible in the above graphics: the region of medium curvature (Coil 04 through Coil 09 and SIET facility) shows the greatest depressed zone. In addition, the above explained "casually zero" relative error value in the red curve and the departure from laminar flow in the yellow curve are nearly coincident: in line of this distinct position the starting point of the depression can be located. Focusing therefore the attention on red profile, the depth of the depression never exceeds the value 15% for all the coils tested: this fact signifies that, if Ito's equation for turbulent flow was used to calculate friction factor in transition zone, the maximum relative error committed would be quite limited. In other words, if one is interested in the prediction of the frictional component of pressure drop, this situation suggests the possibility to approximate the critical region as point-wise, being this Reynolds number value almost near to the beginning of turbulence emergence; then, standard equations for friction factor in laminar and turbulent zone can be employed with an acceptable uncertainty.

1.7.2 Critical Reynolds number determination

Different options can be applied in order to determine the critical Reynolds number, making use of the relative error profiles; a simple method involving both Ito's correlations was employed.

For each coil, the Reynolds number of the experimental point, whose sum of the absolute values of the two relative errors is minimum, was chosen as the critical value.

$$Re_{crit} = min\left(\left|err\%_{Ito\_laminar}\right| + \left|err\%_{Ito\_turbulent}\right|\right) \tag{1.38}$$

Evidently, the result is situated near the beginning of the depression because of the presence of the "casually zero" value close to the departure from laminar flow. Hence, one can assume that Re_{crit} in eq. (1.38) marks the start of turbulence emergence[5]. The important advantage of this method is the fact that no arbitrary thresholds for the relative error must be chosen: a simple objective value is obtained directly from experimental data. Since for strongly curved coils the transition zone deduced from friction factor profiles appears point-wise, this kind of approach is able to identify for Coil 01 and Coil 02 quite exactly the Reynolds number value at which the changing in law of the experimental profile, and therefore the laminar to turbulent flow transition, is located.

1.7.3 Linear model

In Table 1.8 the results of this procedure are summarized.

By multiplying the critical Reynolds number with the respective curvature ratio, a linear dependence with the curvature diameter is observable (Figure 1.47). All the points lie quite perfectly on the fitting line obtained with the least square method ($R^2 = 0.9969$):

$$Re_{crit\_1}\left(\frac{D_{coil}}{d_{tube}}\right) = 2200\frac{D_{coil}}{d_{tube}} + 93000 \tag{1.39}$$

and rearranging this equation, a correlation for critical Reynolds number is obtained:

$$Re_{crit\_1} = 93000\frac{d_{tube}}{D_{coil}} + 2200 \tag{1.40}$$

Coil no.	***D_{coil}/d_{tube}***	***Re_{crit_1}***	***$Re_{crit\_1}\left(\frac{D_{coil}}{d_{tube}}\right)$***
Coil 01	*6.9*	*12606*	*87367*
Coil 02	*16.8*	*8562*	*144128*
Coil 03	*24.0*	*7140*	*171156*

---

[5] for the sake of clearness, in the following equations the Reynolds number at beginning of the transition zone will be marked with the subscript "1" and that at the ending with the subscript "2", i.e. Re_{crit_1} and Re_{crit_2}

Coil 04	*35.3*	*4774*	*168181*
Coil 05	*42.9*	*4274*	*183395*
Coil 06	*53.3*	*4206*	*211093*
Coil 07	*65.2*	*3536*	*230447*
SIET Facility	*79.8*	*3247*	*337894*
Coil 08	*84.9*	*3242*	*275352*
Coil 09	*103.7*	*3044*	*315680*
Coil 10	*153.0*	*2764*	*422926*
Coil 11	*178.1*	*2710*	*482901*
Coil 12	*369*	*2463*	*909519*

Table 1.8 *Critical Reynolds number evaluation with eq. (1.38)*

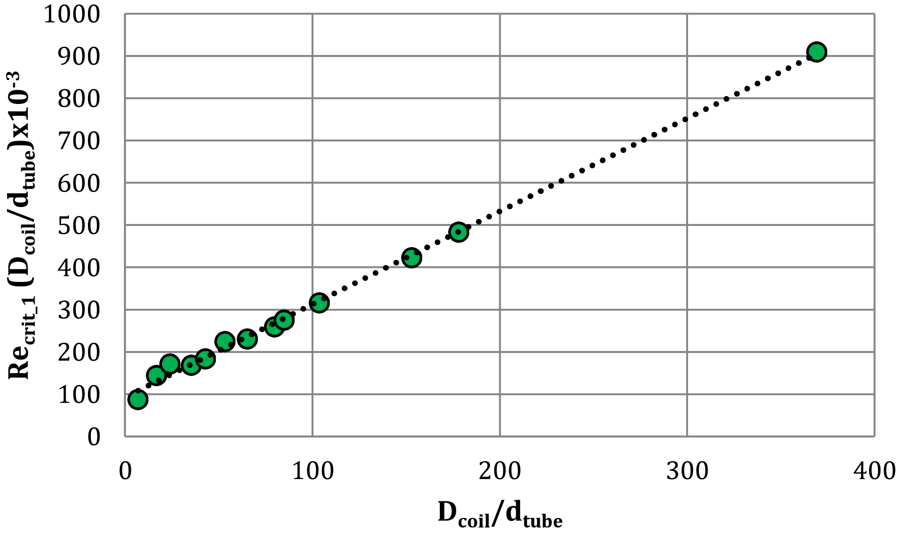

Figure 1.47 *Plot of the product* $Re_{crit\_1} * \left(\frac{D_{coil}}{d_{tube}}\right)$ *vs. curvature ratio and linear fitting*

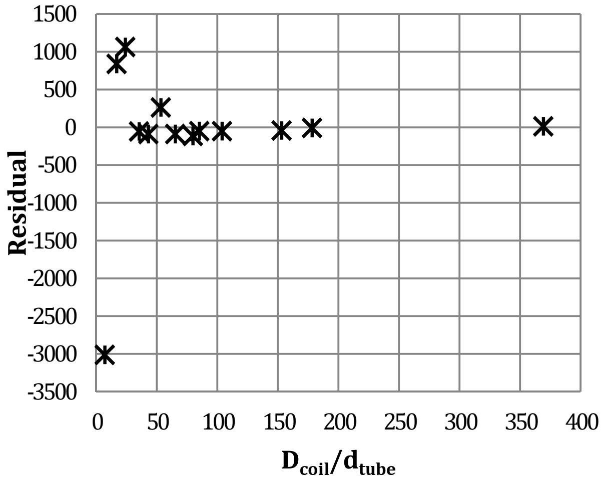

Figure 1.48 *Residual plot for the linear model in eq. (1.40)*

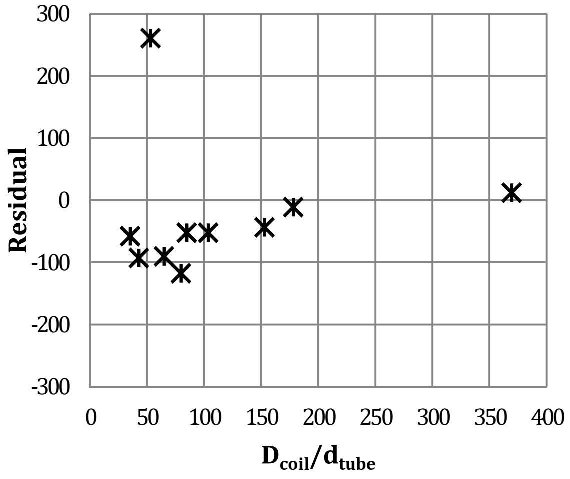

Figure 1.48bis *Residual plot for the linear model in eq. (1.40), only medium and mild curvature points*

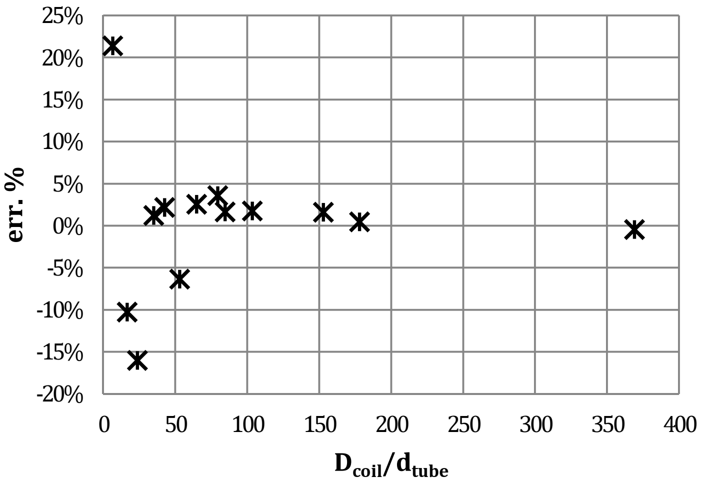

Figure 1.49 *Error plot for the linear model in eq. (1.40)*

The rearranged eq. (1.40) expresses a linear relationship between Re_{crit_1} and the inverse of the curvature ratio: actually, considering the ratio D_{coil}/d_{tube}, the dependence is a hyperbolic function. The residual and the error plots (Figure 1.48, Figure 1.48bis and Figure 1.49) show scattered points in the in the range of medium and mild curvature: here, the linear model is in general appropriate and the distance between experimental points and the predicted values is quite limited (err. < 6.5% and err. < 4% for coils other than Coil 06). On the contrary, for strongly curved coils a greater difference is observed: the relative error for Coil 01 is approximately +25%, whereas Coil 02 and Coil 03 present a negative error that is respectively about -7% and -13%; this fact signify that perhaps a different model would be more suitable when the laminar to turbulent flow transition can be considered as point-wise; Cioncolini and Santini [13] proposed for this region a decreasing exponential model, i.e. eq. (1.11). Despite this, the error is relevant only for very small value of curvature ratio, thus eq. (1.40) can be considered valid for $D_{coil}/d_{tube} > 10$.

The experimental point concerning SIET facility does not lies below the line: the destabilization of the flow due to the increasing in height is not visible and its effects on turbulence emergence are negligible. However, the experimental uncertainty on the specific point chosen to mark the beginning of the transition is about 19%: more accurate works are needed in order to carry out more confident conclusions.

It is very interesting to notice that, if the inverse of the curvature ratio in eq. (1.37) is settled to zero, i.e. $D_{coil} \gg d_{tube}$, the critical Reynolds number value tends approximately to that of a straight tube: actually, when the effect of curvature becomes irrelevant, the condition of horizontal rectilinear channel is achieved and the beginning of the laminar to turbulent flow transition agrees with the typical value of straight tubes. This fact confirms the correctness of the approach.

1.7.4 Exponent optimization

As shown in Figure 1.50, the obtained values for critical Reynolds number are correlated to the curvature ratio by an exponential decreasing function ($R^2 = 0.926$):

$$Re_{crit\_1} = 26500 \left(\frac{D_{coil}}{d_{tube}}\right)^{-0.45} \tag{1.41}$$

An attempt to balance the weight of the two quantity in the product $Re_{crit\_1} * \left(\frac{D_{coil}}{d_{tube}}\right)$ was made, by providing an exponent lower than 1 which reduces the weight of the curvature ratio and thus obtaining a decreasing function. With this procedure a roughly constant value marking the beginning of the transition is found:

$$Transition\ value = Re_{crit\_1} * \left(\frac{D_{coil}}{d_{tube}}\right)^{n} \tag{1.42}$$

Different criteria for the optimization of the exponent *n* were tested:

- the least square method used in eq. (1.41) provides $n = 0.45$;
- by minimizing the standard deviation of the product, the value $n = 0.44$ is obtained;
- the lowest difference between the minimum and the maximum value of the product is achieved for $n = 0.41$.

exponent	***Average (eq. 1.42)***	***Standard deviation***	***min – max difference***	***max error***
n = 0.41	*22500*	*14.62%*	*8320*	*±22,75%*
n = 0.44	*25500*	*14.03%*	*10980*	*±29.45%*
n = 0.45	*26500*	*14.07%*	*12054*	*±31.82%*

Table 1.9 *Results of optimization procedure for the exponent n*

In Table 1.9 these results are summarized: generalizing this procedure, the value $n = 0.41$ is chosen and the following correlation for critical Reynolds number is obtained:

$$Re_{crit\_1} = 22500 \left(\frac{D_{coil}}{d_{tube}}\right)^{-0.41} \tag{1.43}$$

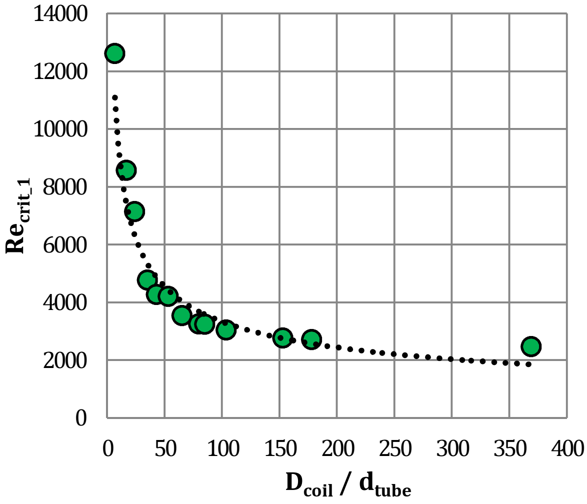

Figure 1.50 *Correlation of experimental points*

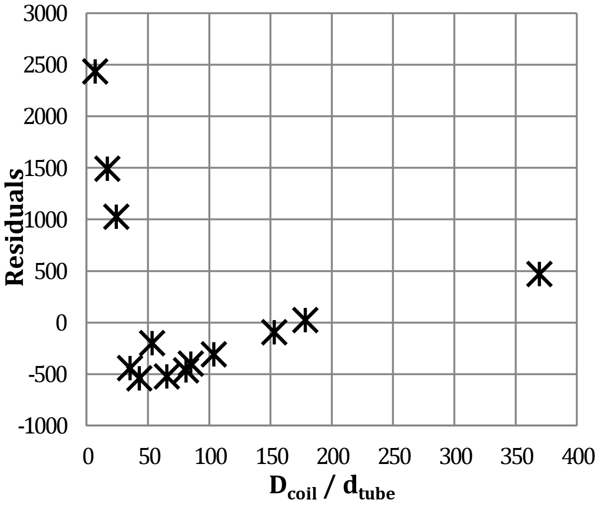

Figure 1.51 *Residual plot of model in eq. (1.43)*

In spite of this result, this model presents an evident correlation among the residual values: as noticeable in Figure 1.51, the residuals in the strong curvature region show a negative linear tendency, while a positive linear trend is visible in the region of medium and mild curvature. In light of this, two corrections can be applied to equation (1.43) and the following resulting correlations are here proposed:

$$Re_{crit\_1\_strong} = 30000\left(\frac{D_{coil}}{d_{tube}}\right)^{-0.41} - 1000 \qquad (1.44)$$

$$Re_{crit\_1\_medium\,\&\,mild} = 17000\left(\frac{D_{coil}}{d_{tube}}\right)^{-0.41} + 700 \qquad (1.45)$$

Eq. (1.44), suitable for strongly curved coil (D_{coil}/d_{tube}<30), provides very accurate predictions, whose relative error with experimental points does not exceed 2%. Nevertheless, the reliability of this equation should be verified with more experimental points, since only three data are available in the region of strong curvature. On the other hand, eq. (1.45) is appropriate for the remaining range of curvature ratio and predicts ten experimental points with a standard deviation equal to 6%, and a maximum error that does not exceeds 11%.

1.7.5 The ending of transition zone

The investigation of the final part of the depression in friction factor profile has been carried out with a different approach: since Ito’s laminar flow resistance formula cannot predict the friction factor at the end of the transition zone, it is not possible using a method based on the relative error without assuming an arbitrary upper limit for it. Therefore, the zone between the two discontinuities has been approximated with a parabolic profile and then the point of intersection with Ito's correlation for turbulent flow was chosen as indicator of the end of the transition zone, providing a correction on the equation due to the not always negligible error in fully turbulent zone. Coil 01 and Coil 02 have been excluded from the application of this procedure, as it does not make sense searching the end of a point-wise transition. Friction factor in Ito's eq. (1.25) is given as a power decreasing function of Reynolds number for a fixed value of curvature ratio; in order to facilitate the individuation of the intersection point, in a Log-Log plot a linear approximation of the resistance formula can be employed: as visible in Figure 1.52 through Figure 1.62 (the blue line indicates Ito's correlation while the black one is the approximation), this assumption does not influence significantly the results in the range of Reynolds numbers investigated. This method needed a correction due to the mean error of Ito's turbulent flow resistance formula in fully turbulent conditions, that in few cases was considerably different from zero: a first set of Reynolds number values marking the end of transition zone, i.e. Re_{crit_2}, was calculated; the mean relative error of Ito's equation for turbulent flow was used to evaluate the absolute error on Re_{crit_2}, in order to shift the linear approximation of the theoretic formula on the experimental data and therefore reducing the difference; then a new intersection point was computed. The results of this procedure are listed in Table 1.10.

Coil no.	**D_{coil}/d_{tube}**	**Ito mean err. %**	**Re_{crit_2} first attempt**	**Re_{crit_2}**
Coil 03	24.0	-0,05	12123	12085
Coil 04	35.3	-0,16	16743	16670
Coil 05	42.9	-0,01	15639	15636
Coil 06	53.3	-0,11	13527	13469
Coil 07	65.2	0,00	12685	12687
SIET Facility	79.8	3,24	10116	11910
Coil 08	84.9	0,30	11306	11430
Coil 09	103.7	0,34	8138	8212
Coil 10	153.0	-3,89	5288	4882
Coil 11	178.1	-1,99	4578	4391
Coil 12	369	-0,39	3363	3348

Table 1.10 *Re_{crit_2} evaluation*

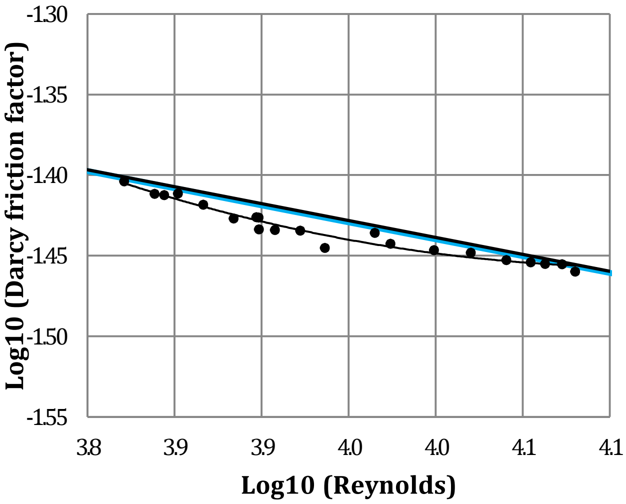

Figure 1.52 *Re_{crit_2} determination for* ***Coil 03***

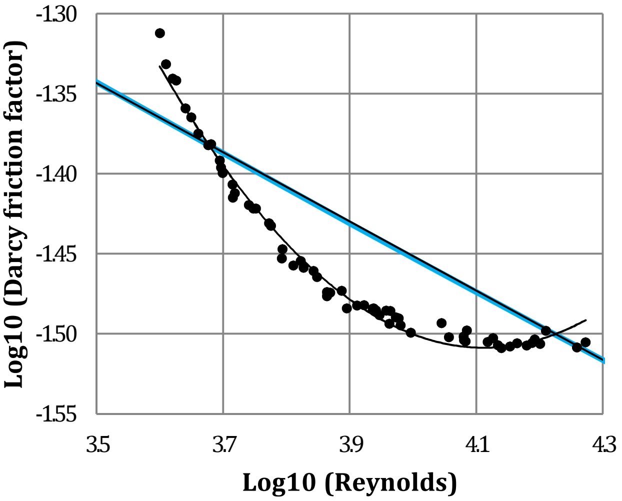

Figure 1.53 *Re_{crit_2} determination for* ***Coil 04***

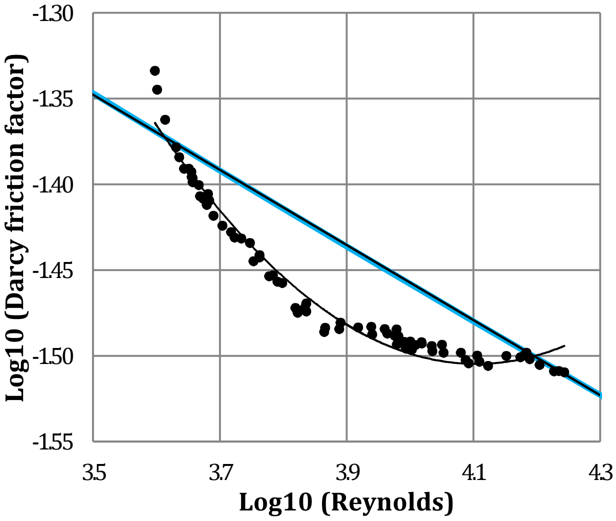

Figure 1.54 *Re_{crit_2} determination for* ***Coil 05***

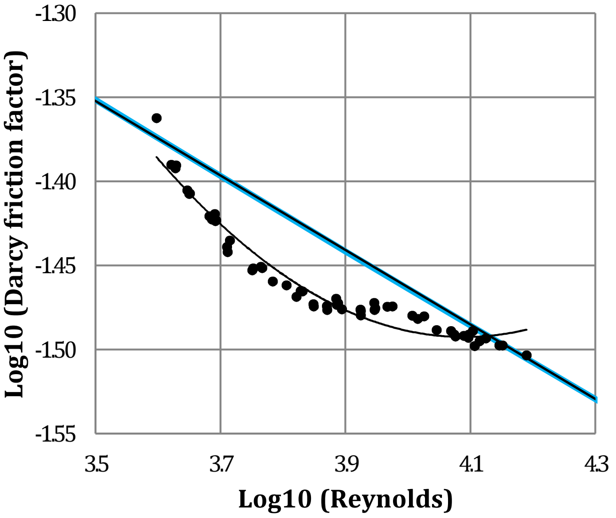

Figure 1.55 *Re_{crit_2} determination for* ***Coil 06***

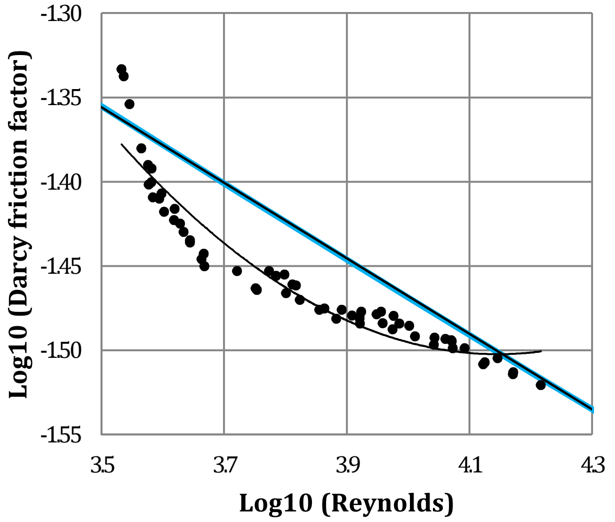

Figure 1.56 *Re$_{crit\_2}$ determination for* ***Coil 07***

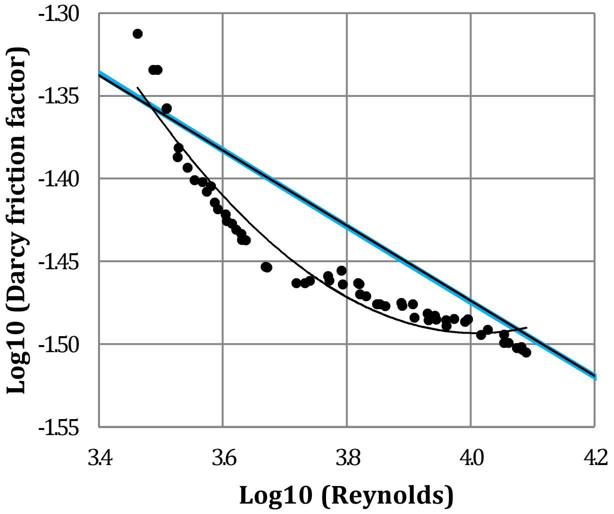

Figure 1.57 *Re$_{crit\_2}$ determination for* ***Coil 08***

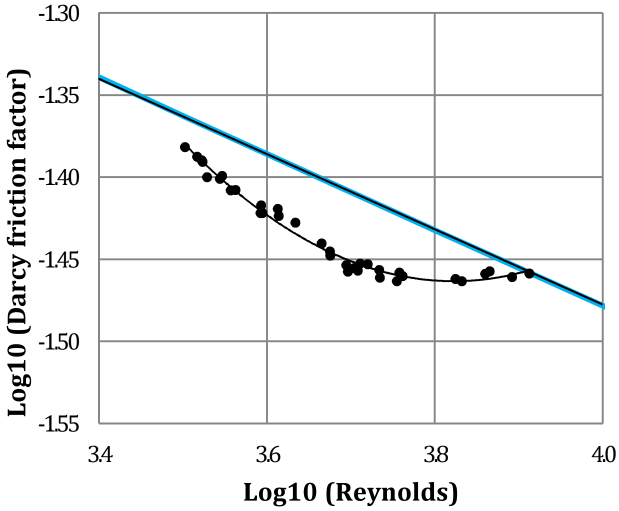

Figure 1.58*Re$_{crit\_2}$ determination for* ***Coil 09***

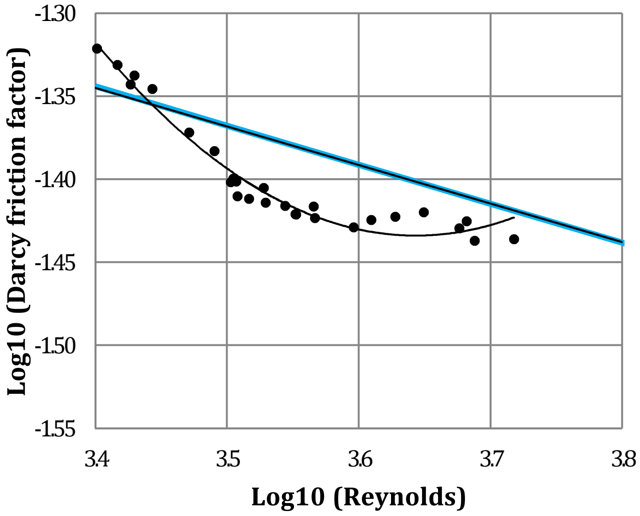

Figure 1.59 *Re$_{crit\_2}$ determination for* ***Coil 10***

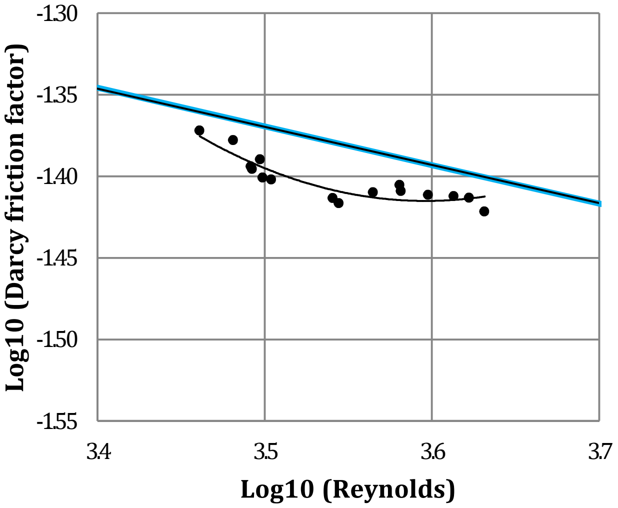

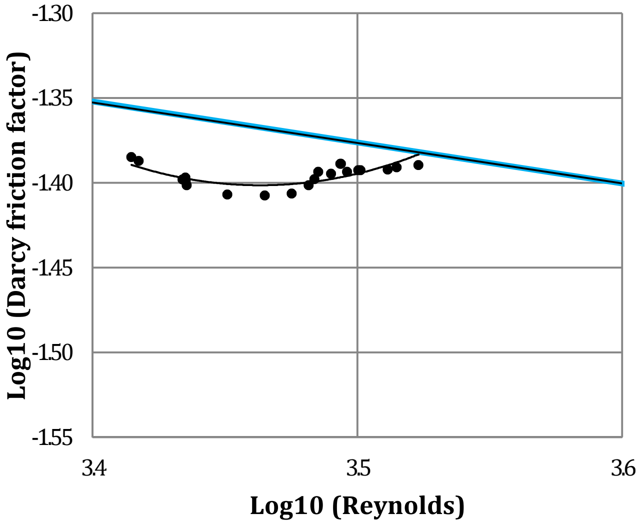

Figure 1.60 *Re*$_{crit\_2}$ *determination for* ***Coil 11***

Figure 1.61 *Re*$_{crit\_2}$ *determination for* ***Coil 12***

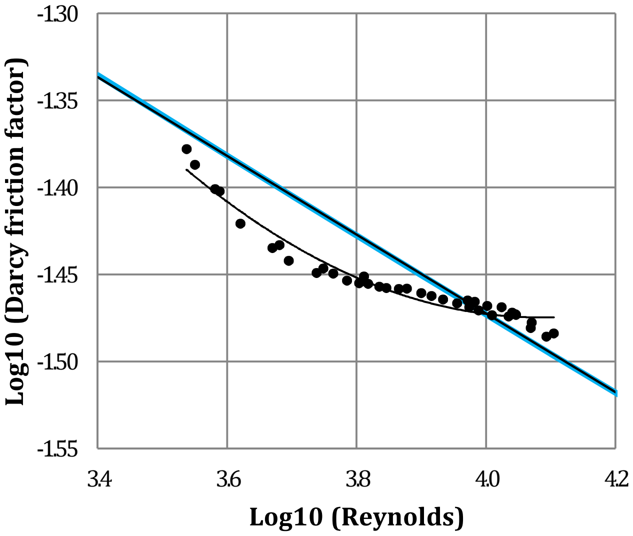

Figure 1.62 *Re*$_{crit\_2}$ *determination for* ***SIET facility***

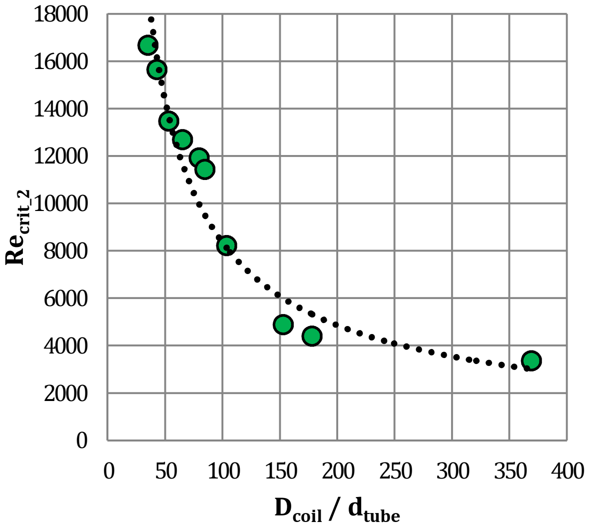

Figure 1.63 *Fitting of values in Table 1.10 for Re*$_{crit\_2}$

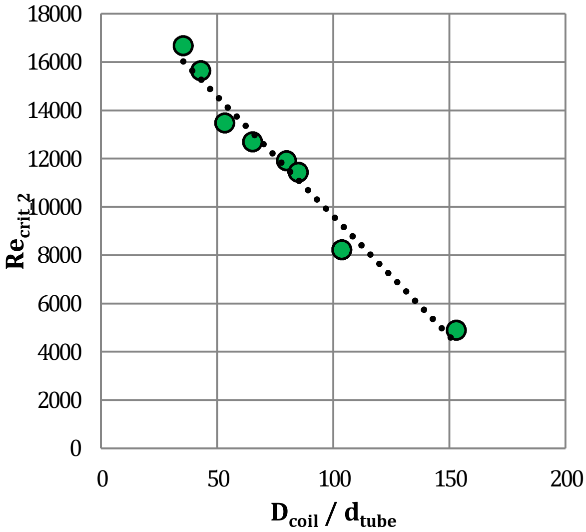

Figure 1.64 *Linear fitting for Re_{crit_2} obtained in a limited range of curvature ratio (eq. 1.47)*

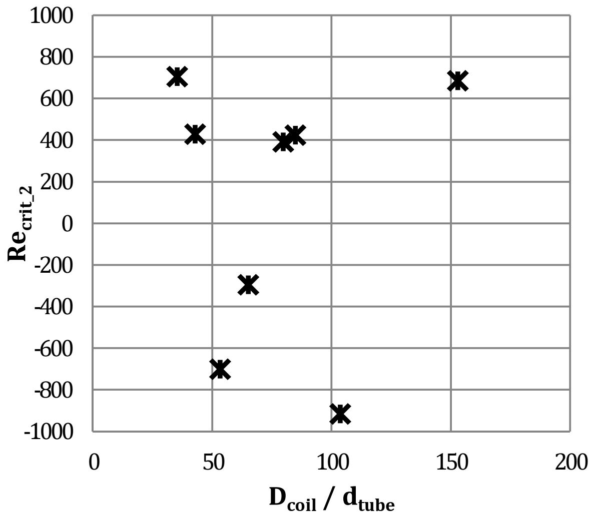

Figure 1.65 *Residual plot for eq. (1.47)*

The higher ending value of the transition is exhibited by Coil 04, while the respective value for Coil 03 is by far lower; thus, it is not possible to include Coil 03 when fitting the experimental points. In Figure 1.63 it is shown how the obtained values can be roughly correlated to the curvature ratio by the function ($R^2 = 0.9396$):

$$Re_{crit\_2} = 305000 \left(\frac{D_{coil}}{d_{tube}}\right)^{-0.78} \qquad (1.46)$$

This formula presents a quite high average relative error (10.30%), with a maximum error reaching 20%, thus it is not proposed as a correlation. A better fitting can be made (Figure 1.64) by excluding Coil 11 and Coil 12, achieving the following linear correlation ($R^2 = 0.9725$):

$$Re_{crit\_2} = -100\frac{D_{coil}}{d_{tube}} + 19500 \qquad (1.47)$$

$$with\ 35 < \frac{D_{coil}}{d_{tube}} < 160$$

The validity field must be limited up to D_{coil}/d_{tube} = 160; the residual plot show scattered points, thus the linear fitting can be considered suitable. The mean relative error is about 4.57%, with a maximum value not exceeding 8.5%.

1.8 Conclusion

The influence of the curvature ratio D_{coil}/d_{tube} on laminar to turbulent flow transition in helically coiled tubes has been investigated by means of experimental pressure drop measures obtained using liquid water as processing fluid. An approach based on the relative error between experimental data and empirical correlations have been tried: among a wide range of formulas available in literature, Ito’s laminar and turbulent flow equations showed the global best accordance with data. Since the analysis of the friction factors profiles [13] has made clear the presence of an often non point-wise transition zone, correlations for the critical Reynolds numbers representing the beginning and the end have been searched.

Two models have been used in order to match the results concerning the beginning of turbulence emergence as function of the curvature ratio: a linear fitting, which has brought to obtain eq. (1.40), and a negative power decreasing model, from which eq. (1.44) and eq. (1.45) have been derived. Eq. (1.40) is retained to be better because of the consistence for curvature ratio tending to infinite and the lower error in respect to experimental data.

The end of transition zone has been determined as the point of intersection between experimental profiles and Ito’s turbulent flow equation. A linear fitting of these points is proposed in eq. (1.47), even though the field of applicability is limited.

An attempt to observe also the influence of coil pitch has been made by analyzing experimental pressure drop data obtained on a facility, i.e. SIET Facility, which does not satisfy Manlapatz and Churchill condition for toroidal assumption. Nevertheless, no deviations due to the increasing in height have been noticed.

1.9 REFERENCES

[1] J. Eustice (1910) “Flow of water in curved pipes” *Proc. R. Soc. London Set. A* 84:107-18

[2] S.A. Berger, L. Talbot and L. S. Yao (1983) “Flow in curved pipes” *Ann. Rev. Fluid Mech. 15,* 461-512.

[3] W.R Dean, (1927) “Notes on the motion of fluid in a curved pipe” *Philos. Mag. 4, 208–233.*

[4] W.R Dean, (1928) “The streamline motion of fluid in a curved pipe” *Philos. Mag. 5, 673–695.*

[5] T.J. Huttl, R. Friedrich, (2000) “Influence of curvature and torsion on turbulent flow in helically coiled pipes” *Int. J. Heat Fluid Flow 21 345–353.*

[6] K. Yamamoto, T. Akita, H. Ikeuchi, Y. Kita, (1995) “Experimental study of the flow in a helical circular tube” *Fluid Dyn. Res. 16 237–249.*

[7] R.L. Manlapaz, S.E.W. Churchill, (1980) “Fully developed laminar flow in a helical coiled tube of finite pitch” *Chem. Eng. Commun. 7 57–78.*

[8] F.P. Incropera, D.P. DeWitt "Fundamentals of Heat and Mass Transfer" (IV ed.), *Wiley, New York 1996.*
[9] C. M. White, (1929) "Streamline Flow through Curved Pipes" *Proc. R. Soc. Lond.* A 1929 123, 645-663
[10] S. Ali, (1999) "Pressure drop correlations for flow through regular helical coil tubes" *Fluid Dynamics Research 28 (2001) 295–310*
[11] H. Ito (1959) "Friction factors for turbulent flow in curved pipes" *J. Basic Eng., 81, 123-134.*
[12] S. Srinivasan, Holland, (1970) "Friction factors for coils" *Trans. Inst. Chem. Eng. , 1970. 48: p. T156–T161.*
[13] A. Cioncolini, L. Santini (2005) "An experimental investigation regarding the laminar to turbulent flow transition in helically coiled pipes" *Experimental Thermal and Fluid Science 30 (2006)* 367-380*.*
[14] Ito H. (1969) "Laminar flow in curved pipes" Z. *Agnew. Math. Mech.*, 11, 653-663.
[15] D. Papini, M. Colombo, A. Cammi, M. E. Ricotti et al. (2011) "Experimental characterization of two-phase flow instability thresholds in helically coiled parallel channels" *Proceedings of ICAPP 2011 Nice, France, May 2-5, 2011 Paper 11183*
[16] C. Lombardi, M. E. Ricotti et al. (2002) "Steam generator of the international reactor innovative and secure" *Proceedings of ICONE-10 10th International Conference on Nuclear Engineering April 14–18, 2002, Arlington, VA*
[17] M. Adler, (1934) "Stromung in Gekrummten Rohren" *Z. Angew. Math. Mech. 14, 257–275.*
[18] L. Prandtl, (1949). "Fuhrer dmchdie Stromungslehre" *3rd Edition p. 159, Braunsschweigh*; English Transl., Essentials of Fluid Dynamics, *Blackie and Son, London, 1954, p. 168.*
[19] D. Hasson, (1955). "Streamline flow resistance in coils" *Res. Corresp 1, S1.*
[20] E.F. Schmidt, 1967. "Warmeubergang and Druckverlust in Rohrschlangen" *Chem. Eng. Technol. 13, 781–789.*
[21] P. Mishra, S.N. Gupta, (1979) "Momentum transfer in curved pipes" 1 *Ind. Eng. Chem. Process Des. Dev. 18, 130–142.*
[22] C.M. White, (1932) "Fluid friction and its relation to heat transfer" *Trans. Inst. Chem. Eng. (London) 10, 66–86*
[23] V. Kubair, C.B.S. Varrier, (1961/1962) "Pressure drop for liquid flow in helical coils" *Trans. Indian Inst. Chem. Eng. 14, 93–97.*
[24] P.S. Srinivasan, S.S. Nandapurkar, F.A. Holland, (1968) "Pressure drop and heat transfer in coils" *The Chem. Eng. (London), 218, CE113–119.*
[25] L. Guo, Z. Feng, X. Chen (2000) "An experimental investigation of the frictional pressure drop of steam-water two-phases flow in helical coils" *International journal of heat and mass transfer 44 (2001) 2601-2610*
[26] A.E. Ruffell, (1974), "The application of heat transfer and pressure drop data to the design of helical coil once-through boilers" *Symp. Multi-Phase Flow Systems, University of Strathclyde, Inst. Chem. Eng. Symp. Ser. 38 (1974) Paper 15.*
[27] D.R. Webster, J.A.C. Humphrey, (1993) "Experimental observation of flow instability in a helical coil" *A.S.M.E. J. Fluids Eng. 115 (1993) 436–443.*
[28] J.H. Lienhard IV and J.H. Lienhard V (2006) "A heat transfer textbook" *Massachusset Institute of Technology, Phlogiston Press Cambridge Massachusset U.S.A.*
[29] T.J. Huttl, R. Friedrich (1999) "Influence of curvature and torsion on turbulent flow in helically coiled pipes" *International Journal of Heat and Fluid Flow 21 (2000) 345-353*

2 Experimental analysis of pressure drop of steam-water flow under adiabatic and diabatic conditions

2.1 Two-phases flow investigation

The large use of helically coiled tubes in steam generators justifies the necessity to study accurately the steam-water two-phase flow: a great knowledge of behavior of pressure drop, flow instabilities and mechanisms of heat transfer should be achieved, especially for those applications, e.g. nuclear industry, which requires high safety standards. In this chapter an experimental investigation regarding pressure drop using a two-phase steam-water mixture is carried out: several measures were made, both in adiabatic and diabatic conditions. The available data set is composed of:

(a) 155 pressure drop measures performed on SIET Facility coil under adiabatic conditions. Water was heated in a steam generator and then sent into the test section at the desired quality; even thought the tube had been accurately insulated, small power input was given to the fluid in order to balance thermal losses.

(b) 188 pressure drop measures performed on SIET Facility coil at various levels of power input. The fluid entered the tube in sub-cooled condition and then was electrically heated inside the test section; SIET facility tube is divided into two independent section, from 0 to 24 meters and from 24 meters to the end of the tube (see sub-paragraph 1.2.1), thus two different power input are possible: some measures were performed with no heat flux in the second part of the tube, while for the other runs a different power input was imposed in order to obtain superheated vapor at tube outlet. The nine pressure taps situated along the test section allow enlarging the diabatic data set: since quality varies because of the presence of heat flux, pressure drop in a wider range of thermodynamic conditions can be measured; in this way, about 1500 different experimental measures are available. The measures obtained without heat flux in the second part of the tube have been added to the adiabatic data set.

In Table 2.1 a list of operative conditions is presented. A total of nine and twelve different pressure – mass flux combinations, respectively for adiabatic and diabatic cases, were tested, but, with the purpose to investigate the effect caused by power input, similar conditions are requested; therefore, the only six corresponding cases are used in present work. Only one type of geometry was tested, i.e. SIET Facility tube whose parameters are reported in subparagraph 1.2.

	No. points		**$G = 200\ kg/m^2s$**	**$G = 400\ kg/m^2s$**	**$G = 600\ kg/m^2s$**	
ADIABATIC	155	**$p = 3000\ kPa$**	17	26	17	
		$p = 4000\ kPa$	17	20	13	
		$p = 6000\ kPa$	16	15	14	
			$G = 200\ kg/m^2s$	**$G = 400\ kg/m^2s$**	**$G = 600\ kg/m^2s$**	**$G = 800\ kg/m^2s$**
DIABATIC	188	**$p = 2000\ kPa$**	26	12	18	11
		$p = 4000\ kPa$	12	14	14	22
		$p = 6000\ kPa$	14	13	18	14

Table 2.1 *Subdivision of experimental points referred to nominal conditions*

After a preliminary examination of the profile of the frictional component of pressure drop in boiling conditions, an attempt to quantify and graphically visualize the difference between the cases without and with power input was made. Two complementary approaches were tried, and the quite good accordance between the results demonstrates the correctness of the procedures; an uncertainty analysis on experimental data was also carried out and proved the reliability of the measures. The obtained results showed that the effects of thermal input on a steam-water flow in a helically coiled tube are strongly dependent on thermodynamic mass quality and mass flux; on the contrary, pressure seems not to affect so much the difference between diabatic and adiabatic case; the influence of geometric parameters, i.e. tube inner diameter, coil diameter and coil pitch, was not investigated. The complexity of this situation does not allow obtaining any valid relation and suggests the use of more refined instruments, that is to say Computational Fluid Dynamics study.

2.2 Frictional pressure drop in two-phases flow

In literature the influence of pressure and mass flux on two-phase flow frictional pressure drop is well known: a high operative pressure is believed to limit the friction inside the flow and against the wall: this happens because the difference between the specific volumes of liquid and vapor, and then between the velocities, reduces with increasing pressure; thus pressure drop decreases with increasing operative pressure. On the contrary, an increasing mass flux tends to amplify flow frictional effects and therefore pressure drop. The law that links frictional pressure drop and operative pressure can be assumed as linear, whereas an exponent 1.5 should be applied to express the dependence on the mass flux [1]. This behavior, visible in Figure 2.1 and Figure 2.2, is general for either straight or coiled tubes. In formulas:

$$\Delta p_{frict} \sim \tilde{f}(p, G^{1.5}) \qquad (2.1)$$

By plotting the frictional component of SIET helical tube experimental pressure drop measures concerning the adiabatic case as function of mass quality, it is immediately noticeable that the profiles are not monotonic curves, but they present a maximum: frictional pressure drop increases with quality up to the value $x = 0.75 \div 0.85$ and then decreases till the end of the boiling process. The analysis of the profiles in Figure 2.3 through Figure 2.8 (adiabatic case) evidences that this behavior strongly depends on the mass flux, while pressure variations have little effect on the shape of the profile. Because of scale effects due to the representation of three profiles on each graphic, this phenomenon will be more appreciable in Figure 2.10 through Figure 2.15. It is visible that the position of the maximum and the slope beyond it are considerably different at the three different mass flux level (Figure 2.3 through Figure 2.5): the increasing of mass flux tends to shift the maximum at a lower quality value and to amplify this condition. On the contrary, the curves are very similar at the three different pressure level (Figure 2.6 through Figure 2.8): excluding the different pressure drop values, the three profiles present the same behavior. Unfortunately, the case $p = 3000\ kPa, G = 600\ kg/m^2s$ lacks the points at quality higher than 0.70, the maximum cannot be seen.

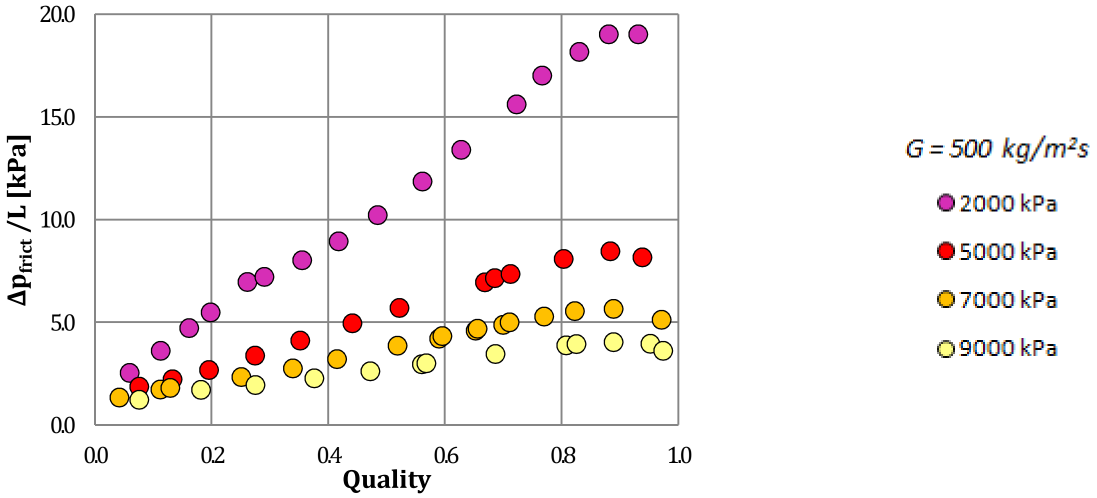

Figure 2.1 *Experimental data of Δp_{frict} per unit of length vs. quality in a straight pipe (tube inner diameter 0.0152 m, no power input) at four different pressure levels for a given mass flux value [2]*

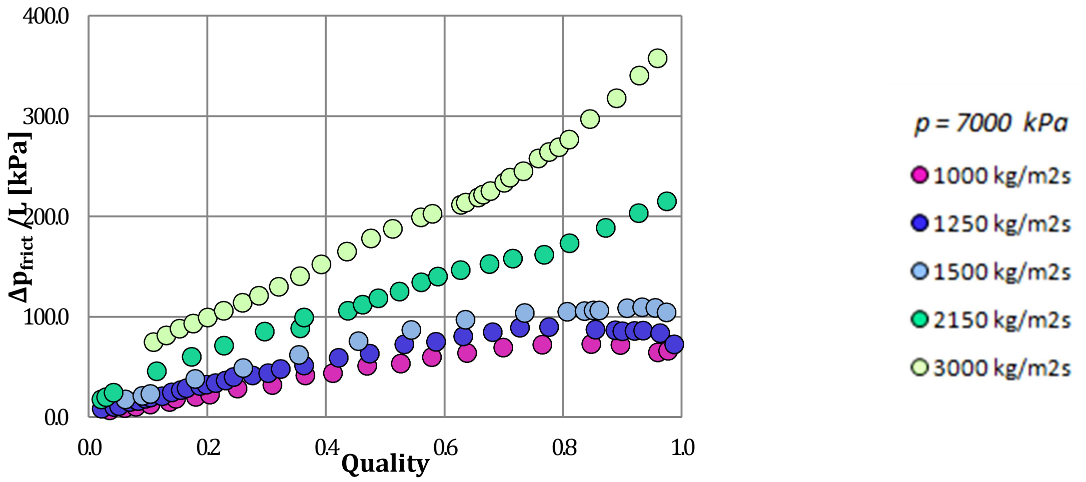

Figure 2.2 *Experimental data of Δp_{frict} per unit of length vs. quality in a straight pipe (tube inner diameter 0.00508 m, no power input) at five different mass flux levels for a given pressure value [2]*

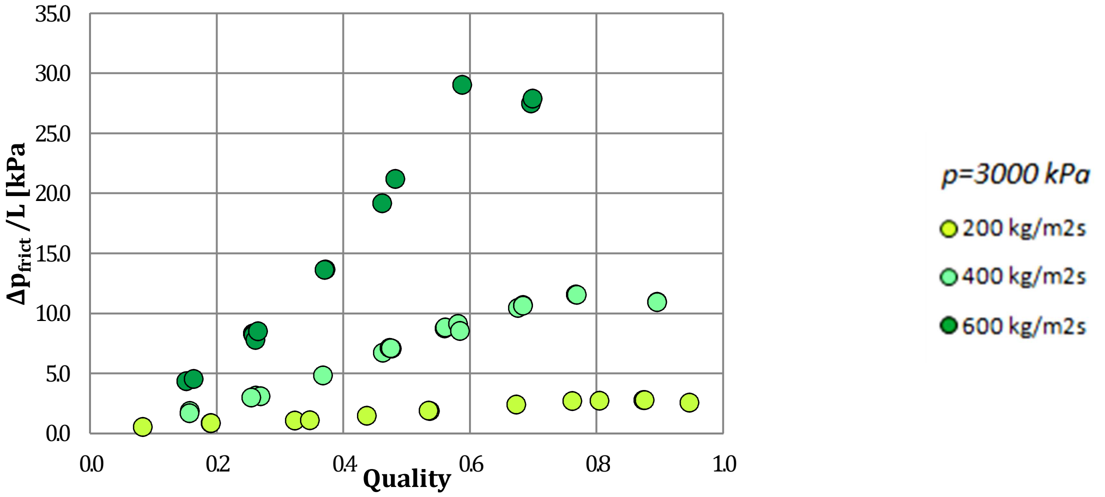

Figure 2.3 *Experimental data of Δp_{frict} per unit of length vs. quality in SIET Facility helically coiled pipe (no power input) at three different mass flux levels for a given pressure value*

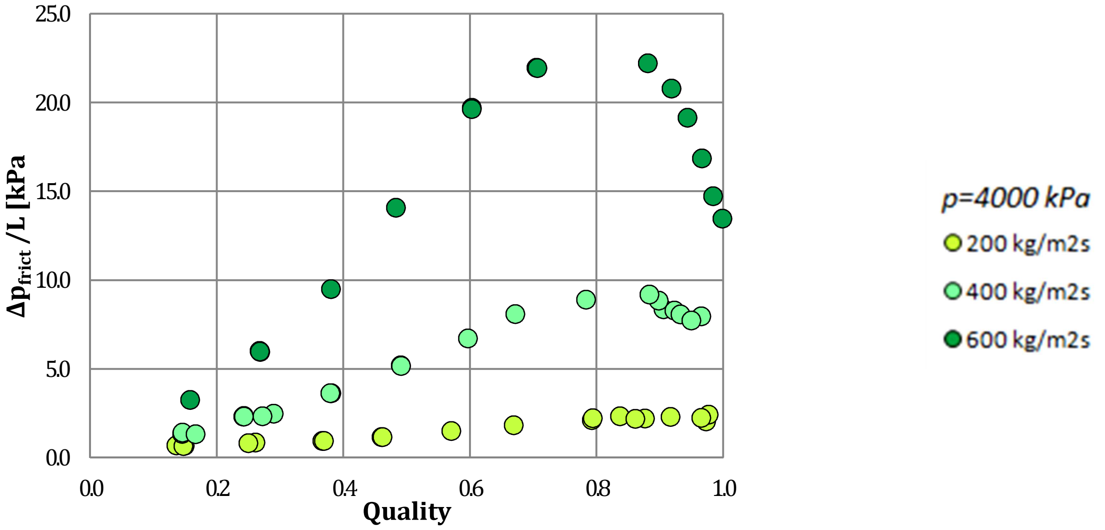

Figure 2.4 *Experimental data of Δp_{frict} per unit of length vs. quality in SIET Facility helically coiled pipe (no power input) at three different mass flux levels for a given pressure value*

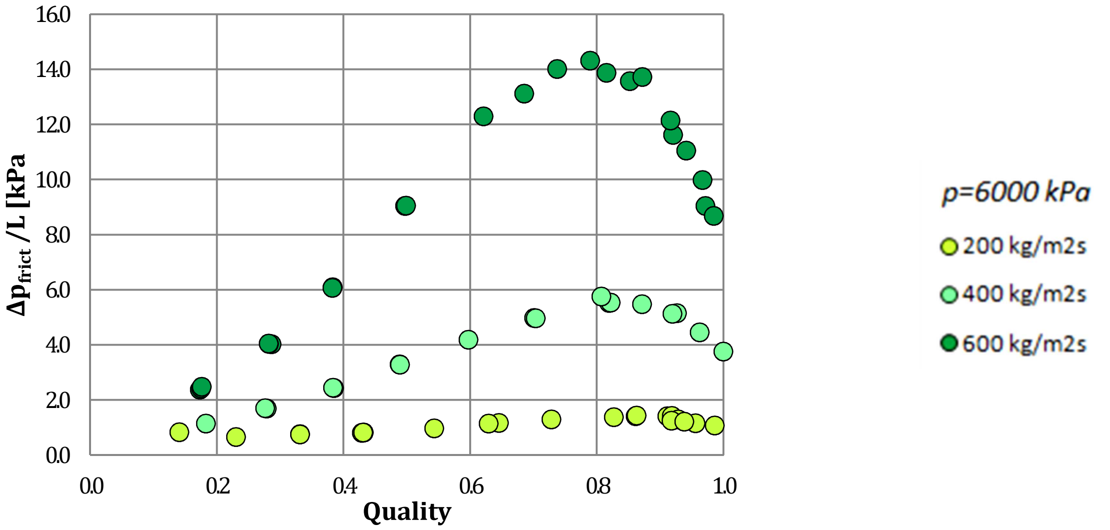

Figure 2.5 *Experimental data of Δp_{frict} per unit of length vs. quality in SIET Facility helically coiled pipe (no power input) at three different mass flux levels for a given pressure value*

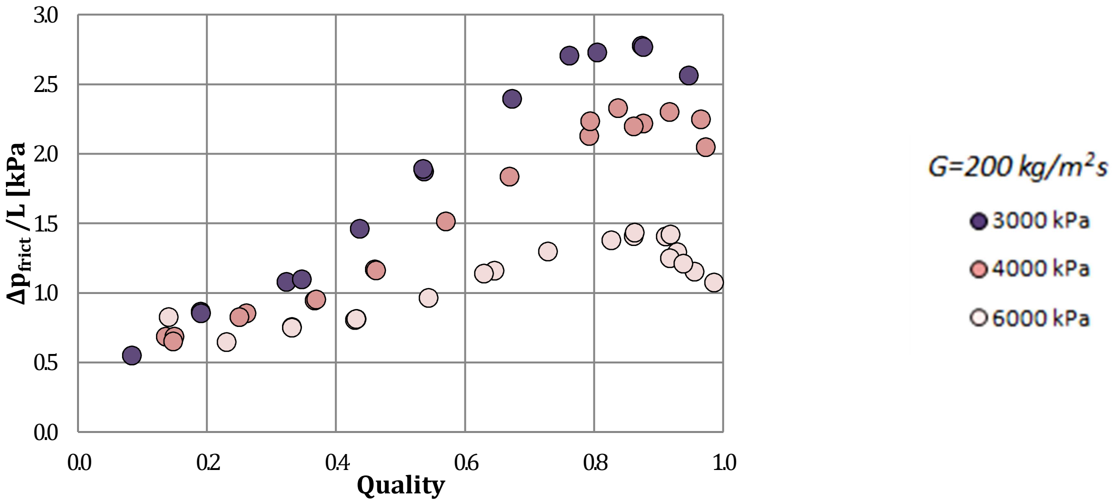

Figure 2.6 *Experimental data of Δp_{frict} per unit of length vs. quality in SIET Facility helically coiled pipe (no power input) at three different pressure levels for a given mass flux value*

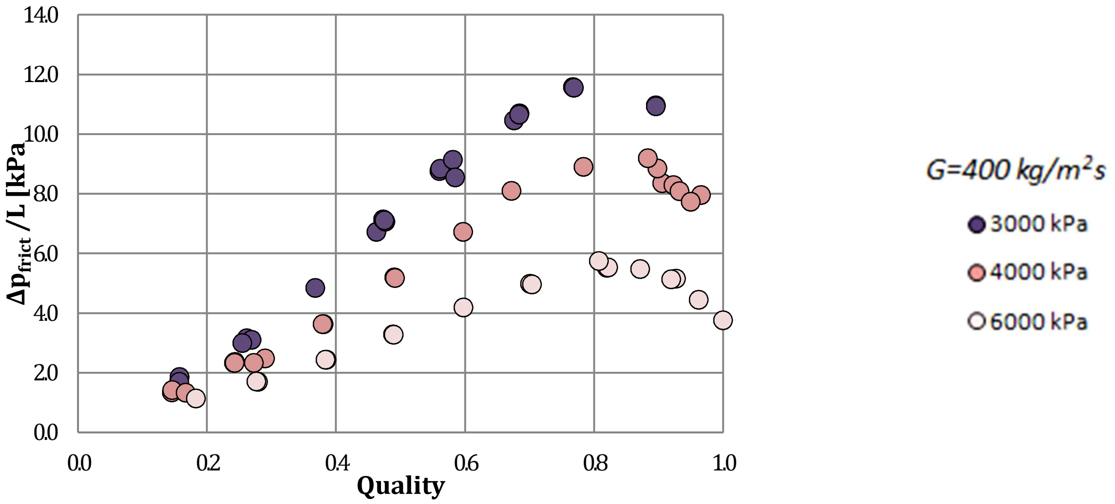

Figure 2.7 *Experimental data of Δp_{frict} per unit of length vs. quality in SIET Facility helically coiled pipe (no power input) at three different pressure levels for a given mass flux value*

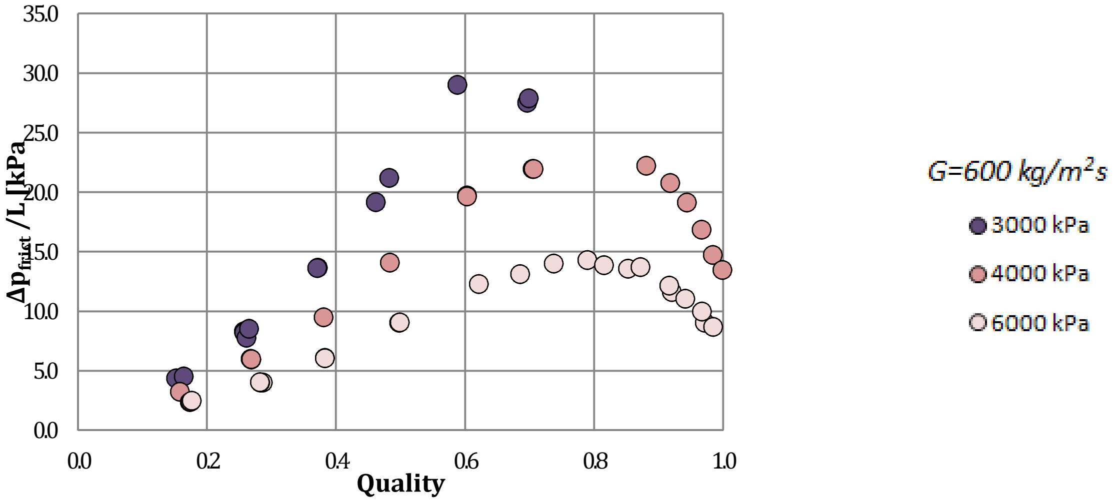

Figure 2.8 *Experimental data of Δp_{frict} per unit of length vs. quality in SIET Facility helically coiled pipe (no power input) at three different pressure levels for a given mass flux value*

The presence of a maximum in frictional pressure drop profile is also noticeable in some cases of rectilinear ducts: a slight decrease of Δp_{frict} in the range of quality very close to the unit can be observed; this situation was already observed in straight tubes by other authors [3] [4]. Nevertheless, the position and the size of the maximum in Figure 2.1 and Figure 2.2 are significantly different from the cases of helical pipes, and the change in slope of the curve can often be neglected; the maximum is by far more visible in coiled tubes. The physical explanation of this phenomenon is quite complicated and cannot be understood only by mean of the observation of experimental data: a hypothesis concerning the effects of centrifugal force on the wall shear stress in annular flow regime will be discussed in Chapter 3 with a CDF study.

2.3 Models for two-phases pressure drop correlation

A large number of two-phase flow pressure drop correlations can be found in literature; these correlations can be classified into the following four general categories.

(1) Empirical correlations based on the homogeneous model. In the homogeneous flow model, the two-phase frictional pressure gradient is calculated in terms of a friction factor, as in single-phase flow. Fluid thermo-physical properties (viscosity and density) are calculated with specific models; in this work the following equation will be used:

$$\frac{1}{\rho_{homogeneus}} = \frac{(1-x)}{\rho_{ls}} + \frac{x}{\rho_{vs}} \qquad (2.2)$$

$$\frac{1}{\mu_{homogeneus}} = \frac{(1-x)}{\mu_{ls}} + \frac{x}{\mu_{vs}} \qquad (2.3)$$

eq. (2.3) is due to McAdams (1942); several other models for the viscosity can be found in literature. The friction factor is calculated using the correlations for single-phase flow. It will be shown that this model is not suitable for helically coiled tubes because of the presence of the above mentioned maximum, which cannot be recognized with a single phase correlation: in fact, as already evidenced in paragraph 1.4, friction factor for single phase flow is a monotone decreasing function of Reynolds number.

(2) Empirical correlations based on the two-phase friction multiplier concept. The two-phase pressure drop is calculated from the single-phase pressure drop by multiplying with a two-phase friction factor multiplier. The following definitions of two-phase friction multipliers are often used:

$$\Phi_{lo}^2 = \frac{(dp/dz)_{two-phases}}{(dp/dz)_{lo}} \quad \text{(a)} \qquad \Phi_{go}^2 = \frac{(dp/dz)_{two-phases}}{(dp/dz)_{go}} \quad \text{(b)}$$

$$\Phi_{l}^2 = \frac{(dp/dz)_{two-phases}}{(dp/dz)_{l}} \quad \text{(c)} \qquad \Phi_{g}^2 = \frac{(dp/dz)_{two-phases}}{(dp/dz)_{g}} \quad \text{(d)} \qquad (2.4)$$

The denominators refer to the single-phase pressure gradient for flow in the same duct with mass flow rates corresponding to the mixture flow rate in case of Φ_{lo}^2 and Φ_{go}^2 and individual phases in case of Φ_{l}^2 and Φ_{g}^2; numerous correlations for the multipliers are available in literature. This kind of approach is capable to predict the maximum of the curve and therefore allows studying also the case of coiled tubes; in paragraph 2.2 a comparison between few correlations and experimental data demonstrates this fact. Actually most of the correlations for two-phase flow in helically coiled tubes make use of this concept.

It is worth mentioning the method of Lockhart-Martinelli [5] for pressure drop evaluation: although it is not a correlation specific for coiled tubes, it is able to predict the maximum in the profile of frictional pressure drop. It is based on equation (2.4c), where the term Φ_l^2 is calculated by means of the following formulas:

$$\Phi_l^2 = 1 + \frac{C}{X} + \frac{1}{X^2} \tag{2.5}$$

$$X^2 = \left(\frac{\mu_f}{\mu_g}\right)^{0.25} \left(\frac{1-x}{x}\right)^{1.75} \left(\frac{\rho_g}{\rho_f}\right) \tag{2.6}$$

The constant C depends on the type of phase flow: 20 for turbulent liquid and turbulent vapor, 12 for laminar liquid and turbulent vapor, 10 for laminar liquid and turbulent vapor, 5 for laminar liquid and laminar vapor. By using Ito's turbulent flow (1.25) equation for single-phase friction factor in coiled tubes, the profile in Figure 2.9 is obtained:

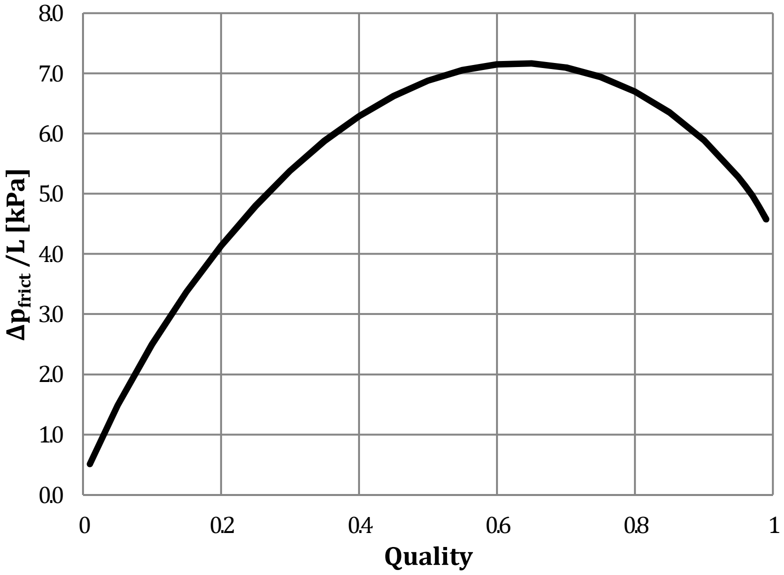

Figure 2.9 *Frictional pressure drop profile obtained with the method of Lockhart-Martinelli*
(p=3800 kPa, G=389 kg/m^{2}s, SIET Facility geometry)

Nevertheless, Lockhart and Martinelli's approach is interesting only from the theoretical point of view: in fact, it has been experimentally proved that frictional pressure drop in two-phase flow is proportional to the mass flux like $G^{1.4}$, whereas the normalization to the single-phase model used by these authors implies a dependence like $G^{1.8}$ [7].

(3) Direct empirical models. The two-phase friction pressure drop is directly expressed as a function of

mass flux, mixture density, length, equivalent diameter, etc. without reference to single-phase pressure drop. An example in this category is the correlation "CeSNEF" proposed by Lombardi et. al. [7]

(4) Flow pattern specific models. In general, two methods are being used to generate flow pattern specific correlations: in the first, empirical correlations are obtained by correlating the data for each flow pattern; in the second method mechanistic models which take into account the distribution of phases in each flow pattern have been developed.

In addition, various correlations for interfacial friction in addition to wall friction have been developed for two-fluid models used in many of the advanced system codes.

2.4 Pressure drop correlation for two-phase flow in helical tubes

In literature a large amount of correlations for pressure drop is available; in general, this kind of correlations makes use of the two-phase friction multiplier concept. In 2001 Guo et al. [8] proposed a comparison among five formulas, showing that the predictions are quite different: this analysis evidences the difficulty of predicting two-phase pressure drop in helically coiled tubes. The author refers to Guo et al.'s work for an exhaustive review of available correlations.

An empirical correlation was made by Santini et al. [8], specific for SIET Facility geometry, by means of a fitting on the diabatic experimental data used also in present work. They obtained the following formula:

$$\left(\frac{dp_{frict}}{dz}\right) = K(x)\frac{G^{1.91}v_m}{d^{1.2}} \qquad (2.7)$$

$$K(x) = -0.0373x^3 + 0.0378x^3 - 0.00479x + 0.0108$$

with v_m representing the mean specific volume of the mixture. They showed also that in this case of helically coiled tube the frictional pressure drop are proportional to $G^{1.91}$.

2.5 Heat flux input

The presence of a positive or negative heat flux at the tube wall surely modifies the value of total pressure drop in a generic tube: the heating or cooling process generates a variation in the specific volume of the mixture, thus the accelerative component of pressure drop, which linearly depends on the difference of specific volumes at the inlet and outlet of the tube, shows a great variation compared with to the adiabatic case. As far as the frictional component is concerned, one can think that if the tube wall temperature is greater (or lower) than the fluid one, a new motion normal to the tube surface is introduced: the axial velocity gradient and the wall shear stress are modified, and bubbles created at the wall may destabilize the liquid film; moreover, the mean viscosity of the fluid is influenced by the presence of a heat flux. Thus in principle one can expect that also the frictional component of pressure drop varies with the presence of a heat flux. Since the variation of quality has a strong influence on pressure drop, the comparison between two-phase pressure drop in two different situations should be made considering the same quality of the mixture. A direct comparison between the diabatic case and that without power input at the same quality is not possible, since the presence of heat flux renders not constant the quality in the diabatic case; in order to obtain an evaluation of the differences, two approaches will be proposed in the next paragraphs.

Up to the author knowledge, the only experimental investigations regarding the effect of heat flux on two phase pressure drop was carried out by Santini et al. [8]: this study excludes any heat flux effect on frictional pressure drops in the range of heat fluxes lower than 200 kW/m^2 and specific enthalpy input lower than 2000 – 2500 kJ/kg. Instead, several works are available in literature concerning the straight tube: the obtained results are not always in accordance. Tarasova et al. [10] observed that two phase friction pressure drop is higher in a heated channel compared to that in an unheated channel for same flow condition. Studies conducted by Leung and Groeneveld [11] indicate that the surface condition is significantly influenced by heat flux: effective surface roughness increases due to the formation of bubbles at heated surface leading to larger pressure drop; they concluded that for the same flow conditions, the two phase multiplier is larger for low heat flux than high heat flux. Koehler and Kastner [12] showed that, when tube wall is still wetted, the two-phase multiplier is unchanged passing from the diabatic to the adiabatic case, while in the dry-out region it tends to decrease. This result has been confirmed also by other works [14].

2.6 Purpose of present work

In this chapter an accurate analysis of the available data is presented, trying to understand the effects of power input on the frictional component of pressure drop in a helically coiled pipe. It will be shown that the difference between the diabatic and the adiabatic case cannot be easily interpreted, since it is highly variable with quality and strongly influenced by the mass flux: a general behavior is identified, but no conclusion can be carried out, even thought the experimental uncertainty is quite low.

Since the experimental facility is the same used for the single-phase study, the description of the test section is reported in paragraph 1.2.

2.7 A visual representation of frictional pressure drop profiles

2.7.1 Data analysis

The experimental pressure drop data obtained during the adiabatic and diabatic runs have been reduced in order to obtain the frictional component of pressure drop, by following the energy balance method explained in the introduction of this work. In formulas:

$$\Delta p_{frict} = \Delta p_{measured} - \Delta p_{acc} - \Delta p_{grav} \tag{2.8}$$

$$\Delta p_{acc} = G^2(v_{out} - v_{in})\Delta z$$

$$\Delta p_{grav} = \rho_m g \cos\left(\frac{\pi}{2} - \gamma\right)\Delta H$$

The accelerative term is negligible for the adiabatic data, since in the absence of heat flux the variation of specific volume is due to pressure gradient only, thus in general very low. The gravitational term is the main component of pressure drop in liquid single-phase flow and in two-phase flow at low quality; for SIET Facility the value of the angle γ is 14.48°.

The thermodynamic conditions of the inlet flow are the result of the operations at the pre-heater, which serves as steam generator, and the passage into the connection line to the test section. For the adiabatic experiences, thermal power has been given to the fluid at ambient temperature entering the steam generator, in order to obtain the desired thermodynamic conditions of the steam-water mixture; the inlet mass quality was then calculated with a balance, considering the input power at the pre-heater and the thermal losses. The inlet conditions of the diabatic runs have been set by heating the liquid water in the pre-heater until the desired temperature and pressure; sub-cooled liquid was then sent to the test section, the negative thermodynamic quality was about -0.15.

The presence of nine pressure taps along the test section plays a fundamental role in the composition of the data set: since the diabatic experiences contemplated sub-cooled liquid at the tube inlet and saturated or superheated vapor at the tube outlet, the continuous monitoring of the tube allows to obtain a great amount of measures at different qualities; the position of the taps is reported in Table 1.2 Excluding the first section of the tube, in which the flowing fluid is still liquid for almost half of the length, seven pressure drop measures can be achieved from each run; this fact allows calculating the mean density between a lower interval of conditions, thus obtaining a better evaluation of the gravitational component of pressure drop. The imposed heat flux is included in the range $50\ kW/m^2 < q'' < 200\ kW/m^2$. Since three level of mass flow rate were tested, a more convenient quantity has been defined in order to express the heating grade, which represents the enthalpy given to each kg of fluid flowing in the test section:

$$h_{input} = \frac{(\dot{Q}_{in} - \dot{Q}_{loss})}{\Gamma} \left[\frac{kJ}{kg}\right] \tag{2.9}$$

where Γ is the mass flow rate. The thermodynamic equilibrium quality of the mixture flowing along the heated tube is calculated imposing an enthalpy balance at each pressure tap:

$$x = \frac{h(tap_j) - h_f}{h_g - h_f} \tag{2.10}$$

where $h(tap_j)$ represents the specific enthalpy of the fluid as function of the curvilinear coordinate; under the hypothesis of uniform heat flux on the tube wall, this value is given by the relation:

$$h(tap_j) = h_{inlet} + \frac{h_{input}}{\tilde{L}} \sum_{i=1}^{j} \Delta p^{i}_{section\_lenght} \tag{2.11}$$

where $\tilde{L}$ is the total uniformly heated length. Since the power input is kept constant only in the first 24 m of the test section, whereas in the second part of the tube adiabatic conditions or a different input is introduced, eq. (2.10) is appropriate only of the first six pressure tap; convenient corrections were applied for pressure taps 7, 8 and 9. Since the heat flux is constant only in the first 24 meters of the test section, only the pressure drop measures between Tap 2 and Tap 6 have been considered diabatic.

2.7.2 Comparing diabatic and adiabatic data

The graphic representation of the adiabatic pressure drop measures as function of the mass quality does not present difficulties, since for each run the mass of vapor can be assumed as constant for all the tube length; this operation is visible in Figure 2.3 through Figure 2.8. Some difficulties arise when power is given to the test section, because there is a production of vapor inside the tube: in order to plot the two cases on the same graphic, the local quality is determined with the arithmetic average between the values at two consecutive pressure taps. This procedure allows observing the differences between the adiabatic and the diabatic conditions; the results are visible in Figure 2.9 through Figure 2.14. The region between Tap 6 and Tap 7 is heated by the same power input for nearly 2/3 of the length, while the rest of the section is left adiabatic or subjected to a lower heat flux; since the exclusion of these point would cause a great lack of data in the last part of the boiling process, rendering the comparison less significant, these points have been plotted as well.

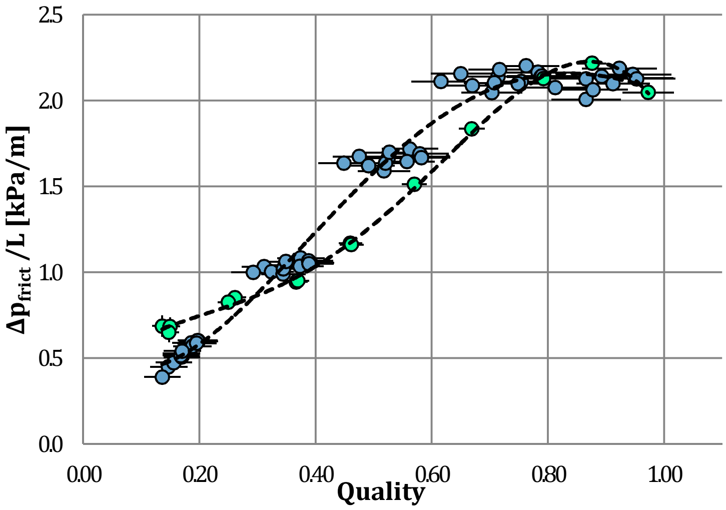

p=4000 kPa G=200 kg/m^{2}s

Figure 2.10 *Experimental pressure drop measures under adiabatic conditions (●) and with power input (●)*

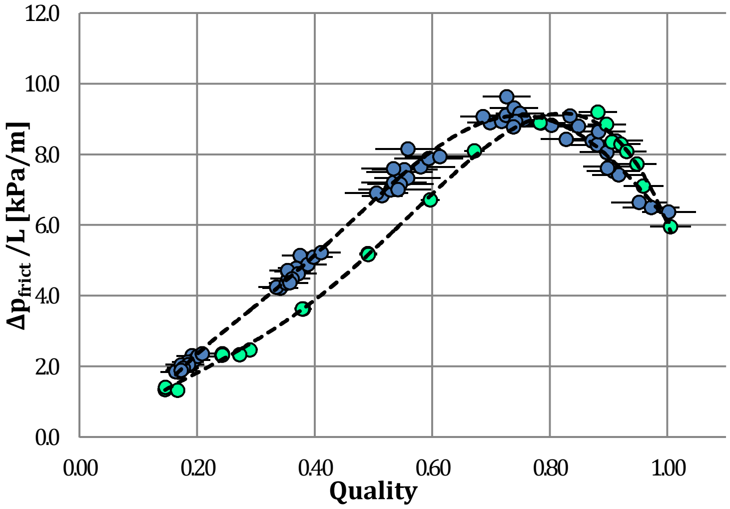

p=4000 kPa G=400 kg/m^{2}s

Figure 2.11 *Experimental pressure drop measures under adiabatic conditions (●) and with power input (●)*

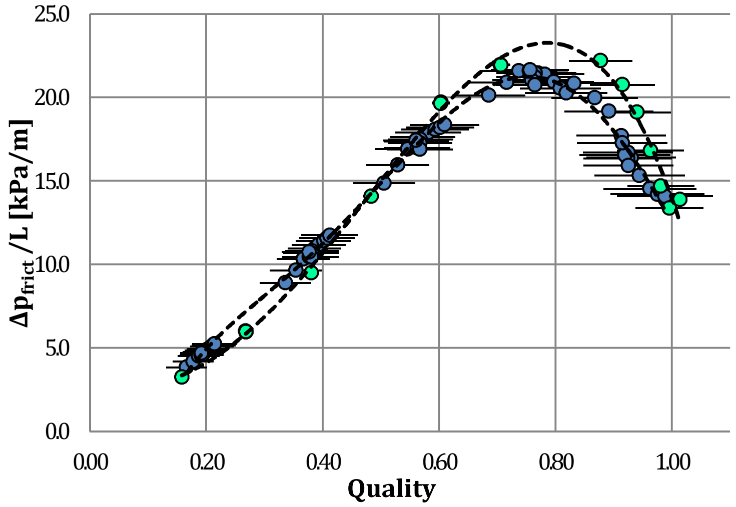

p=4000 kPa G=600 kg/m^{2}s

Figure 2.12 *Experimental pressure drop measures under adiabatic conditions (●) and with power input (●)*

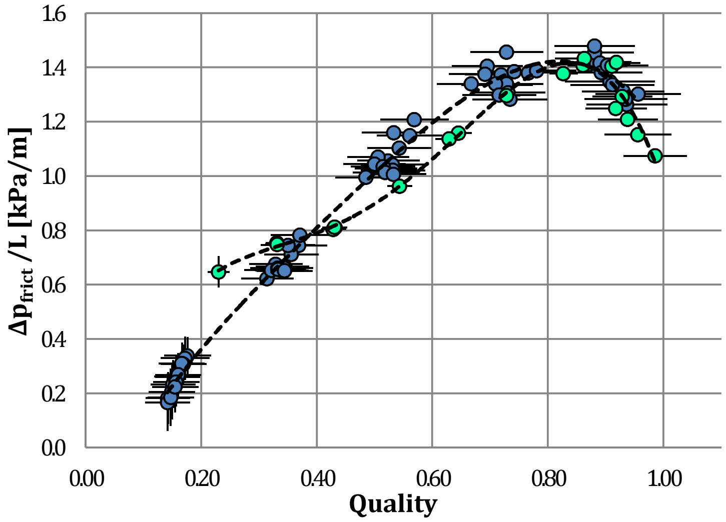

p=6000 kPa G=200 kg/m^{2}s

Figure 2.13 *Experimental pressure drop measures under adiabatic conditions (●) and with power input (●)*

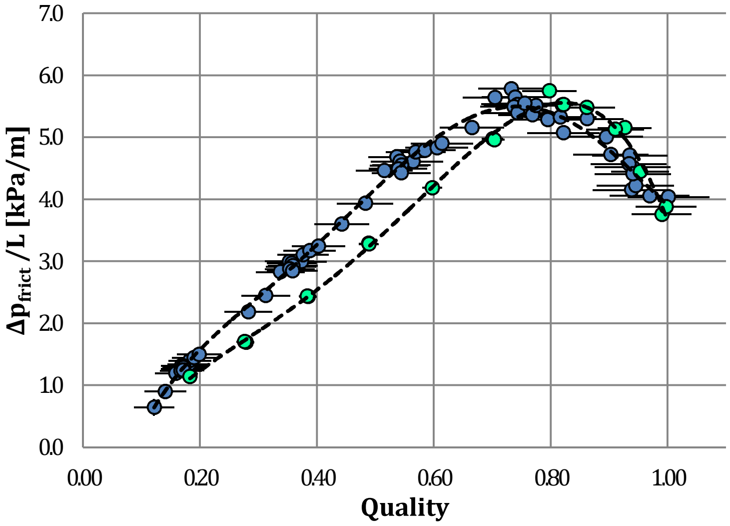

p=6000 kPa G=400 kg/m^{2}s

Figure 2.14 *Experimental pressure drop measures under adiabatic conditions (●) and with power input (●)*

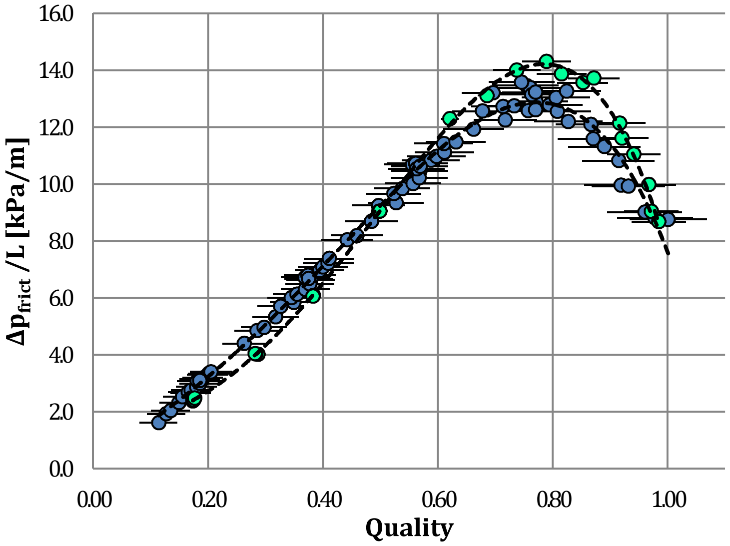

p=6000 kPa G=600 kg/m^{2}s

Figure 2.15 *Experimental pressure drop measures under adiabatic conditions (●) and with power input (●)*

2.7.3 Discussion of results

Uncertainty on experimental data has been evaluated with standard techniques (See Appendix 1). As reported in the description of SIET Facility, pressure drop measures show a quite low error (0.4%). In the range of quality $x>0.2$ the frictional component represents the predominant fraction of pressure gradient (more than 80%), thus, even thought the uncertainty on the gravitational and the accelerative terms is high (5% - 10%), the error cannot be much great; in this range it never exceeds the value 5% and it is lower than 1% if $x>0.5$. Instead, in some measures with low mass flux and quality $x<0.2$, where the gravitational component of pressure drop is important, a higher uncertainty have been estimated: the case $p=6000\ kPa\ G=200\ kg/m^2s$ presents few experimental points with an uncertainty ≈40% while for all the others operative conditions the error does not exceeds the value 10%. On the other hand, the mass quality evaluation is affected by a high error because of the uncertainty on power input (2.5%) and on thermal losses at the pre-heater and along the tube (15%). The result is an uncertainty on mass quality varying in the range [0.01 – 0.08]; the greater values were observed in the diabatic case, since thermal losses are greater when power input in given to the test section.

The above graphics show a strongly variable difference between two situations under examination: in general, frictional pressure drops measured with power input seems to be greater than the adiabatic case in the central phase of the boiling process and lower in the ending part of the spectrum of mass quality; moreover, mass flux seems to affect the size of this difference, while pressure does not. Noticed this unusual and unexpected behavior, no definitive conclusion can be carried out; further analysis are needed in order to understand this phenomenon.

2.8 Evaluation of the differences

2.8.1 The integration method

With the purpose to quantify the differences observed in paragraph 2.2, a mathematical artifice is applied to the data. It is assumed that variations of mass quality along the length of the tube can be caused only by power input, i.e. equal mass quality at tube inlet and outlet in the adiabatic runs. For given operative conditions, i.e. pressure and mass flux, the only free parameter in the adiabatic data is the inlet mass quality, whereas the diabatic measure of pressure drop in a two-phase flow depends also on the amplitude of the interval $\Delta x = x_{out} - x_{in}$ in addition to the single values x_{in} and x_{out}; for a fixed homogeneous heat flux, Δx is proportional to the length of the tube. Since x_{in} has approximately the same value for all the diabatic runs, in this analysis it can be considered a constant parameter, while, for a fixed homogeneous heat flux, x_{out} is determined once established a value of the length on the tube. Thus, ΔL, Δx and x_{out} are substantially the same variable. In this situation, the adiabatic measures can be interpreted as the derivative, in respect to x_{out}, of a function Δp_{frict_d} expressing the dependence between pressure drop and quality outlet for a fixed inlet. In formulas:

$$\text{fixed} \quad p_0\,, G_0, q'', \qquad \Delta p_{frict\_d} = \tilde{f}(x_{in},\ x_{out},\ \Delta L,\ \Delta x)$$

$$\text{fixed} \quad p_0\,, G_0, q'', x_{in} \qquad \Delta p_{frict\_d} = \tilde{f}(\Delta x)$$

$$\Delta p_{frict\_a}(x) = \frac{\partial \Delta p_{frict\_d}(\Delta x)}{\partial \Delta x} \tag{2.11}$$

where in the subscripts the letter "d" means "diabatic" and the letter "a" means "adiabatic". The function $\Delta p_{frict\_a}(x)$ can be easily achieved with a polynomial fitting of the experimental data, after having subtracted the gravitational and the accelerative components of pressure drop. In order to determine $\Delta p_{frict\_d}(\Delta x)$, for each value of power input an expression of the total relative pressure inside the tube as a function of the curvilinear coordinate, and subsequently of the mass quality, has been obtained by subtracting the pressure drop measures of the nine taps to the inlet pressure, and then fitting those values; thanks to this function, it has been possible to calculate, for each value of power input tested, the pressure drop for two generic values of mass quality. Hence, one obtains:

$$\Delta p_{tot\_d}(\Delta x) = p(z_1) - p(z_2) = p(x_1) - p(x_2) \tag{2.12}$$

where z_1 and z_2 express the curvilinear coordinates at which the mass quality reaches the values x_1 and x_2. Again, Δp_{frict_d} is obtained from the total pressure drop by subtracting the gravitational and the accelerative terms.

Eq. (2.11) suggests the idea of integrating the function $\Delta p_{frict\_a}(x)$, thus rendering comparable diabatic and adiabatic data. Thanks to this method, it is possible to choose an arbitrary interval of integration and then to evaluate the difference in many phases of the boiling process. This concept is summarized by the following equation:

$$\Delta p_{int}(x_2 - x_1) = \frac{1}{x_2 - x_1}\int_{x_1}^{x_2} \Delta p_{frict\_a}(x)dx \tag{2.13}$$

A physical interpretation of Δp_{int} can be given: this term is representative of frictional pressure drop under an ideal condition in which the fluid changes its quality while flowing in the tube with no power input at the wall. Since for each Δx a corresponding length $\Delta L = (z_2 - z_1)$ of the tube is defined, depending only on the level of power input, the integrated value must be divided for the total length of SIET Facility test section, i.e. 32 meters, and then multiplied for ΔL. Theoretically, if this quantity is greater / lower than the corresponding diabatic measure, it means that in the considered range of quality power input reduces / increases frictional pressure drop; in practice, the fitting procedures may have added some uncertainty, which sums to the experimental error discussed in paragraph 2.2; thus, only high value of the difference can be considered significant.

$$\frac{\Delta p_{int}(x_2-x_1)*\Delta L}{L_{SIET}} \quad \overset{vs.}{\Leftrightarrow} \quad \Delta p_{frict_d}(\Delta x) \tag{2.14}$$

Finally, the variation among the different power inputs was not taken into account and only the difference between adiabatic and adiabatic conditions is considered; this assumption may be a cause of uncertainty.

2.8.2 Results

Three situations are here proposed:

(a) global boiling process, considering the entire range of quality [$x_1 = 0.0$; $x_2 = 1.0$];
(b) central phase of boiling process, that is to say [$x_1 = 0.15$; $x_2 = 0.8$], in which annular flow regime is assumed;
(c) ending of boiling process, i.e. [$x_1 = 0.8$; $x_2 = 1.0$], where the tube surface is dry and dispersed regime is established.

No data are available in the beginning phases of boiling process, thus the range [$x_1 = 0.0$; $x_2 = 0.15$] was not individually investigated.

Since the purpose of this work is to evidence the effects of power input in respect to the adiabatic situation, the relative difference between the two quantities in eq. (2.14) was calculated as follow:

$$Difference = \frac{\Delta p_{frict_d}(\Delta x) - \dfrac{\Delta p_{int}(x_2 - x_1) * \Delta L}{L_{SIET}}}{\dfrac{\Delta p_{int}(x_2 - x_1) * \Delta L}{L_{SIET}}} \tag{2.15}$$

For each run in diabatic conditions a corresponding adiabatic term was obtained. The fitting procedure of pressure data concerning the diabatic case imposed the exclusion of those runs in which the outlet mass quality is lower than the chosen value x_2; in other words, if the condition of saturated vapor is not physically reached in the tube, the obtained value of comparison cannot be reliable in the analysis when $x_2 = 1.0$ is set and must be neglected. The integration of the function $\Delta p_{frict\_a}(x)$ does not present difficulties, as it is a polynomial; therefore the standard analytical procedure was employed.

The results are summarized in Table 2.2 and plotted in Figure 2.15 through Figure 2.17

	Pressure [kPa]	G [kg/m^{2}s]	Average difference %	Std. Dev
(a) $x_1 = 0.00$ $x_2 = 1.00$	4000	200	16.237	3.468
	4000	400	12.807	11.416
	4000	600	3.429	2.313
	6000	200	22.591	6.514
	6000	400	22.424	11.699
	6000	600	3.100	2.528
(b) $x_1 = 0.15$ $x_2 = 0.80$	4000	200	18.791	4.593
	4000	400	17.039	8.587
	4000	600	2.983	2.109
	6000	200	6.726	6.994
	6000	400	23.882	10.555
	6000	600	1.486	2.270
(c) $x_1 = 0.80$ $x_2 = 1.00$	4000	200	-0.601	10.028
	4000	400	-8.677	14.656
	4000	600	-4.445	5.754
	6000	200	17.706	10.069
	6000	400	-2.277	11.849
	6000	600	-2.037	5.138

Table 2.2 *Results of the integration method*

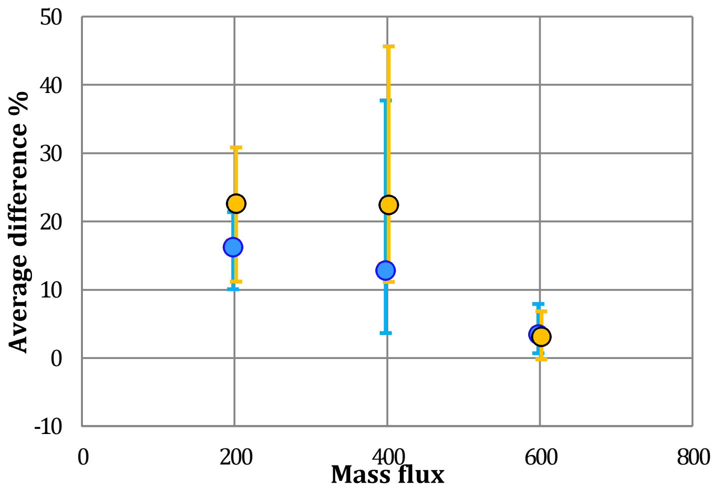

Case (a) [$x_1 = 0.0$; $x_2 = 1.0$]

Figure 2.16 *Difference between the adiabatic and the diabatic conditions for the three tested values of mass flux, at two pressure levels: 4000 kPa (•) and 6000 kPa (•)*

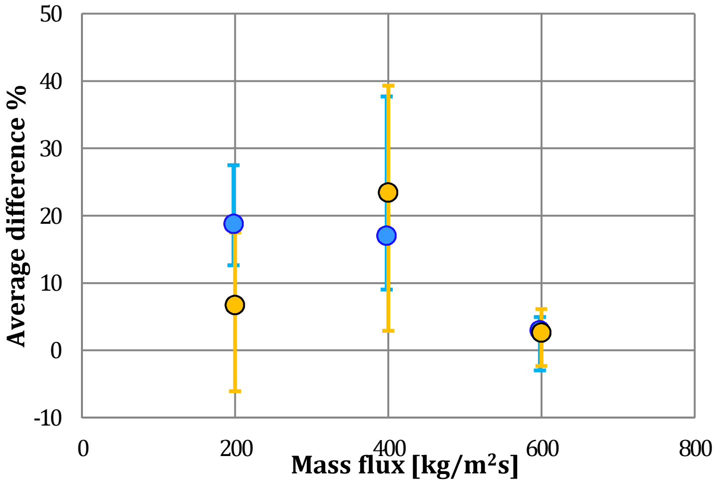

Case (b) $[x_1 = 0.15 ; x_2 = 0.8]$

Figure 2.17*Difference between the adiabatic and the diabatic conditions for the three tested values of mass flux, at two pressure levels: 4000 kPa (•) and 6000 kPa (•)*

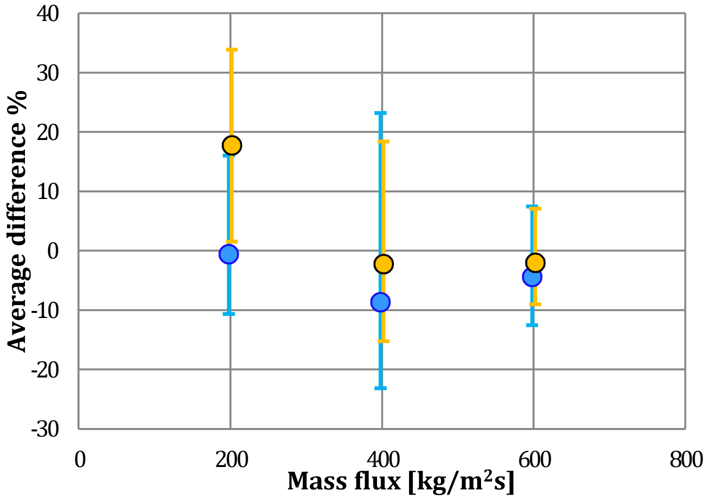

Case (c) $[x_1 = 0.8 ; x_2 = 1.0]$

Figure 2.18 *Difference between the adiabatic and the diabatic conditions for the three tested values of mass flux, at two pressure levels: 4000 kPa (•) and 6000 kPa (•)*

2.8.3 Discussion of results

The intrinsic problem of a method based on integration is the fact that the average value obtained causes a loss of information about possible changes in sign of the difference into the interval of integration: in order to understand this behavior, the match with the graphic profiles is therefore essential. In general, the average values reported in Table 2.2 tend to confirm the visual evaluation made in paragraph 2.2: the sign of the difference always corresponds to what assessable in Figure 2.9 through Figure 2.14 and also the numerical values seem to be roughly consistent. Nevertheless, the great uncertainty affecting some cases, due to the experimental error on quality evaluation and the neglected variation of power input, forbids a quantitative estimate in many situations. The results of this procedure presents again the unusual behavior of the profiles already evidenced: power input seems to influence the frictional component of pressure drop, by increasing it in the central phases of the boiling process and slightly reducing it in the dry-out region; no conclusion can be carried out regarding the beginning of the boiling process because of the lack of experimental data. Furthermore, this method confirms the already observed strong influence of mass flux on this phenomenon and the weak effects of the operative pressure on this phenomenon.

In Case (a) a correlation between the average difference and the mass flux is visible: the increasing mass flux renders less important the effects of power input; however the absence of experimental measures in the range $[x_1 = 0.0 \; ; \; x_2 = 0.15]$ puts some doubts on the validity of this result. Case (b), which does not account for the zone lacking of data, seems to confirm this interpretation, even though the point G=200 kg/m^{2}s – p=6000 kPa is not in agreement with the others; in addition, the high uncertainty of the points at G=200 kg/m^{2}s and G=400 kg/m^{2}s is another element against the significance of this relationship. Considering these facts, the obtained result can be retained only an indication of the effects of mass flux on the phenomenon under investigation; in order to ascertain it, a more accurate analysis is required.

Case (c) shows greater uncertainty compared to the others: the reason is the fact that the adiabatic measures in the range of quality close to 1.0 were obtained during the diabatic runs by removing the power input in the second part of the test section; this means that the inlet qualities of these points are affected by a greater uncertainty, as explained in sub-paragraph 2.2.3. With the exception of the point G=200 kg/m^{2}s – p=6000 kPa, whose behavior is strongly irregular because of a high uncertainty, the obtained values demonstrates that the impact of power input on frictional pressure drop in the drying region is quite different in respect to what happens in the central phases of the boiling process. However, this results, shown also by some research available in literature concerning the straight tube [12 – 14] and mentioned in sub-paragraph 2.1.4, seems to confirm qualitatively the fact that, even for the helically coiled tube, the presence of power input tends to reduce frictional pressure drop in the final phase of boiling process.

2.9 Conclusions

The analysis of pressure drop of steam-water two-phase flow has been conducted, focusing the attention on the effects of power input on frictional pressure drop. Two complementary methods have been used, in order to represent and quantify the differences between the adiabatic and the diabatic case.

The theoretical approaches have reported in general quite compatible results, demonstrating the correctness of the procedure. Even thought the differences between the two cases are small, the high uncertainty on quantitative results and the irregular behavior of the profiles do not allow determining a governing law for this phenomenon. This fact is principally due to the experimental uncertainty on the determination of the quality. Thus, no quantitative conclusion can be carried out from this work. Nevertheless, the shape of the profile in the drying zone, which indicates that power input reduces frictional pressure drop, is coherent with some research concerning the straight tube.

The influence of pressure and mass flux over pressure drop and, in particular, over the dependence of frictional pressure drop on power input has been also examined: it has been found that a variation of mass flux tends to modify the shape of the profiles, while a variation of operative pressure does not.

2.10 REFERENCES

[1] C. Lombardi (2004) "Impianti Nucleari" - *CUSL*

[2] E. Brega, B. Brigioli, C.G. Carsana, C. Lombardi, L. Maran – "MIDA: data bank of pressure drops and densities of two-phase mixtures flowing in rectilinear ducts" *CeSNEF, Politecnico di Milano, ENEL / CRNT Milano*

[3] K. Stephan (1992) "Heat transfer in condensation and boiling" *Springer-Verlag, 1992*.

[4] G.P. Gaspari, C. Lombardi, G. Peterlongo (1964) "Pressare drops in steam-water mixtures" *CISE Report R 83, January 1964.*

[5] R.W. Lockhart, R.C. Martinelli (1949) "Proposed correlation of data for isothermal two-phase two component flow in pipes" *Chem. Eng. Prog. 45 : n o . 39. 1 949.*

[6] N.E. Todreas, M.S. Kazimi (1989) "NUCLEAR SYSTEMS I Thermal Hydraulic Fundamentals" *Copyright © 1990 by Hemisphere Publishing Corporation*

[7] C. Lombardi, C.G. Carsana (1992) "A dimensionless pressure drop correlation for two-phase mixtures flowing up-flow in vertical ducts covering wide parameter ranges" *Heat and Technol. 10, 125–141.*

[8] L.J. Guo, Z. Feng, X. Chen, "An experimental investigation of the frictional pressure drop of steam-water two-phase flow in helical coils" *Int. Journal of Heat and Mass Transfer 44 (2001) 2601-2610.*

[9] L. Santini, M. Ricotti, A. Achilli (2008) "Adiabatic two-phase pressure drops in a helically coiled heat exchanger" *LEAP Laboratorio Energia e Ambiente Piacenza*
[10] N.V. Tarasova et al (1966), "Pressure Drop of boiling subcooled water and steam-water mixture flow in heated channels" *Proc.3rd. Int.Heat Transfer Conf., pp. 178-183, American Society of Mechanical Engineers, New York (1966).*
[11] L.K.H. Leung, D.C. Groeneveld, (1991) "Frictional pressure gradient in the pre- andpost-CHF heat-transfer regions" *Multiphase flows' 91, Tsukuba, 1991, Tsukba, Japan.*
[12] W. Koehler, W. Kastner, (1988) "Two-phase pressure drop in boiler tubes, in Two-phase flow heat exchangers (Thermal-Hydraulic fundamentals and design)" *Edited by S.Kakas, A.E.Bergles, E.O.Fernandes, Kluwer Academic Publisher 1988.*
[13] IAEA-TECDOC-1203 (2001) "Thermo-hydraulic relationships for advanced water cooled reactors" *Nuclear Power Technology Development Section International Atomic Energy Agency, Vienna, Austria*
[14] E. Faimali, C. Lombardi, A. Cammi, (2012) "Survey of two phase pressure drops correlations: verifications, comparisons, improvements"*, Dipartimento di Ingegneria Nucleare, Politecnico di Milano, Milan, Italy.*
[15] C. Lombardi, Private communications

3 CFD investigation regarding pressure drop of a steam water two-phase flow in a helically coiled pipe

3.1 The challenge of two-phase flow CFD

Two-phase flow regime is frequently encountered in various industrial applications: the most important ones are surely the long distance transfer pipelines (e.g. steam and water, natural gas and oil flows) in power generation, petrochemical and process plants. The requirements for economic design, optimization of operating conditions and assessment of safety factors create the need for quantitative information about such flows; therefore, reliable estimates of hydrodynamic properties associated with this type of flow are considered essential for the safe design and efficient operation of two-phase problems. Nevertheless, the complexity of the phenomena, both from physical and numerical point of view, poses a great obstacle to its comprehension, rendering the modeling of a rigorous two-phase flow and the prediction of the hydrodynamics and heat transfer behaviors a real challenge for scientists and engineers all over the world. An example of this fact has been shown in Chapter 2, where the sophisticated mechanisms of heat transfer do not allow understanding the influence of power input on pressure drop by means of experimental measures only. Unfortunately, the complexity of this phenomenon has always prevented from defining universally applicable Computational Fluid Dynamics (CFD) codes: the several possible flow regime (e.g. annular flow, slug flow, bubbly flow, dispersed flow, etc.), the lack of complete physical as well as mathematical knowledge of many phenomena occurring in presence of the two phases (interface dynamics, coalescence, break-up, drag, etc.) and the extreme complexity of numerical methods for solving the governing equations and closure laws of two-phase flows, generating often a inherent oscillatory behavior, are the main reasons.

An attempt to understand some aspects of the hydrodynamic behavior of a gas-liquid steam-water two-phase flow in helically coiled tubes is presented in this work, paying particular attention to pressure drop and wall shear stress. The problem is investigated by means of three-dimensional numerical simulations performed with the most popular commercial software FLUENT 14.0. FLUENT provides numerical solutions to the governing equations using the finite volume approach to discretization: the transport equations (PDE's) are integrated over each finite volume as defined by the grid and an average value of the variable is assumed over the volume. An appropriate grid has been built with GAMBIT 2.4.6, i.e. FLUENT preprocessor for geometry modeling and mesh generation, reconstructing the exact features of a small part of SIET facility helically coiled tube. Once established the operative conditions, a set of numerical simulation has been carried out in order to examine the behavior of the two-phase mixture at different values of quality under adiabatic conditions. The results have been then matched against the same two-phase steam-water pressure drop measures performed on SIET Facility and discussed in chapter 2, finding a quite good accordance with experimental results and validating the approach. Finally, the analysis of the simulated numerical results of the wall shear stress has suggested a physical explanation of the frictional pressure drop profiles evidenced in chapter 2.

3.1.2 Previous CFD works on two-phase flow in helically coiled tubes

Because of the expensive computational load required to carry out numerical simulations of two-phase flow, the earliest CFD models were presented only in the eighties and the major development was made in the last decade. Indian researchers have given an important contribution to the analysis of this subject, proposing a large amount of works investigating principally the two-phase flow in different configurations of rectilinear tubes with various processing fluids. Nowadays, numerical simulation of multi-phase flow has become an important matter of study all over the world. Nevertheless, the literature concerning two-phase flow CFD studies in coiled tubes is still quite poor and has been worked out only in the last few years; a brief review is now presented.

Vashisth and Nigam [3] investigated the local variables and interfacial phenomena for unsteady laminar two-phase flow in coiled tube, by means of a three-dimensional CFD model using volume of fluid (VOF) approach for predicting the development of velocity fields, local and average friction factor, interfacial friction factor, phase distribution and entry length; they examined also the effects of geometrical parameter and operative conditions, considering various working fluids (steam–water, air–water, SF6–water and organic liquids (glycerine, butanol)–water). Thanks to this approach they succeeded in evidencing the asymmetry in the radial distribution of the main flow velocity, which leads to a significant, non-uniform increase in the wall shear stress; they also obtained a good agreement with literature experimental data.

Bandyopadhyay et al. [4] performed an hydrodynamic modeling of a two-phase gas-non Newtonian liquid flow through a helically coiled tube, by first treating both phases separately as homogeneous and then coupling through pressure and inter-phase exchange coefficients; the non-Newtonian fluid flow was assumed laminar. Their CFD modeling matches well with specific experimental results.

Rahimi et al. [5] studied air-water two-phase flow and heat transfer in helical coils using CDF and population balance modeling (PBM) for bubble size distribution and coalescence and breakage of bubble groups: with this method bubbles can be equally divided into 5 classes of diameter; they used the realizable k-ε turbulence model for turbulence modeling in continuous phase and the Sato Enhanced Eddy Viscosity model for taking into account induced turbulence of bubbles. These authors calculated important flow quantities such as local void fraction, liquid velocity, pressure drop, temperature distribution, and found that CFD-PBM model has more ability to capture the main flow features compared to CFD model without PBM.

A recent work of Jayakumar et al. [6 - 7] applied the two-fluid Eulerian-Eulerian scheme, modeling turbulence using a multiphase "mixture k-ε model", which is based on the realizable k-ε model: they carried out a CFD analysis on air-water flow by varying geometric parameters (coil diameter, coil pitch, tube diameter), in order to bring out their influence on thermal hydraulic characteristics of the two-phase flow, and subsequently the inlet void fraction for a given value of the flow velocity. They managed to show the effects of geometry on two-phase flow and heat transfer properties.

Up to the author knowledge, no attempts of rigorous modeling steam-water two-phase flow in helically coiled tubes have ever been published in literature.

3.2 Modeling method

3.2.1 Generalities

The purpose of the CFD study is to almost reproduce the experimental steam-water two-phase flow under adiabatic conditions observed on SIET Facility helical tube and discussed in Chapter 2. Thanks to this simulations, it is possible to examine features and estimate quantities, such as volume fraction, wall shear stress, velocity profiles etc., that otherwise would not be recognizable or would require complex and expensive experimental investigations. The experimental pressure drop data can be used to validate the results: it is assumed that, if the simulations are able to approximately predict the profiles of Figure 2.3, Figure 2.4 and Figure 2.5, then a good reliability of the above mentioned features is proved and the obtained data can be used to at least qualitatively explain some physical phenomena. Actually, the first main goal of this study concerns pressure drop and consists in defining a code that is capable to virtually reconstruct the experimental pressure drop profile of a steam-water two-phase flow in helically coiled tubes as function of quality. In particular, the attention is focused on the maximum at $x \approx 0.8$ noticed in the profile of frictional pressure drop: the second main goal of this investigation is therefore to individuate the physical cause of the decrease of pressure drop in the final part of the boiling process.

Simulation no.	01	02	03	04	05	06	07	08	09	10	11	12
Quality	0.01	0.025	0.075	0.15	0.25	0.38	0.50	0.59	0.67	0.78	0.85	0.93

Table 3.1 *List of quality values for a series of numerical simulation*

Some preliminary operations have been made to set the CFD. First of all, the operative conditions have been established by taking into consideration the available experimental data: for a first series of numerical simulations pressure and mass flux have been set to respectively 3800 kPa and 389.27 kg/m^{2}s, because these value are the most representative of the corresponding experimental measured used to validate the results. Since no heat flux is imposed to the flow, the variation of thermo-physical properties, i.e. density, viscosity and surface tension, has been neglected and constant values have been set. This assumption is reasonable, since the length of the tube considered in the simulations is very limited and therefore the decreasing of absolute pressure cannot cause a significative variation of fluid properties. The following step to approach the CFD study is to discretize the quality spectrum: twelve values of quality, representative of all the phases of the boiling process, have been chosen, performing a numerical simulation for each point.

3.2.2. Geometry construction and meshing

The geometry of the grid has been built with the intention to reproduce the exact characteristics of SIET Facility: tube inner diameter, coil diameter and coil pitch listed in Table 1.1 have been used. While defining the grid, a problem arises because of two contrasting exigencies. Frictional pressure drop is strictly correlated to what happen at the interface between the fluid and the tube surface. During the experiences of pressure drop measuring under adiabatic conditions, no signals of thermal crisis were noticed, thus it is believable that, without the imposition of power input that increases quality and modifies the behavior of the flow, the annular flow regime is established and a thin liquid film covers all the inner surface; the existence of this layer may have a great influence on pressure drop. In view of this fact, a geometry including a high definition of the near wall zone, i.e. a boundary layer, is necessary; obviously, this kind of approach produces a strong growth of the computational load[6] of the numerical simulation, hence the length of the mesh must be limited in order to reduce the total number of volumes and only a small section of the tube, e.g. a dozen centimeters, can be considered. On the other side, since homogeneous values of velocity and volume fraction have been imposed at the inlet of the tube, the mesh must be long enough to exhaust the initial transition in the calculation and to allow the achievement of stationary conditions: under adiabatic conditions, the flow can be considered fully developed when pressure drop, volume fraction, velocity profiles and all the other quantities concerning the flowing fluid become constant along the tube; a complete round of the helical tube (3.14 meters) can be reasonably considered sufficient for this process. This difficulty has been solved by building two different meshes shown in Figure 3.1 and Figure 3.2, whose features are listed in Table 3.2.

	Section area [m^2]	***Length [m]***	***Number of cells on the section***	***Number of cells on the length***	***Total number of volumes***	***Boundary layer***	***Maximum aspect ratio***	***Number of control surfaces***
Coarse Mesh	$1.228*10^{-4}$	1.047	300	720	216000	No	3.0	7
Fine Mesh	$1.228*10^{-4}$	0.080	1280	280	352800	Yes	9.5	3

Table 3.2 *Geometric parameters and features of the two meshes*

Notice that some control surfaces inside the two meshes have been arranged, in order to monitor the progress of the flow and to get more reliable results, since the inlet and the outlet surface are believed to provide unstable values. The exact positions of the control surfaces are reported in Table 3.3:

Position [m]	***Inlet***	***Surf 1***	***Surf 2***	***Surf 3***	***Surf 4***	***Surf 5***	***Surf 6***	***Surf 7***	***Outlet***
Coarse Mesh	0.000	0.131	0.262	0.393	0.523	0.654	0.785	0.916	1.047
Fine Mesh	0.000	0.020	0.040	0.060	-	-	-	-	0.080

Table 3.3 *Position of control surfaces*

A first series of simulations using the coarse mesh has been performed by setting homogeneous conditions at the inlet of the tube, with the sole purpose to obtain developed profiles of flow velocity, volume fraction and turbulence parameters calculated on Surf 7; the choice to consider the final profiles on Surf 7 instead of at the end of the tube is due to the fact that the numerical

---

[6] Giving some numbers, a calculator needs approximately a 2 GB sized RAM to read a 250000 volumes mesh.

results at the outlet are believed to be less reliable because of the setting of a fixed pressure as boundary condition. Then, a new series has been performed using these profiles as input and conveniently rotating the mesh to avoid instabilities due to the different direction of the vectors. Finally, these procedure has been repeated twice in order to obtain the above mentioned development length. Anticipating a little part of the discussion of the results, in the next paragraph it will be shown that the numerical results deriving from a two-phase flow CFD carried out with a mesh lacking of boundary layer cannot predict the experimental profile of pressure drop. Thus, once obtained the developed profiles, five series of numerical simulations with the fine mesh have been performed.

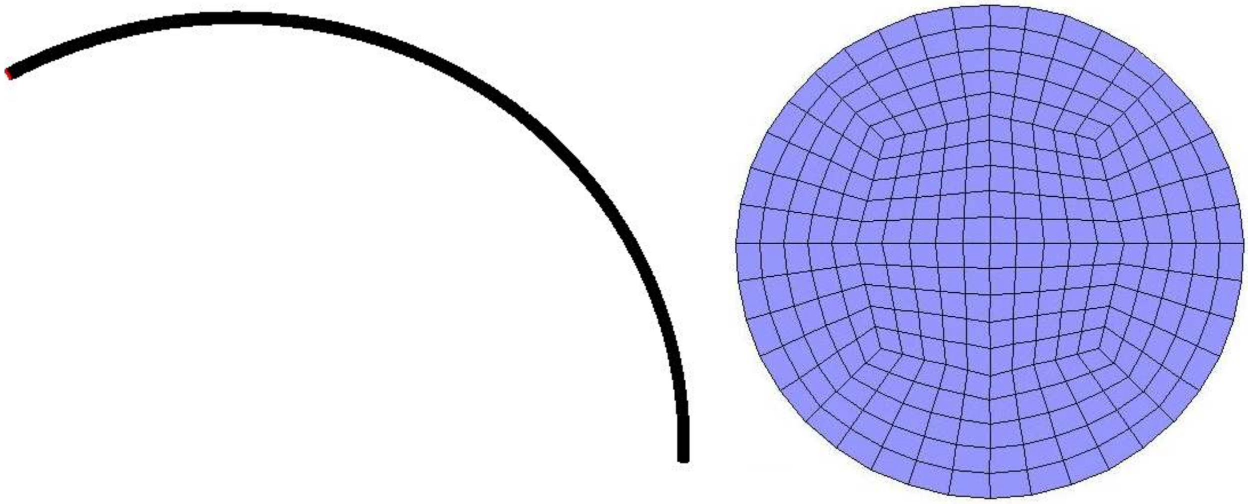

(a) (b)

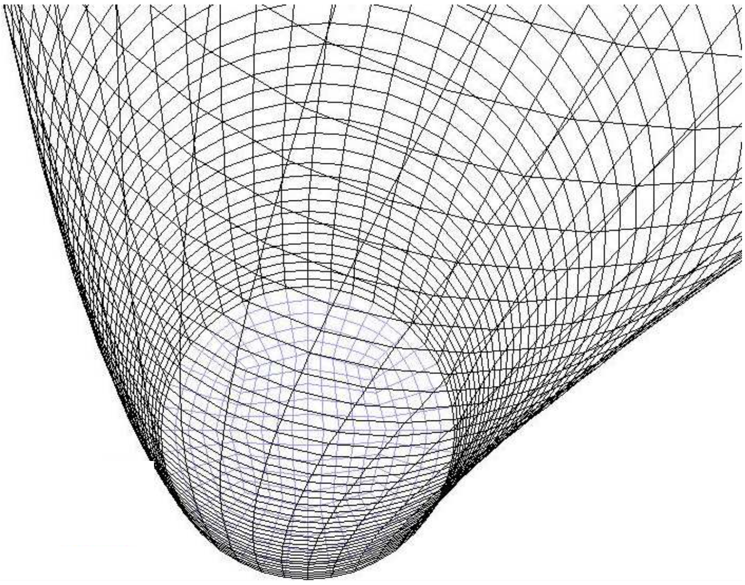

(c)

Figure 3.1 *Global view (a), section view (b) and wall view (c) of the coarse mesh*

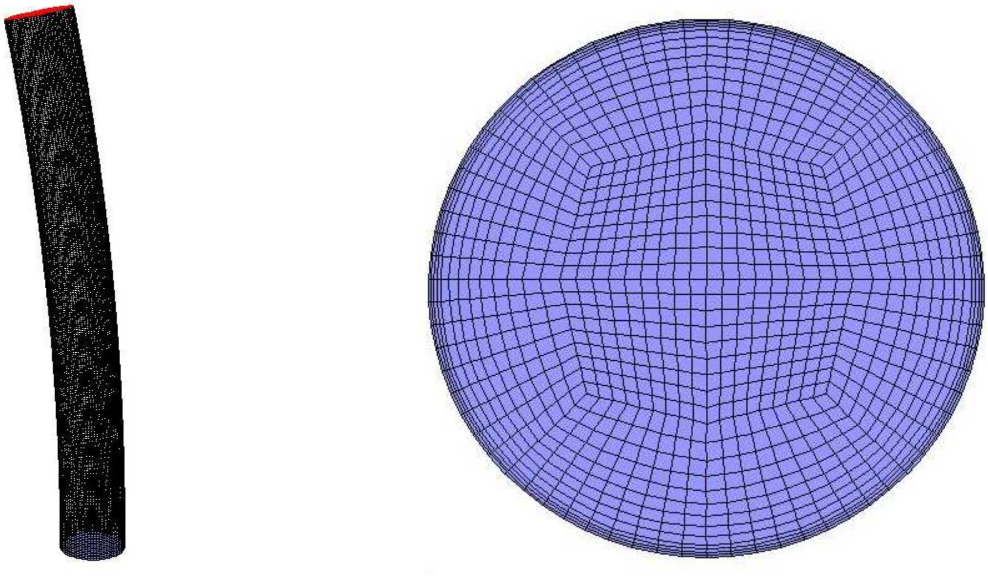

(a) (b)

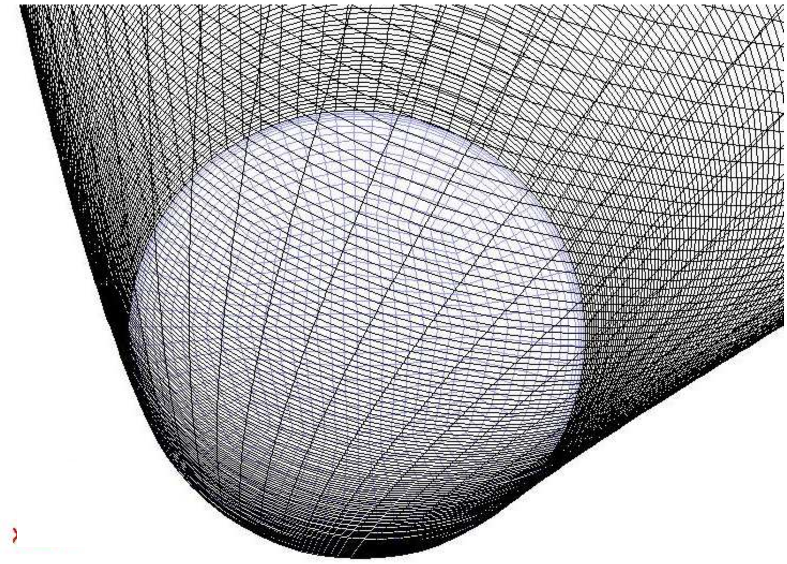

(c)

Figure 3.2 *Global view (a), section view (b) and wall view (c) of the fine mesh*

The boundary layer of the fine mesh has been built by trying to follow the principle that the size of two contiguous volumes must not vary more than 20%: by doing this, the averaged values for each volume should not be much different and therefore the computation should be more stable. Unfortunately, this approach generates a very large amount of volumes, since the nearest-wall cells must be small enough to resolve the liquid film covering the inner surface; hence, higher differences have been used. The maximum aspect ratio[7] of the fine mesh, found in the nearest-wall cells of the boundary layer, does not exceed the value 9.5, while the aspect ratio of 83% of elements does not exceed the value 6.0. The maximum aspect ratio of the coarse mesh is clearly far lower.

3.2.2 Turbulence modeling

Turbulence modeling is a critical topic of a CFD simulation: in literature one can found a huge amount of theoretical analysis, which generates tens of models applicable for diverse situations. Herein the theoretical descriptions are reduced to the bare minimum needed to justify the most important choices made; the author refers to dedicated works for further explanation.

The simplest "complete model" of turbulence is the standard *k-ε:* because of its good sensitivity to flow conditions, robustness, economy, and reasonable accuracy for a wide range of turbulent flows, it has become the workhorse of practical engineering flow calculations in the time.

---

[7] GAMBIT computes the aspect ratio of hexahedral elements with the formula: $Q_{AR} = \frac{\max(e_1, e_2, \ldots, e_n)}{\min(e_1, e_2, \ldots, e_n)}$ where e_i is the average length of the edges in a coordinate direction (i)

Presented by Launder and Spalding (1972) [9] and Patankar et al. (1975) [10], it is an easy method consisting of two transport equations, in which two additional variables are the kinetic energy k of the turbulence and its dissipation rate ε. The effective turbulent viscosity is then calculated from k and ε with the formula:

$$\mu_t = \rho C_\mu \frac{k^2}{\varepsilon} \tag{3.1}$$

where C_μ is a constant which has the default value 0.09; with the aid of this the Reynolds stresses are related to the velocity gradients. The realizable k-ε model, an enhanced version of the standard k-ε, is likely to provide superior performance for flows involving rotation, boundary layers under strong adverse pressure gradients, separation, and recirculation: it has shown substantial improvements over the standard model where the flow features include strong streamline curvature, vortices, and rotation [11]. Thanks to these features, the realizable k-ε model was chosen by many researchers in the study of non rectilinear ducts and has been used also in present work. In literature there are many other models which may be more suitable for this kind of problem (k-ω model, Large Eddy Simulation, etc.); however, the realizable k-ε model represents the best compromise between accuracy of the results and computational load. Moreover, the mentioned works available in literature [3 though 7] have shown that this model provides good results when applied to a helically coiled tube.

It is well known that turbulent flows are significantly influenced by the presence of walls. Although the mean velocity field is affected through the no-slip condition that has to be satisfied at the wall, the turbulence is also changed by the presence of the wall in non-trivial ways. Hence, the k-ε models, as well as many others, are primarily valid for turbulent core flows, i.e. the flow in the regions somewhat far from walls, and require a specific treatment for the near-wall region. Since the coarse mesh lacks of a boundary layer, it does not require an advanced methods and the FLUENT standard wall function was employed [11]. Thus, the software assumed a logarithmic law-of-the-wall for mean velocity and a homogeneous Neumann type boundary condition for solving the turbulent kinetic energy transport equation, i.e.:

$$u^* = \frac{1}{\kappa} \ln E y^* \tag{3.2}$$

$$\frac{\partial k}{\partial n} = 0 \tag{3.3}$$

here $u*$ is the dimensionless mean velocity, $y*$ is the dimensionless distance to the wall used by FLUENT (nearly equal to the y^+)[8], κ is the Von Karman constant (=0.42), E is an empirical constant (= 9.793), k is the turbulent kinetic energy and n is the local coordinate normal to the wall. Eq. (3.2) is recommended for y^+ of the first near wall node greater than 15, because below this limit, wall functions typically deteriorate and the accuracy of the solutions cannot be maintained. In the simulations performed with rough mesh, y^+ is not expected to exceed this limit. However, in FLUENT the log-law is employed when $y* > 11.225$; when the mesh does not satisfy this conditions at the wall-adjacent cells, the software applies the laminar stress-strain relationship $u* = y*$. On the other hand, when a boundary layer is applied and the mesh is supposed to be fine enough to be able to resolve the viscous sub-layer on the wall (y^+ value of the first near wall node ≈1), the enhanced wall treatment is adopted [11]. In this situation, the two-layer model for enhanced wall treatment is used to specify both ε and the turbulent viscosity in the near-wall cells: the whole domain is subdivided into a viscosity-affected region and a fully-turbulent region by the calculation of a local Reynolds number; the fully turbulent zone is treated with k-ε model whereas the viscosity-affected near-wall region the one-equation model of Wolfstein [12] is employed. Such a type of wall treatment is essential in order to achieve the resolution of the liquid film covering the inner surface of the tube.

3.2.3 Boundary conditions

At the inlet of the very first numerical simulation, uniform profiles for all the dependent variables were employed, whereas for the others the procedure mentioned in sub-paragraph 3.2.2 has been used. First of all, vapor volume fraction has been calculated with the homogeneous model, i.e. assuming slip ratio s=1:

$$\alpha_v = \frac{1}{\left(1 + \frac{1-x}{x} * \frac{\rho_v}{\rho_l} * s\right)} \tag{3.4}$$

Then, identical velocities for liquid and vapor have been set, derived from the mass flux value with the following formulas:

$$u_l = \frac{(1-x)G}{(1-\alpha_v)\rho_l} \qquad u_v = \frac{xG}{\alpha_v \rho_v} \tag{3.5}$$

The realizable k-ε model has been implemented by providing initial value for turbulence intensity and length scale as suggested by FLUENT User Guide [11]:

---

[8] The non-dimensional wall distance for a wall-bounded flow is defined as: $y^+ = \frac{\sqrt{\rho \tau_w}}{\mu} y$

$$Turbulence\ intensity = 0.16Re^{-0.125} \tag{3.6}$$

$$Lenght\ scale = 0.07d_{tube} \tag{3.7}$$

In Eq. (3.6) the Reynolds Number of the mixture has been calculated with a homogeneous model for the viscosity. Since the purpose of this CDF study is to reproduce an upward flow motion in a helical tube, gravity has been set as well. A non-slip boundary condition is imposed on the wall of the pipe; the treatment of turbulence in the near wall region has been already discussed in sub-paragraph 3.2.3. The outlet boundary conditions were set up as a pressure outlet boundary instead of as an outflow boundary to avoid difficulties with backflow. The inlet homogeneous boundary conditions used for the first series of simulation with the coarse mesh are reported in Table 3.4:

Simulation no.	***Quality***	***Void fraction homogeneous***	***Velocity (s=1) [m/s]***	***Turbulence intensity %***	***Turbulence length scale***
01	0.01	0.298	0.684	4.163	0.00088
02	0.025	0.519	0.983	4.126	0.00088
03	0.075	0.774	1.980	4.021	0.00088
04	0.15	0.881	3.476	3.899	0.00088
05	0.25	0.934	5.470	3.776	0.00088
06	0.38	0.963	8.062	3.657	0.00088
07	0.50	0.977	10.454	3.571	0.00088
08	0.59	0.984	12.249	3.517	0.00088
09	0.67	0.988	13.844	3.474	0.00088
10	0.78	0.993	16.037	3.423	0.00088
11	0.85	0.996	17.433	3.393	0.00088
12	0.93	0.998	19.028	3.362	0.00088

Pressure [kPa]	3800	***Temperature [K]***	247.3
Mass flux G [kg/m^{2}s]	389.268	***Surface tension σ [N/m]***	0.027
Saturated liquid density ρ_{ls} [kg/m^3]	802.823	***Saturated vapor density ρ_{vs} [kg/m^3]***	19.059
Saturated liquid viscosity μ_{ls} [Pa m]	1.078e-04	***Saturated vapor viscosity μ_{vs} [Pa m]***	1.744e-05

Table 3.4 *List of initial values employed in the first series of simulation with the coarse mesh*

3.2.4 Two-phase model

The Euler-Euler approach has been employed, so that the different phases are treated mathematically as interpenetrating continua: in this way, the software solves conservation equations for each phase and then these equations are closed by providing constitutive relations that are obtained from empirical information. At the interface, in order to take into consideration the momentum exchanges between the phases, the Eulerian model is the best choice, since the software solves two set of *n* momentum and continuity equations for liquid and vapor sharing the same pressure, and then achieves the coupling through the pressure and inter-phase exchange coefficients. The continuity and momentum governing equations for the liquid phase and the vapor phase are:

CONSERVATION OF MASS

$$\frac{\partial}{\partial t}(\alpha_l \rho_l) + \nabla\left(\alpha_l \rho_l \overrightarrow{V_l}\right) = \Gamma_{vl} - \Gamma_{lv} \tag{3.8}$$

$$\frac{\partial}{\partial t}(\alpha_v \rho_v) + \nabla\left(\alpha_v \rho_v \overrightarrow{V_v}\right) = \Gamma_{lv} - \Gamma_{vl} \tag{3.9}$$

CONSERVATION OF MOMENTUM

$$\begin{aligned}\frac{\partial}{\partial t}\left(\alpha_l \rho_l \overrightarrow{V_l}\right) + \nabla\left(\alpha_l \rho_l \overrightarrow{V_l}\overrightarrow{V_l}\right) &= -\alpha_l \nabla p + \nabla \bar{\bar{\tau}}_l + \alpha_l \rho_l \vec{g} + \overrightarrow{F_{l-CF}} + \overrightarrow{F_{l-VM}} + \\ &+K_{vl}\left(\overrightarrow{V_v} - \overrightarrow{V_l}\right) + \Gamma_{vl}\overrightarrow{V_{vl}} - \Gamma_{lv}\overrightarrow{V_{lv}}\end{aligned} \tag{3.10}$$

$$\begin{aligned}&\frac{\partial}{\partial t}\left(\alpha_v \rho_v \overrightarrow{V_v}\right) + \nabla\left(\alpha_l \rho_l \overrightarrow{V_v}\overrightarrow{V_v}\right) \\ &\qquad = -\alpha_v \nabla p + \nabla \bar{\bar{\tau}}_v + \alpha_v \rho_v \vec{g} + \overrightarrow{F_{v-CF}} + \overrightarrow{F_{v-VM}} + \\ &\qquad +K_{lv}\left(\overrightarrow{V_l} - \overrightarrow{V_v}\right) + \Gamma_{lv}\overrightarrow{V_{lv}} - \Gamma_{vl}\overrightarrow{V_{vl}}\end{aligned} \tag{3.11}$$

NOMENCLATURE

α = *volume fraction*
ρ = *fluid density*
$\vec{V}_l \vec{V}_v$ = *velocity of liquid and vapor*
$\Gamma_{lv}\, \Gamma_{vl}$ = *mass flow rate exchanged by the phases*
p = *relative pressure*

$\bar{\bar{\tau}}$ = *stress-strain tensor*
g = *gravitational constant*
F_{CF} = *centrifugal force*
F_{VM} = *virtual mass forces*
$\overrightarrow{V_{lv}}\, \overrightarrow{V_{vl}}$ = *inter-phase velocities*
$K_{vl}\, K_{vl}$ = *see eq. (3.12)*

Notice the presence of centrifugal force due to the tube curvature. The term of virtual mass forces arises because the secondary phase, i.e. vapor, is believed to accelerate relative to the primary phase, i.e. liquid; then, the inertia of the liquid generates a force on the vapor and this term account for it with an appropriate expression [11]. Despite the presence of many terms that model the interaction between the phases, that is to say $\Gamma_{lv}\overrightarrow{V_{lv}}$, $\Gamma_{vl}\overrightarrow{V_{vl}}$, $\overrightarrow{F_{v-VM}}$, K_{lv} in eq. (3.11) and the respective terms in eq. (3.10), only the latter, i.e. the momentum exchange due to the drag, has been considered. Also Γ_{lv} , Γ_{vl} in eq. (3.08) and eq. (3.09), which represent the mass exchange between the phases, i.e. condensation and evaporation of fluid at the interface, have been neglected. The universal drag law was used for the calculation of the drag coefficients in bubble-liquid or droplet-gas flow regimes, then the coefficient K_{vl}, and similarly K_{lv}, is defined as follow:

$$K_{vl} = \frac{18\mu_l \alpha_v \alpha_l f}{d_v^2} \tag{3.12}$$

where the drag coefficient C_D is included in the drag function f [13]. Here d_v is the diameter of the bubbles of vapor (and similarly d_l is the diameter of the droplet of liquid). This parameter was found to be highly critical, since a too small size of the bubbles/droplets generates a homogeneous flow, while if the dimension is excessively big the software underestimates the interaction between the phases and then liquid and vapor appear more separate. After a sensitivity study, the optimized value $d_v = 0.0001\ m$ has been set.

3.2.6 Solution strategy and convergence criterion

A pressure based transient solving method has been employed. Since the Eulerian model was selected, the Phase Coupled SIMPLE scheme, an extension of the SIMPLE algorithm to multiphase flows [14], has been adopted for pressure-velocity coupling. The spatial discretization schemes used in the simulations are listed in Table 3.3, while a First Order Implicit scheme has been employed for time discretization; these schemes ensured, in general, satisfactory accuracy, stability and convergence. The time step value t utilized in temporal discretization depends on the velocity of the flow and on the type of mesh: the formula suggested by FLUENT User's Guide [11] has been employed:

$$\frac{l_c * V}{t} \approx 10 \tag{3.13}$$

where l_c represents the length of a cell and V is the initial velocity of the mixture.

Gradients	*Least Square Cell Based*
Momentum	*Second Order Upwind*
Volume fraction	*QUICK*
Turbulence kinetic energy	*Second Order Upwind*
Turbulence dissipation rate	*Second Order Upwind*

Table 3.5 *Spatial discretization schemes*

The convergence criterion is based on the residual value of the calculated variables, i.e. mass, velocity components for each phases, turbulent kinetic energies, turbulent dissipation energies and volume fraction. The numerical computation was considered converged when the residual summed over all the computational nodes at n^{th} iteration, $R_n(\varphi)$, satisfies the following criterion:

$$\frac{R_n(\varphi)}{R_m(\varphi)} \leq 10^{-5} \tag{3.14}$$

with the exception of the mass convergence, for which the value is 10^{-3}, where $R_m(\varphi)$ denotes the maximum residual value of the variable φ after m iterations. In order to accelerate the convergence, some under-relaxation factors lower than the default value has been set, as reported in Table 3.4.

Pressure	*0.2*
Density	*1*
Body forces	*1*
Momentum	*0.6*
Volume fraction	*0.4*
Turbulence kinetic energy	*0.7*
Turbulence dissipation rate	*0.7*
Turbulence viscosity	*1*

Table 3.6 *Under-relaxation factors*

3.3 CFD with the homogeneous model

3.3.1 Modeling the homogeneous model

In addition to the approach explained in Paragraph 3.2, also a CFD study concerning the homogeneous model has been performed. A series of numerical simulation has been carried out, using a liquid only flow under adiabatic conditions with homogeneous averaged thermo-physical properties instead of the two-phase steam-water mixture under consideration. In particular, the density and the viscosity of the fluid have been calculated as follow:

$$\frac{1}{\rho_{hom}} = \frac{(1-x)}{\rho_{ls}} + \frac{x}{\rho_{vs}} \tag{3.15}$$

$$\frac{1}{\mu_{hom}} = \frac{(1-x)}{\mu_{ls}} + \frac{x}{\mu_{vs}} \tag{3.16}$$

The operative conditions $p = 3800\ kPa$ and $G = 389.27\ kg/m^2s$ have been imposed and the presence of gravitational force has been taken into account. Seven values of quality were considered (Table 3.5).

Simulation no.	1	2	3	4	5	6	7
Quality	0.15	0.25	0.38	0.50	0.67	0.78	0.93

Table 3.7 *List of quality values for the homogeneous model numerical simulation*

This type of single-phase flow numerical simulation does not require a much refined grid, since the physical phenomena, and therefore the governing equations, are by far simpler than the multi-phase situation. Hence, the coarse mesh, whose features are listed in Table 3.2, has been used for this purpose. The standard *k-ε* model with standard wall function was retained appropriate for turbulence modeling. A transient first order implicit temporal formulation of the problem was adopted. SIMPLEC scheme has been used for pressure-velocity coupling, while second order schemes have been employed for spatial discretization of pressure, momentum, turbulent kinetic energy and turbulent dissipation rate. The under-relaxation factors have been kept at the default values. Time step was calculated as in eq. (3.13).

3.3.2 Results and discussion

The homogeneous model is substantially a simplified model that in principle allows studying the two-phase flow with the methods of single-phase flow. In practice, this approach is not able to forecast a great number of phenomena occurring in a two-phase flow; hence, this study would not provide information about volume fraction, flow regime, velocity profiles etc. The only result achievable with this approach regards pressure drop and a comparison with experimental data have been made. As noticeable in Figure 3.3, the homogeneous model does not succeeded in predicting the experimental profiles of pressure drop: the numerical calculations of pressure drop are in general underestimated, especially in the range of quality greater than 0.50. Moreover, the numerical results do not reproduce the profile of pressure drop and the maximum of the curve at *x*≈0.8. Then, it is important to underline that the correctness of the modeling procedure is demonstrated by the excellent accordance between simulated values and single-phase Ito's turbulent flow equation (eq. 1.25), in which Reynolds number is calculated with eq. (3.16) for the viscosity; the gravitational component of pressure drop has been added to the theoretical values in order to compare them to the results of the numerical simulation.

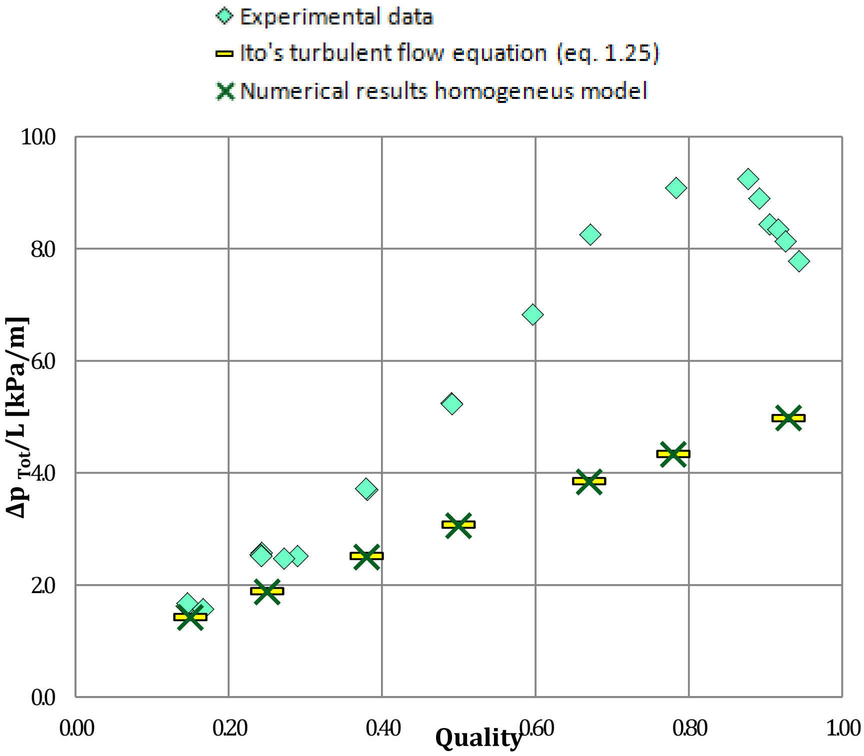

Figure 3.3 *Pressure drop results of CFD study with the homogeneous model*

It is clearly noticeable the unsuitability of the homogeneous model to study the two-phase flow in a helically coiled tube at the given operative conditions. Thus, it can be concluded that a multi-phase model is necessary for the purpose of present study. Nevertheless, many literature works suggest that better results can be achieved in case of higher values of mass flux, i.e. $G \geq 2700\ kg/m^2s$ [15]. Unluckily, the available experimental data set does not include such measures on helically coiled tubes and then it is not possible to validate the results of a numerical simulation. Hence, this situation has not been considered in present work.

The excellent agreement between pressure drop computed with the numerical simulation using the homogeneous model and with Ito' s turbulent flow equation is an important achievement, since two radically different approaches provide very close results. This fact implies that CFDs predictions of pressure drop in single-phase flow are highly reliable. Despite this, a CFD multi-phase approach is by far more complicated, thus this result does not help in order to reach the purpose of this work.

3.4 Two-phase CFD with the Coarse Mesh: results and discussion

3.4.1 Results monitoring

The presence of seven control surface inside the tube allows monitoring the stability of the numerical results: in fact, since adiabatic steady conditions are imposed, when the initial transitory is completed and the results do not depend on inlet boundary condition anymore, surface average values of pressure drop, volume fraction and all the quantity of interest must no vary with the curvilinear coordinate. In general, convergence of pressure drop and wall shear stress has been achieved quite soon, thus the first series of numerical simulation with the coarse mesh has been sufficient. Instead, in order to obtain the convergence of volume fraction and velocity profiles, three series of simulation with the coarse mesh were necessary, as explained in Paragraph 3.2. After this procedure, the final values of pressure drop and volume fraction have been obtained by averaging the numerical results on the seven surfaces (excluding inlet and outlet).

3.4.2 Volume fraction

Vapor volume fraction profiles are shown in Figure 3.4: for the sake of clearness and simplicity, all the sections of the tube have been translated and rotated in order to appear on a plane x-z; the outer part of the tube lies on the left side of the images, while the position of the zero angle conventionally used in trigonometry corresponds to the inner part.

The most apparent element that is revealed by the examination of the twelve profiles is that the numerical simulations managed to reproduce the asymmetry induced on the flow by centrifugal and gravitational forces, since the heavier phase is more subjected to the effect of body forces. Gravity breaks the symmetry on the x-axis, while curvature causes a shift of the heavier phase, i.e. liquid, on the outer side of the tube. The contribution of gravity is strongly important, since the slope of SIET facility helical test section is only 14.48°, rendering this tube more similar to a horizontal rectilinear pipe than to a vertical one. Thus, once annular flow regime is established, the typical film covering the wall is characterized by an evident liquid buildup in the down-left zone of the section. The behavior of this layer is crucial in this investigation, therefore this aspect is better discussed in sub-paragraph 3.5.2 and sub-paragraph 3.5.4, where the analysis of the more accurate results obtained with the fine mesh allows dealing with the wall shear stress. The liquid film covering the inner surface is visible only in the accumulation zone. The software allow the visualization of a hint of the entire layer in some cases at high quality (Simulation 10, Simulation 11 and Simulation 12): this fact is principally due to the different scale used in the visualization of the graphics, since the difference between the higher grades of the colors is very small. Nevertheless, this represents an important signal that the resolution of the liquid film could be achievable with a finer mesh. In the profiles in which annular flow regime is clearly visible, the solution does not show a marked stratification of the two phases, but there is a mixing region that gradually leads from the liquid zone to the vapor zone.

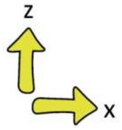

Simulation 02 - x=0.025

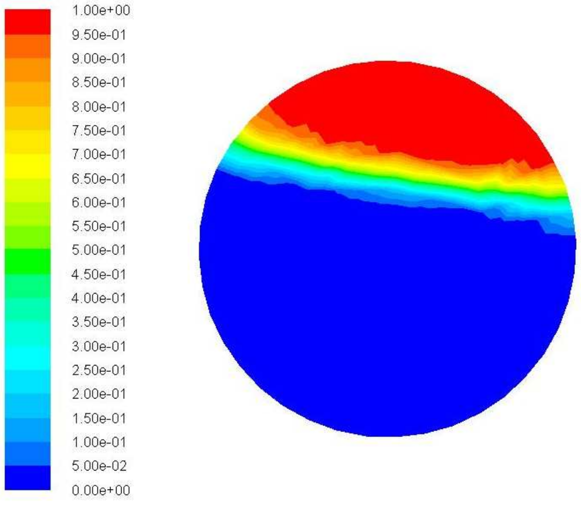

Simulation 01 - x=0.01

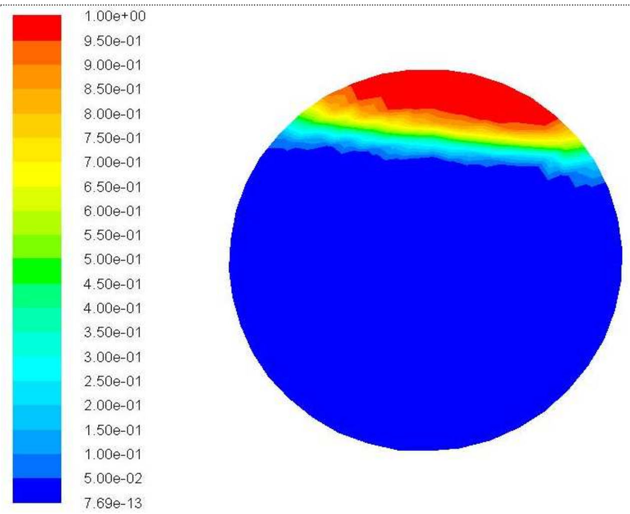

Simulation 03 - x=0.075

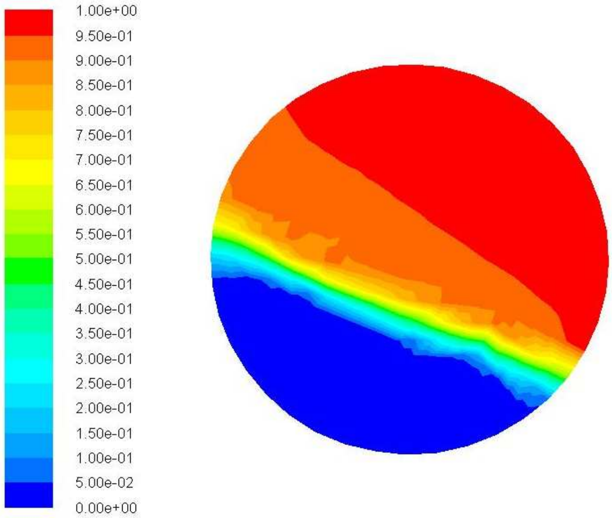

Simulation 04 - x=0.15

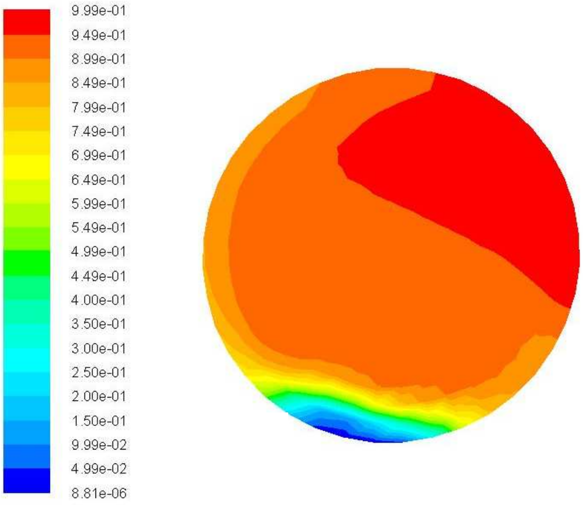

Simulation 05 - x=0.25

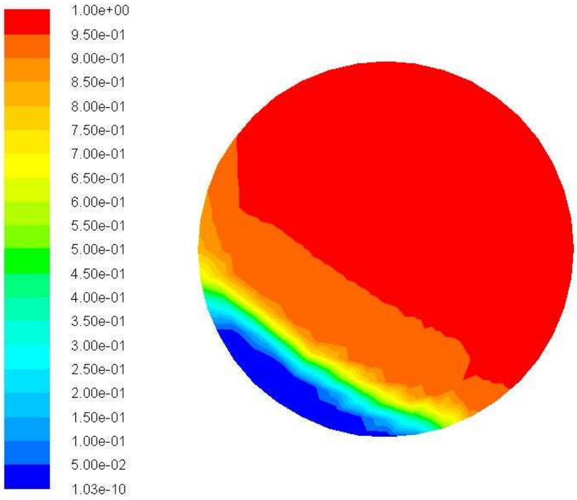

Simulation 06 - x=0.38

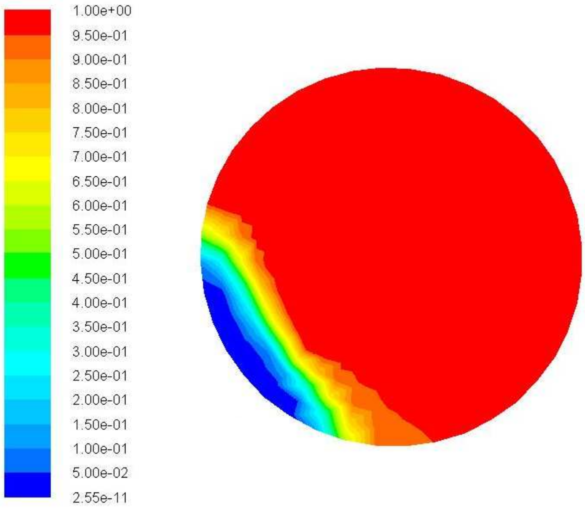

Simulation 07 - x=0.50

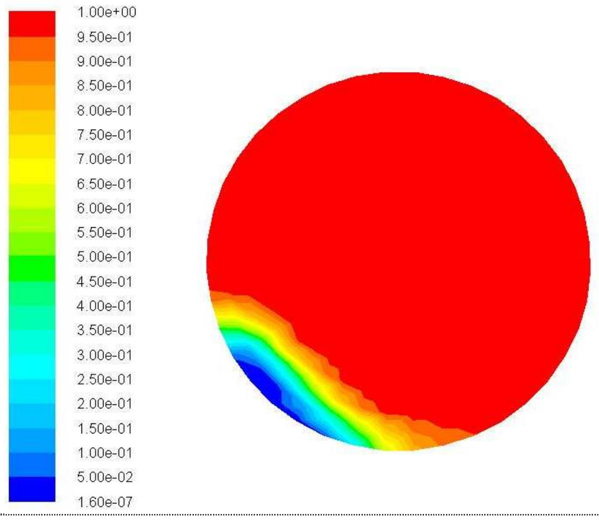

Simulation 08 - x=0.59

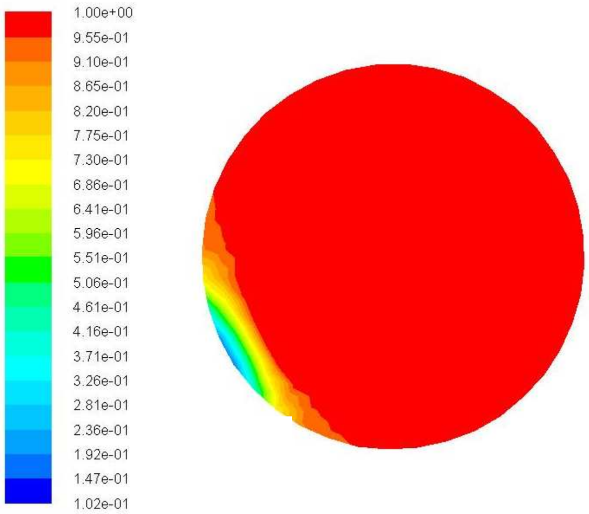

Simulation 09 - x=0.67

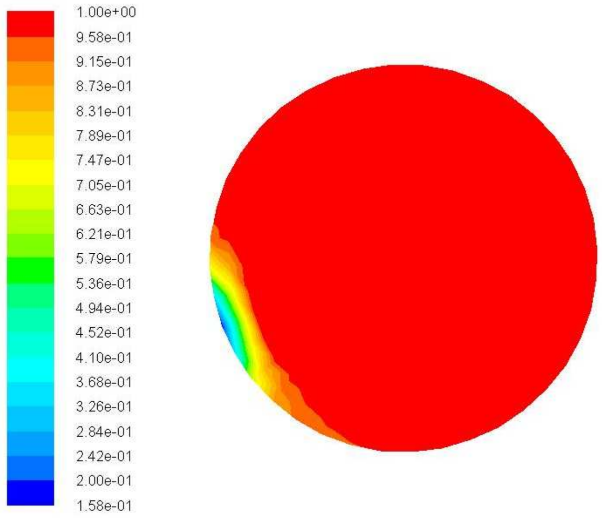

Simulation 10 - x=0.78

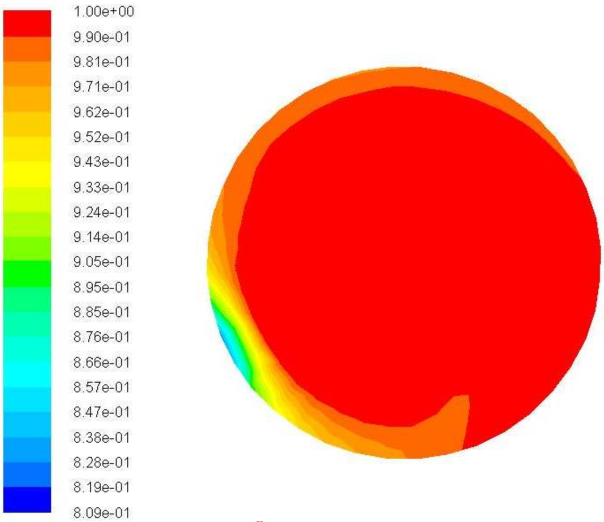

Simulation 11 - x=0.85

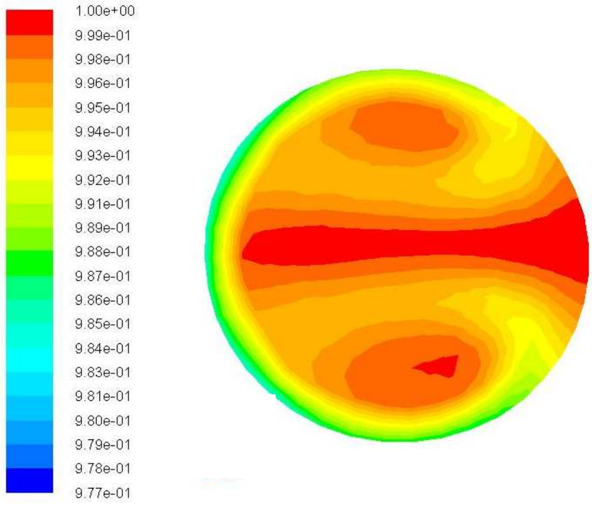

Simulation 12 - x=0.93

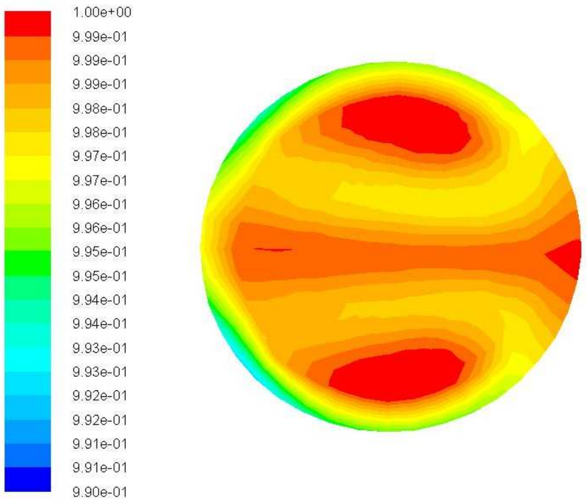

Figure 3.4 *Numerical void fraction profiles obtained with the Coarse Mesh.*

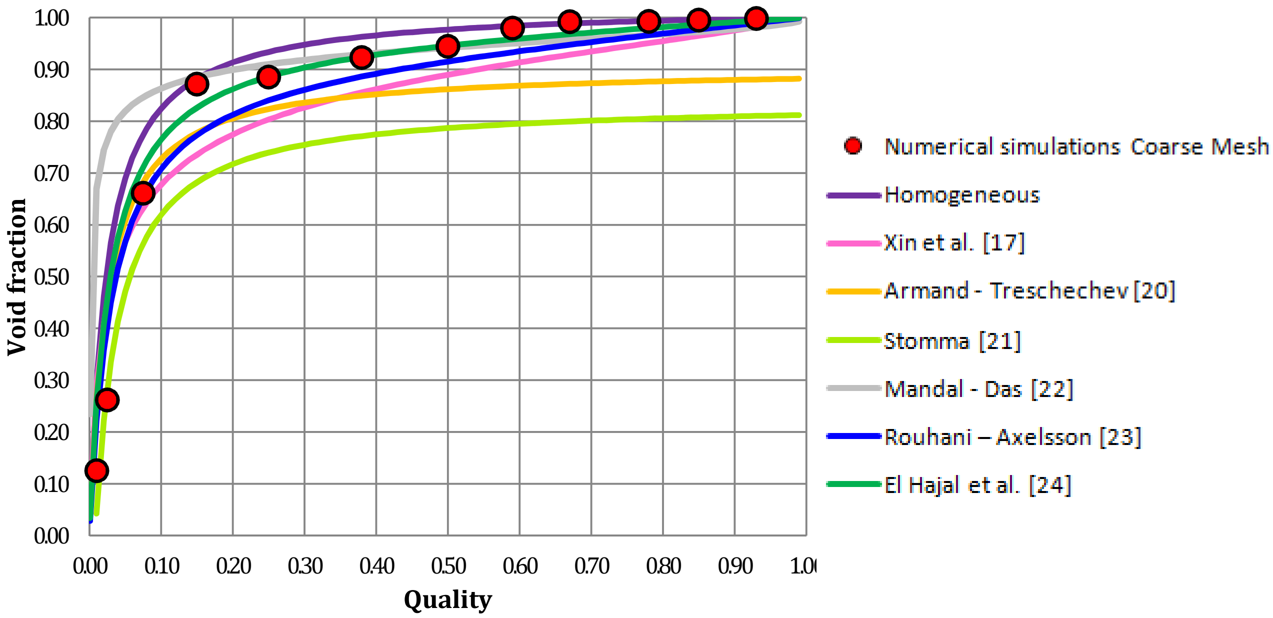

Figure 3.5 *Numerical results of void fraction (Coarse Mesh) and comparison with literature correlations*

The surface integral averages of vapor volume fraction are reported in Figure 3.5. It is believable that these values of volume fraction are overestimated, since they may still feel the effects of the beginning condition of unitary slip ratio: in fact, the condition of uniform velocity of the two phases leads to a very high theoretical value of volume fraction, because it is ascertained that in a steam-water two-phase flow vapor is faster than liquid. Unfortunately, a validation of the results is not possible because of the lack of experimental data. However, a comparison between some correlations for void fraction available in literature confirms the hypothesis of overestimation: in fact, theoretical predictions are in general lower than numerical results, especially in the range of quality greater than 0.50; moreover, in this region numerical values are very similar to those predicted by the homogeneous model derived from eq. (3.17) imposing unitary slip ratio *s*: this approach surely overestimates the void fraction, because the true value of slip ratio, i.e. the ratio of vapor and liquid velocity, is greater than 1.

$$\alpha_{vapor} = \frac{1}{\left(1+\frac{(1-x)}{x}\frac{\rho_v}{\rho_l}\,s\right)} \tag{3.17}$$

Nevertheless, a moderately good accordance is obtained with Rouhani and Axelsson’s equation [23] and with El Hajal et al.’s method [24], which consider the logarithmic mean void fraction between the homogeneous value and Rouhani and Axelsson’s equation, although these formulas are proper for straight horizontal tubes. A quite good accordance has been obtained also with Lockhart and Martinelli’s approach [16] used in Xin et al.’s equation:

$$\alpha_{vapor} = \frac{\Phi_l - 1}{\Phi_l} \tag{3.18}$$

where Φ_l is defined in eq. (2.5) and the constant is set to the value $C = 10.646$ [17]. Even thought Lockhart and Martinelli’s work is not specific for coiled tubes, some authors [17 18 19] achieved quite good results providing modified correlating parameter to the formula. For the benefit of completeness, it worth state that Armand and Treschechev’s equation, and similarly Stomma’s equation, were derived under bubble flow regime, thus they are not able to predict void fraction in the range of high quality. That is why the respective curves do not reach the value 1.0 at the end of boiling.

The closeness to the void fraction values obtainable with the homogeneous approach is a signal that these results cannot be considered reliable. Probably, a better profile could be achieved using the fine mesh.

3.4.3 Pressure drop

The numerical results and the comparison with experimental data are visible in Figure 3.6; all the series are provided of a fitting curve obtained with the least square method. The plotting of the total pressure drop instead of the sole frictional component has been preferred: this choice is motivated by the fact that the subtraction of gravitational and accelerative pressure drop to the numerical results as well as to the experimental measure is supposed to add uncertainty to the final result, since the standard theoretic expressions reported in eq. (0.4) contain some terms, such as density and mass flux, that are different in experimental and numerical case.

Pressure drop numerical evaluations obtained using the coarse mesh does not show a good agreement with experimental data: even though in the range of qualities $x \leq 0.25$ a good correspondence is observable, the simulated profile does not follow the experimental curve when quality increases and does not recognize the maximum at $x \approx 0.8$, underestimating the experimental values with a maximum error greater than 40%. Nevertheless, this result was expectable, since the main phenomena responsible of pressure drop take place at the tube inner surface and the coarse mesh has a bad resolution of the near wall zone. In fact, as observable in Figure 0.1, in the central and final part of the boiling process the main contribution to pressure drop is given by the frictional component, whose theoretical expression is strictly related to the wall shear stress. One can therefore suppose that the inaccurate resolution of the liquid film covering the tube inner surface leads to a incorrect evaluation of wall shear stress and, in consequence, of total pressure drop, the higher the error the greater the contribution of friction. Despite the bad agreement with experimental data, these numerical simulations represent an improvement in respect to the homogeneous model, since a non-monotone trend is recognizable: simulations no. 9 through 12 (*x=0.67*, *x=0.78*, *x=0.85* and *x=0.93*) form a plateau and the numerical estimation of pressure drop does not increase in the end of boiling process. This occurrence may happen because of the bad capabilities of the coarse mesh to resolve complicated hydrodynamic behaviors: actually, with the progressive reduction of the liquid fraction, the liquid buildup on the outer surface become thinner until it dries. Thus, it is plausible that in Simulation 09 and Simulation 10 the near-wall grid is not fine enough to resolve the characteristics of the layer in this situation and when computing pressure drop the software does not distinguish the difference between these cases and Simulation 11 – 12, whose numerical results tend to the conditions of saturated vapor single-phase flow.

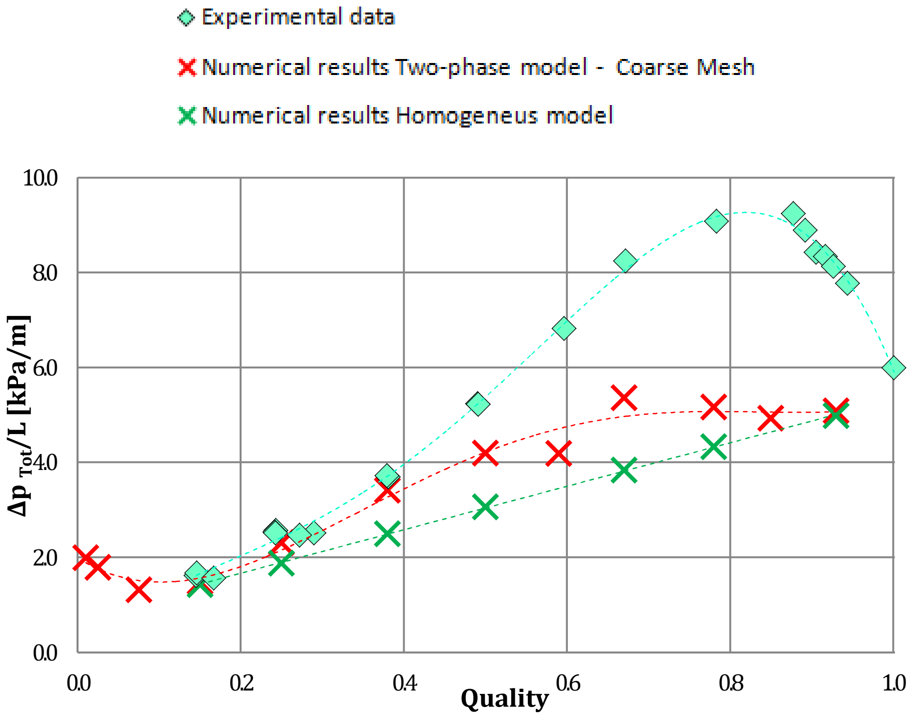

***Figure 3.6** Pressure drop results of CFD study with two-phase model and Coarse Mesh*

The above analysis leads to the conclusion that a numerical simulation employing a coarse mesh is not able to correctly predict the pressure drop profile of a steam-water two-phase flow under the operative conditions under consideration. This result imposes the necessity to use a more refined mesh with a boundary layer for a more exact resolution of the near wall region.

3.5 Two-phase CFD with the Fine Mesh: results and discussion

3.5.1 Results monitoring

After the development of the hydrodynamic profiles with the coarse mesh, the fine mesh, endowed with a boundary layer, described in Table 3.2 have been used in order to achieve a good resolution of the flow and thus obtain accurate numerical results. As already explained, the great amount of volumes necessary for this purpose has imposed a strong limitation on the total length of the grid. Hence, a numerical simulation with the fine mesh has been performed using the results of the development procedure as the inlet boundary conditions for the first run; then the outlet profiles (computed on Surf 3) of velocity, turbulence parameter and volume fraction have been used for the following series. This procedure has been repeated four times to guarantee the development of the flow in the fine mesh; thus for each one of the twelve quality values taken into consideration, five runs have been performed. The three control surfaces set along the grid allow monitoring the stability of the numerical results. With the purpose of increasing the reliability of pressure drop, wall shear stress and vapor volume fraction simulated data, the final results have been computed by averaging the outcomes of the last three series of numerical simulations.

In behalf of comprehensibility during the analysis of the results, the quality spectrum is conventionally subdivided into three parts:

(Zone 1) beginning of boiling process and establishment of annular flow regime, $x \leq 0.38$, Simulation 01 through Simulation 06;

(Zone 2) central boiling, $0.38 < x < 0.78$, Simulation 07 through Simulation 09;

(Zone 3) dry-out region, transition from annular to dispersed flow regime, $x \geq 0.78$, Simulation 10 through Simulation 12.

3.5.2 Volume fraction

Vapor volume fraction profiles are shown in Figure 3.7. In the representation, the same conventions described in sub-paragraph 3.4.2 have been adopted. The considerations concerning gravitational and centrifugal forces explained in sub-paragraph 3.4.2 are valid also for this case:

these forces generate a shift of the liquid phase in the low outer part of the tube. In Simulation 01 through Simulation 02 the effect of centrifugal force is less visible because of the low velocity of the flow. In these cases the liquid volume fraction is still predominant over the vapor one: the numerical simulations have identified a clearly stratified flow. From Simulation 04 the shift of the liquid buildup is clearly appreciable and annular flow regime is established. The thickness of the liquid layer progressively reduces as the vapor mass fraction increases, until the accumulation of liquid disappear in zone 3 and dispersed liquid droplets are transported by the vapor.

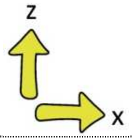

Simulation 01 - x=0.01

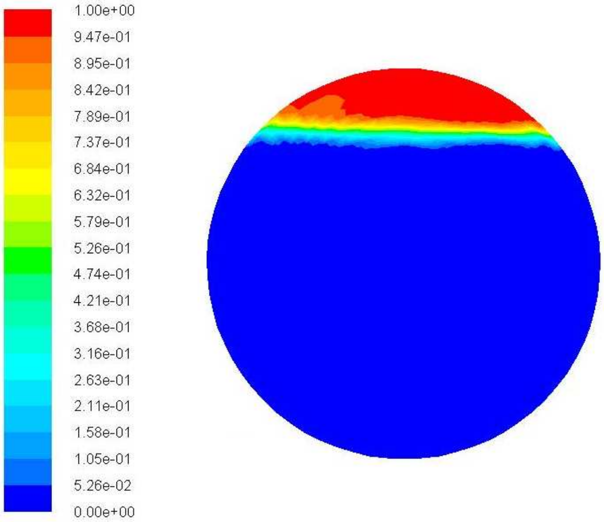

Simulation 02 - x=0.025

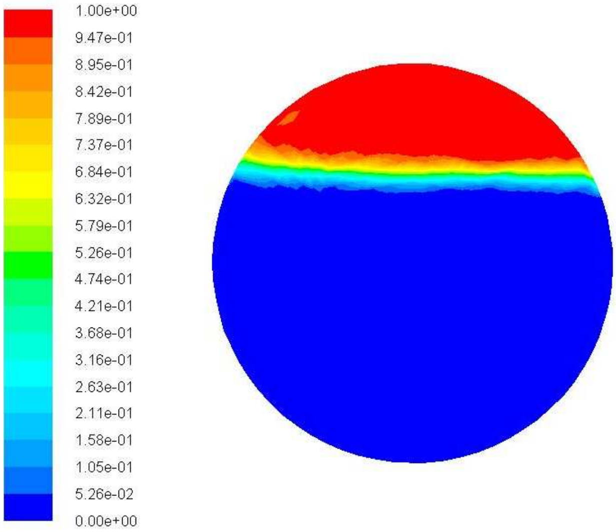

Simulation 04 - x=0.15

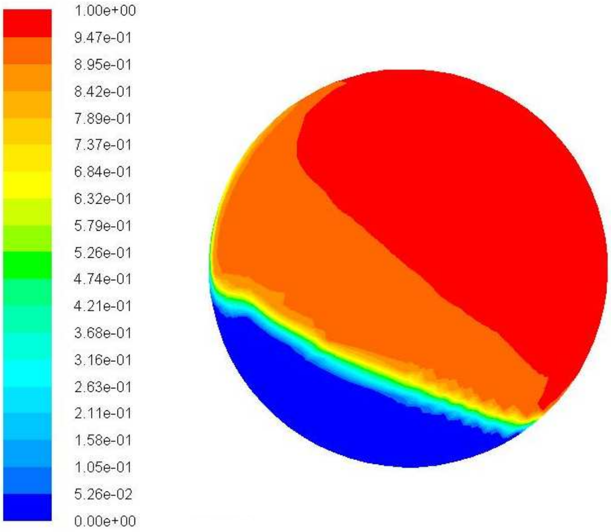

Simulation 03 - x=0.075

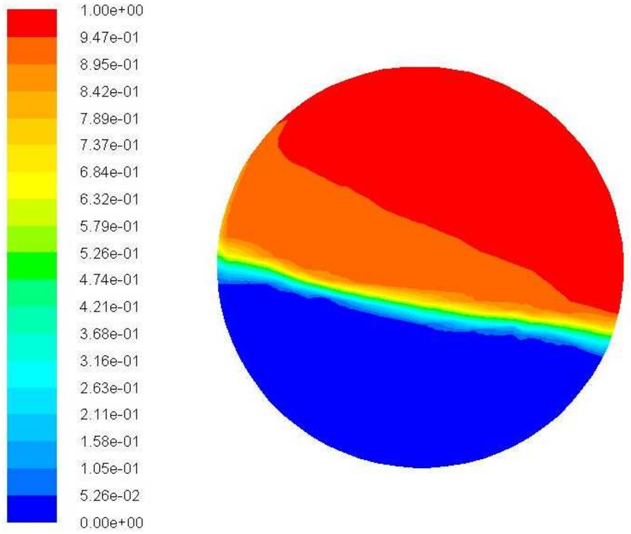

Simulation 05 - x=0.25

Simulation 06 - x=0.38

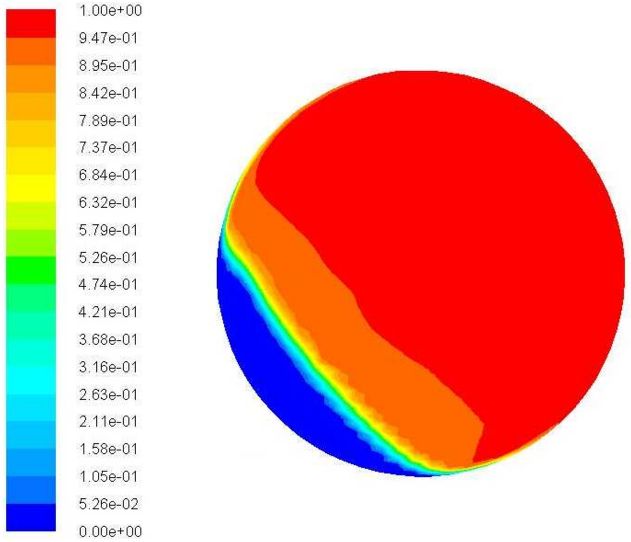

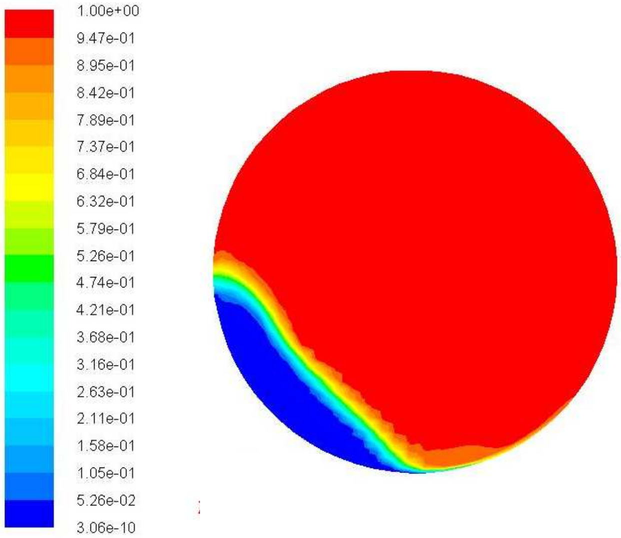

Simulation 07 - x=0.50

Simulation 08 - x=0.59

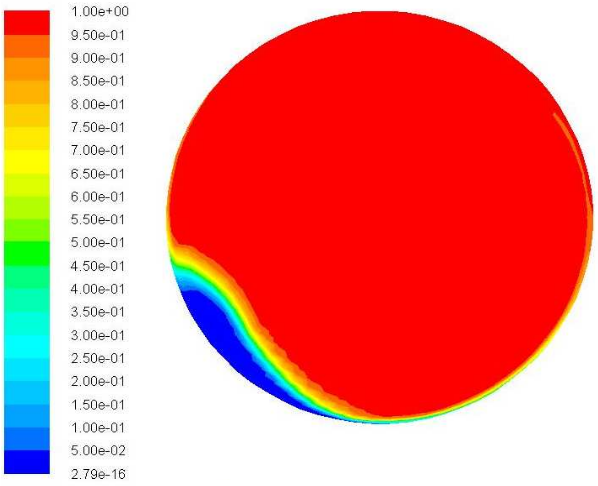

Simulation 09 - x=0.67

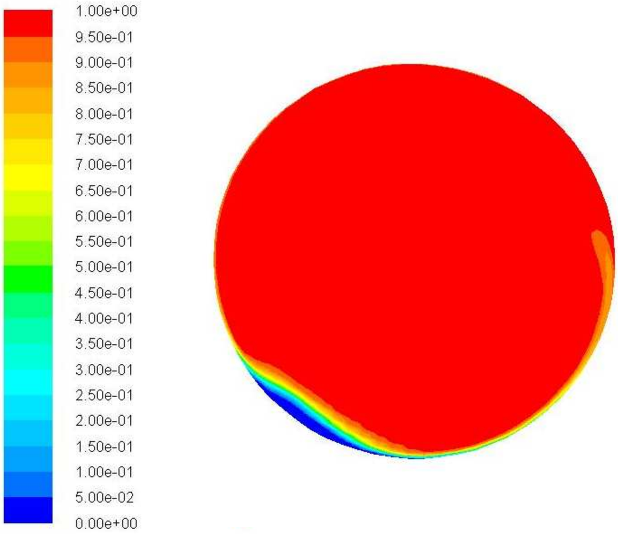

Simulation 10 - x=0.78

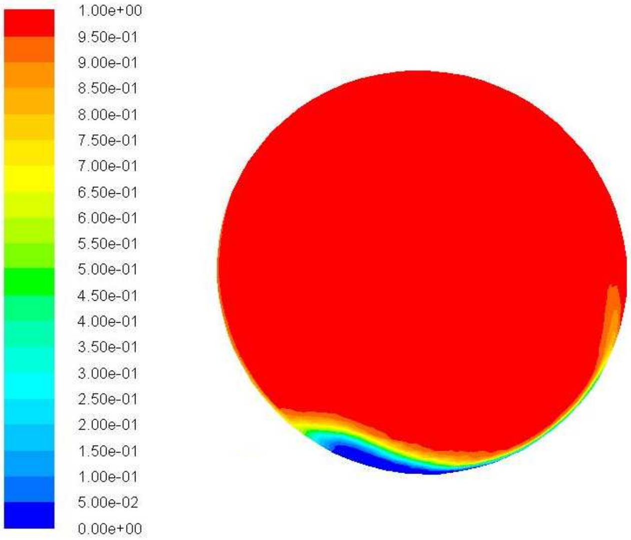

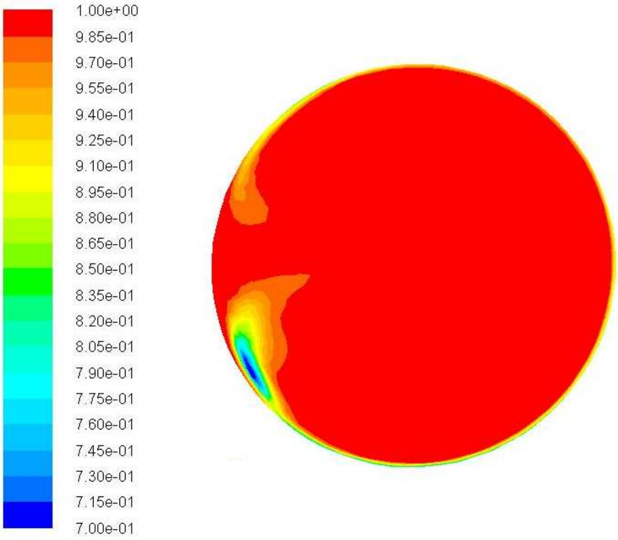

Simulation 11 - x=0.85

Simulation 12 - x=0.93

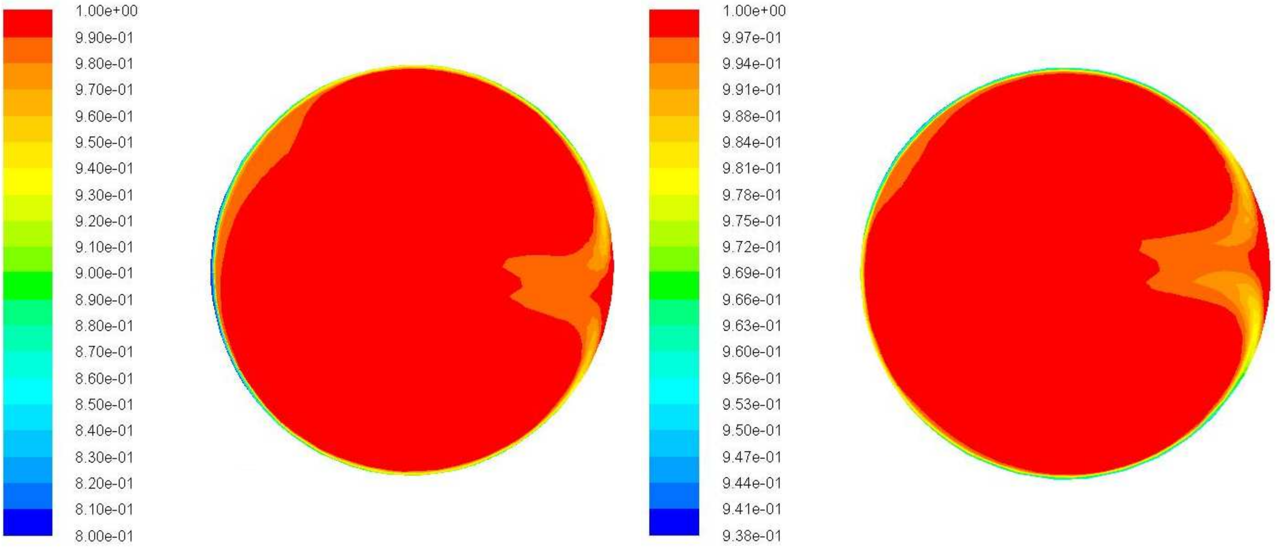

Figure 3.7 *Numerical void fraction profiles obtained with the Fine Mesh.*

The resolution of the liquid film, which is believed to cover the whole inner surface in annular flow regime (part of Zone 1 and Zone 2), is only partially achieved: it is distinctly visible only in the down side of the tube, while along the rest of the perimeter a dry-out condition is evidenced. Given the presence of two body forces that break the symmetry of the flow, it is obvious that the thickness of the layer is anything but constant along the perimeter of the surface. Thanks to the effect of gravity, the film is less thin in the down part of the section and then its resolution is easier. In Figure 3.8 a series of enlargements of the liquid film resolved on Simulation 07 is observable; the grid is also reported. The progressive drying of the film occurs while getting far from the liquid buildup, until the layer become so thin that it is not (or not correctly) resolved. Three hypotheses are formulated in order to explain the happening of this result:

- the boundary layer is not fine enough to resolve the thickness of the liquid film, thus software computes the presence of vapor in the nearest wall cell;
- turbulence model, wall treatment employed are not the most suitable among those available in literature to completely resolve the liquid film;
- the boundary conditions at the interface are highly critical and a non-optimized setting may generate some problem.

Probably, the answer lies in the middle of these suppositions: the employ of either the described fine mesh or the realizable k-ε model with enhanced wall treatment is in general a good approach in order to reach this goal, but, in light of the results, it is not sufficient, allowing only a partial visualization of the layer. In addition, even though the Eulerian model is surely appropriate for the scope, a more accurate optimization of some parameters, such as the drag law and the size of the bubbles / droplets, could allow obtaining better results. Nevertheless, the possibility that the liquid film is really dried in some part of the tube inner surface under annular flow regime must not be neglected, even though no differences in the temperature of the tube were reported in experiments. Actually, the behavior of liquid film is retained to be highly unstable and therefore a correct understanding of annular flow regime is very difficult.

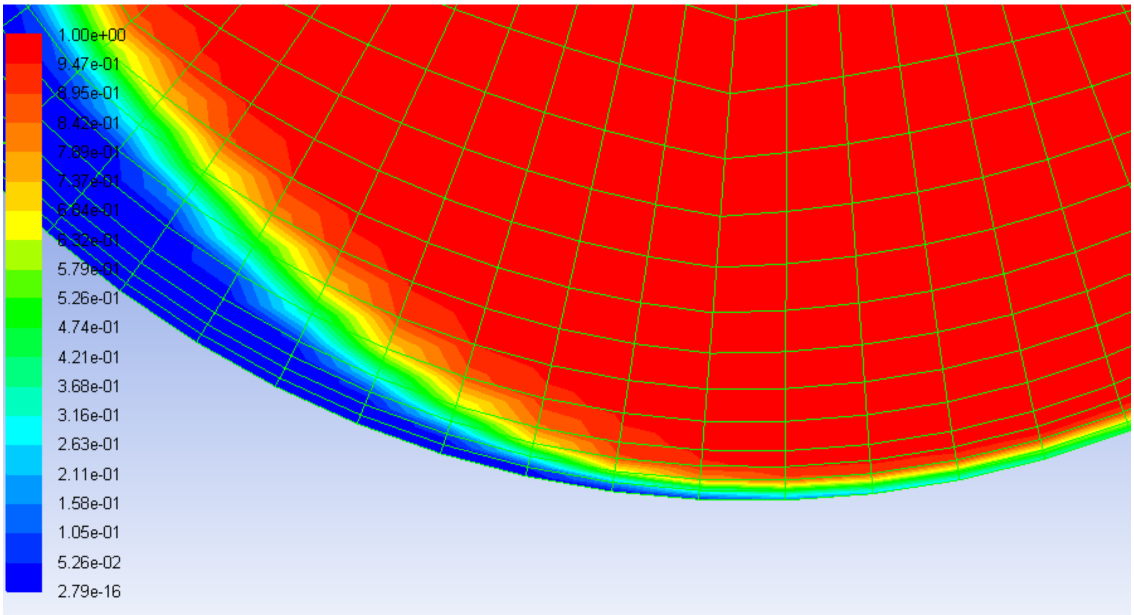

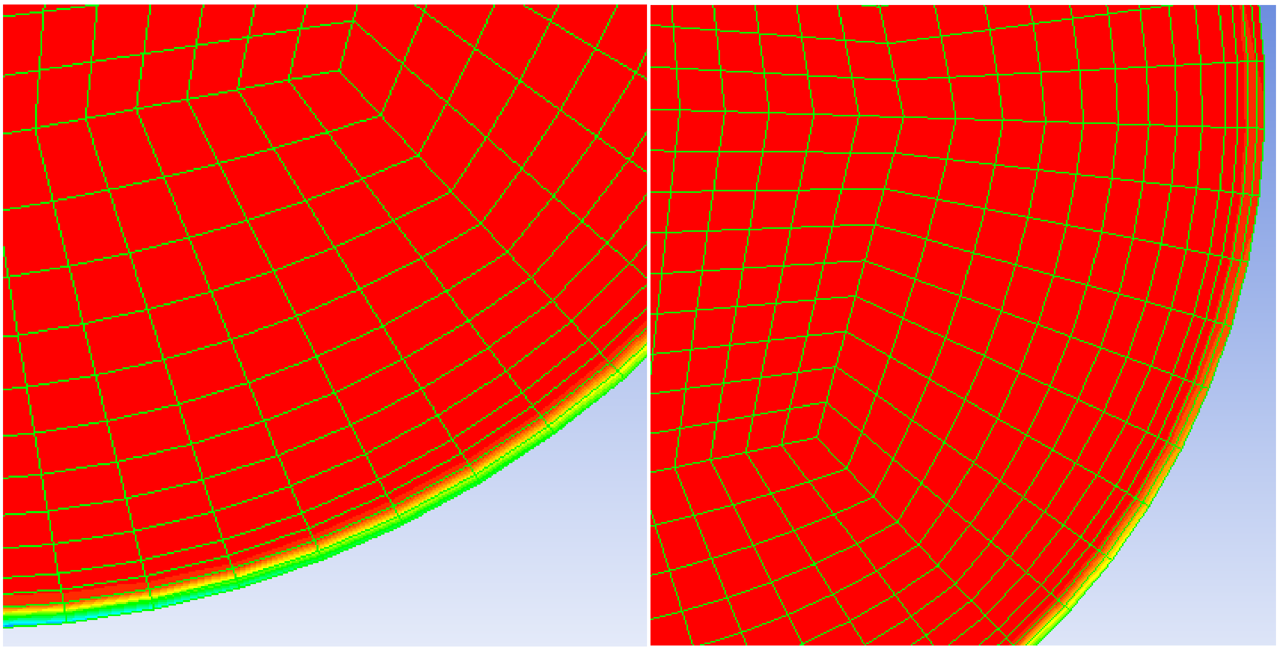

***Figure 3.8** Detailed views of the void fraction profile at x=0.50 (Simulation 0.7)*

Looking at the simulations in Zone 3, the buildup has dried and the presence an inkling of the liquid film on the wall is experienced because of the changing of the scale of visualization. The numerical simulations slightly resolve the dispersed flow regime. As explained in sub-paragraph 3.2.4, it is ascertained that the diameter of liquid droplets / vapor bubbles is a very sensitive parameter, which has a great influence on the definition of void fraction profiles; it is then possible that an optimization of this parameter would lead to a better visualization of the flow regime.

The quantification of average surface vapor volume fraction exhibits an enhancement in respect to what shown in sub-paragraph 3.4.2: the finer resolution of the grid consented a better computation, thus, especially in Zone 1, the global void fraction results are always lower than those obtained with the coarse mesh, and therefore farther from the homogeneous values. Moreover, the profile is more regular and still in accordance with Rouhani and Axelsson's and El Hajal et al.'s equations. In Figure 3.9 and Figure 3.10 this situation is observable. Lastly, it is important to underline the achieved convergence of these results: in the last three series the void fraction is stable and then substantially constant in each simulation.

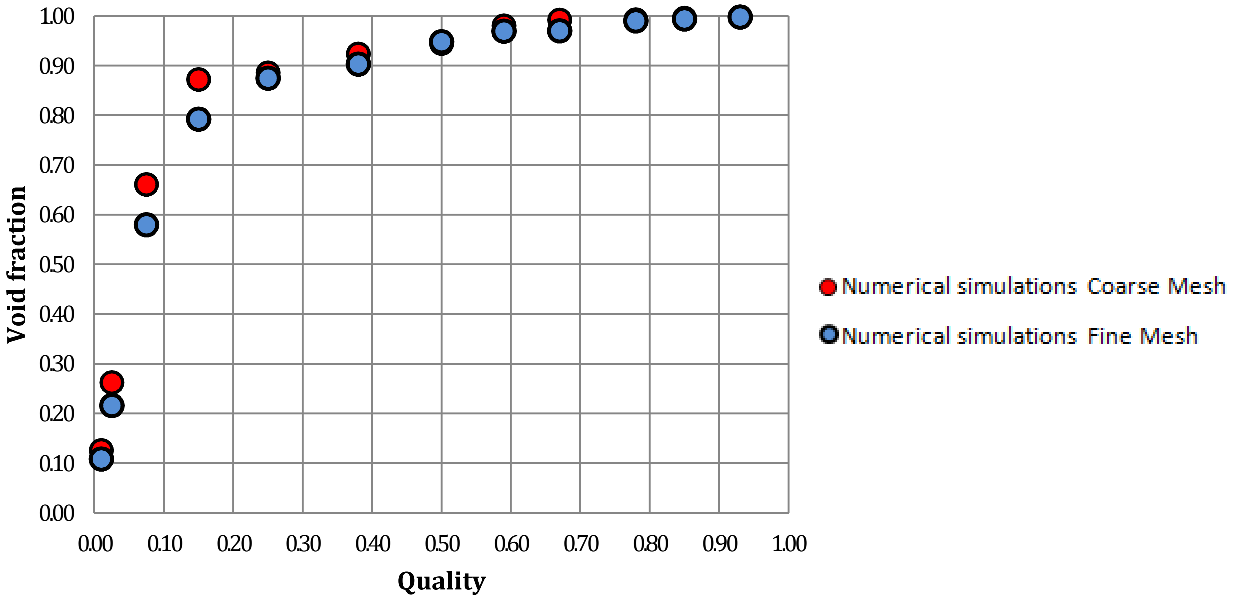

***Figure 3.9** Comparison of numerical void fraction results (Fine Mesh vs. Coarse Mesh)*

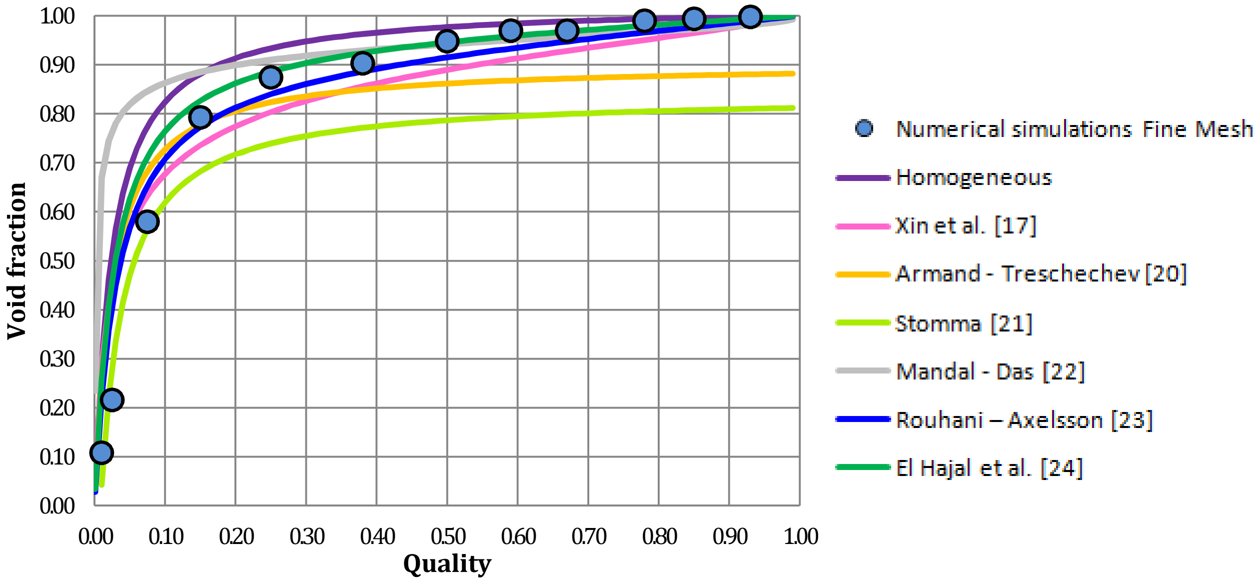

***Figure 3.10** Numerical results of void fraction (Fine Mesh) and comparison with literature correlations*

These quantitative results are surely satisfying. Nevertheless, correlations predicting void fraction in helically coiled tubes available in literature are few and not always in agreement; thus, the impossibility to validate them against experimental data leaves a reserve on their reliability.

3.2.5 Pressure drop

The numerical estimation of total pressure drop profile is reported in Figure 3.11; all the series are provided with a fitting curve obtained with the least square method. For the same reasons explained in sub-paragraph 3.4.3, the above graphics report the total pressure drop in place of the frictional component only. Despite the fact that an incomplete visualization of the liquid film has been obtained, the first thing that comes evident is that the fine mesh has consented to achieve the main goal of the present investigation, that is the reproduction of the maximum characterizing the experimental pressure drop curve. In effect, a good similarity between the experimental and the computed curves is noticeable and a great difference between the two numerical results reported in the graphic is appreciable. Probably, the enhanced mesh allowed a better resolution of the liquid buildup in the down left zone of the tube, which is, as it is shown in next paragraph, the main responsible of the shear stress on the surface. Therefore, it can be deduced that the resolution of the grid play a very important role in this situation: an approach including the employ of a boundary layer for the spatial discretization of the near-wall zone is fundamental in order to correctly reproduce the experimental profile of pressure drop.

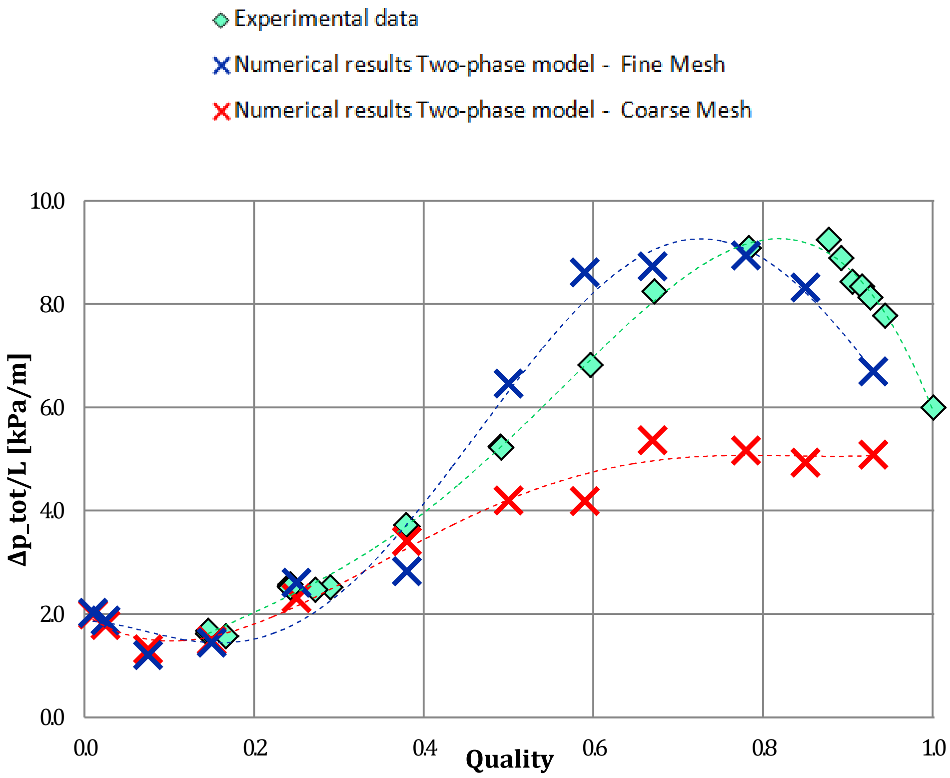

Figure 3.11 *Pressure drop results of CFD study with two-phase model and Fine Mesh*

A quantitative estimation of the difference between the profiles has been performed. Since the quality of experimental and simulated points not always corresponds, a polynomial fit of the experimental data in eq. (3.19) has been done in order to calculate pressure drop at the desired quality and get comparable values.

$$\frac{dp_{tot}}{dz} = -76.995x^4 + 115.58x^3 - 48{,}068x^2 + 15{,}358 + 0{,}0794 \qquad (3.19)$$

In addition, it must be mentioned that the validation of the results has been possible only for Simulation 04 through simulation 12, because of the lack of data in the range of quality $x<0.15$. The general tendency shows that numerical results, in respect to experimental data, are nearly in accordance in Zone 1, overestimated in Zone 2, underestimated in Zone 3. The average relative error is equal to 14.3%, while the maximum difference with the corresponding experimental datum is due to Simulation 08 ($x=0.59$) and is equal to 26.3%.

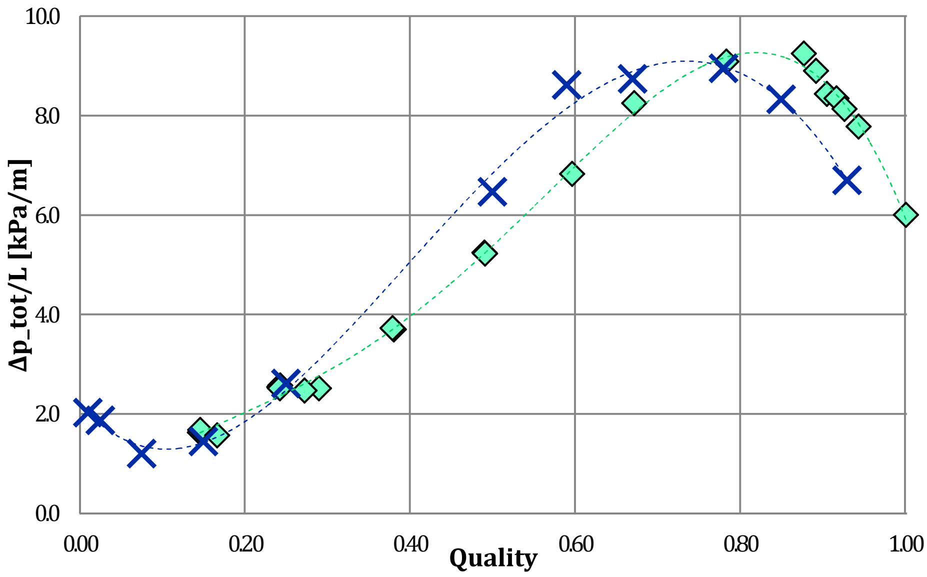

Figure 3.12 *Pressure drop results of CFD study with two-phase model and Fine Mesh (Simulation 06 excluded)*

It is noticeable that the numerical result of Simulation 06 ($x=0.38$) is particularly low compared with the general trend of the curve. Actually, the reliability of this point is doubtful, since the corresponding void fraction profile shows that in this case the part of the liquid film covering the tube inner surface resolved by the numerical simulation is smaller than the others. One can hypothesize that some instabilities occurred in the simulation with the fine mesh or in the development of the hydrodynamic profile with the coarse mesh. Neglecting Simulation 06, the average error reduces to 13.1%; the resulting curve is shown in Figure 3.12 (for the sake of clearness, the red curve obtained with the coarse mesh has not been reported).

Another matter observed concerns the convergence of the values in the three series of numerical simulation taken into consideration when averaging the numerical results. Even though the three runs are expected to provide nearly equal predictions, a quite small difference among the results of simulations in Zone 2 and in simulation 10 is visible. Moreover, the trend shown in Zone 3 is the opposite in respect to the other zones. Possible reasons of the occurrence of these instabilities are the following:

(a) the incomplete development of the profiles, since the hydrodynamic behavior of a flow with quality greater than 0.5 is probably more complicated to be resolved than the case *x<0.5*;

(b) the changing of the flow regime in the last phase of boiling process, from annular flow to dispersed flow.

The case (b) suggests the idea that the same setting of boundary conditions at the interface used might generate different behavior when stratified, annular or dispersed flow regime is established. The principal suspect relapses on the input constant value of the diameter of the bubbles/droplets. If this interpretation is correct, it could explain also the overestimation of experimental data in Zone 2 and the underestimation in Zone 3. This instability is visible in Figure 3.13.

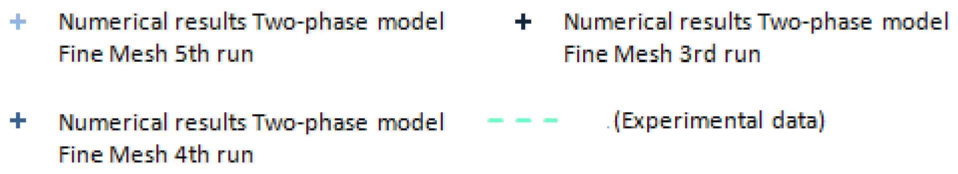

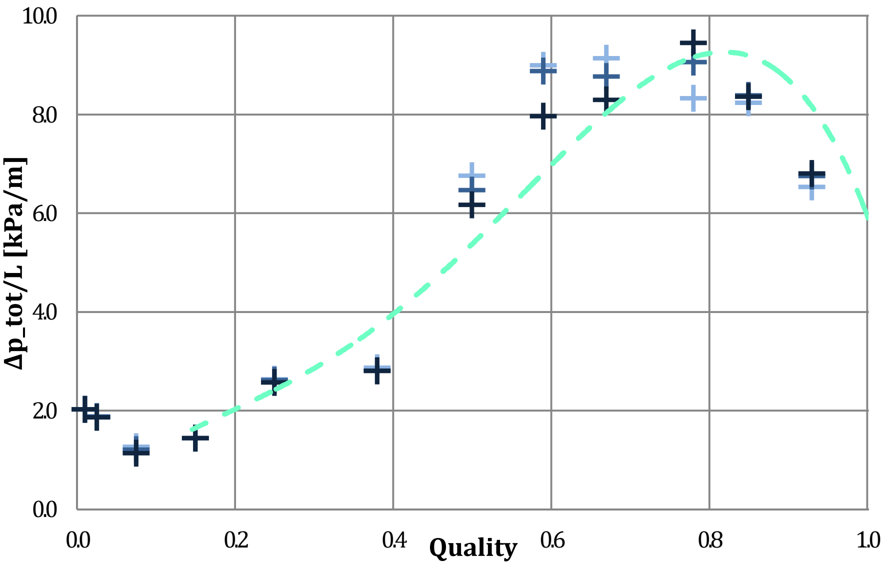

Figure 3.13 *Pressure drop results of CFD study with two-phase model and Fine Mesh (3^{rd}, 4^{th} and 5^{th} runs)*

Despite the arising of these two problems, the obtained results concerning pressure drop can be considered satisfying: the modeling method employed allows reaching a qualitative reproduction of pressure drop profile in the entire spectrum of quality which is validated by experimental data, and also the quantitative values are not so far from physical measures. It is worth emphasizing that this achievement is principally due to the presence of the boundary layer and the consequent variations on turbulence model and wall treatment in respect to what done with the coarse mesh.

3.6 Wall shear stress analysis

3.6.1 Overview

It is expectable that the analysis of wall shear stress concerning the results of the numerical simulations employing the coarse mesh would not lead to a correct evaluation of the profiles of the shear stress at the tube surface, since the wrongness of pressure drop predictions is due to an incorrect evaluation of the force exercised by the fluid against the wall. Instead, a qualitatively and quantitative almost right reproduction of pressure drop profile allows the research of a physical explanation for the maximum at $x=0.8$, investigating the phenomenon that generates frictional pressure drop. In this paragraph, the results obtained with the fine mesh are discussed in detail, while those deriving from the development of the hydrodynamic profiles are sometimes shown only as examples in order to demonstrate the importance of the boundary layer in this analysis.

The relationship between wall shear stress and frictional pressure drop is expressed in eq. (0.6):

$$\frac{dp_{frict}}{dz} = \frac{1}{A_z}\int_{P_z} \tau_w dP_z = \frac{\bar{\tau}_w P_z}{A_z} \qquad (0.6)$$

For circular tubes, the ratio of the wetted perimeter P_z to the cross section A_z is equal to $4/d_{tube}$, hence eq. (0.6) can be rearranged, obtaining a very simple formula:

$$\frac{dp_{frict}}{dz} = \frac{4\bar{\tau}_w}{d_{tube}} \qquad (3.20)$$

Once fixed the diameter of the tube, the mean wall shear stress and the frictional component of pressure drop are linearly depended. When annular flow regime is established, the inner surface is supposed to be covered by liquid, thus, it is believable that only the liquid phase supplies to generate the stress at the wall. Nevertheless, when computing the wall shear stress, the software distinguishes also a contribution of the vapor, because in the numerical simulation the liquid film is not resolved correctly and the presence of vapor is recognized in the nearest-wall cells. These two terms are complementary and a simple sum of them gives the value of the total wall shear stress. It is important to underline that no physical meaning is attributable to liquid and vapor components of wall shear stress, since they derived from a probably incorrect definition of the flow. In reality, in a ideal annular flow regime the whole shear stress at the wall is due to the force exercised by liquid on the inner surface.

3.6.2 Validation of the results

The average global wall shear stress over the entire inner surface of the mesh has been computed for each one of the twelve numerical simulations by summing liquid and vapor component. In light of eq. (3.20), the profile of wall shear stress must reflect that of frictional pressure drop and also that of total pressure drop visible in Figure 3.11, since, as already said, the gravitational and the accelerative terms give only a very small contribute: in Figure 3.14 a good similarity is visible and the wall shear stress profile exhibits also the instability concerning Simulation 06 discussed in sub-paragraph 3.5.3 and the high error of Simulation 08. In the simulations at low quality the gravitational component of pressure drop is relevant, hence in the first part of Zone 1 the profile of wall shear stress is considerably different from that of total pressure drop.

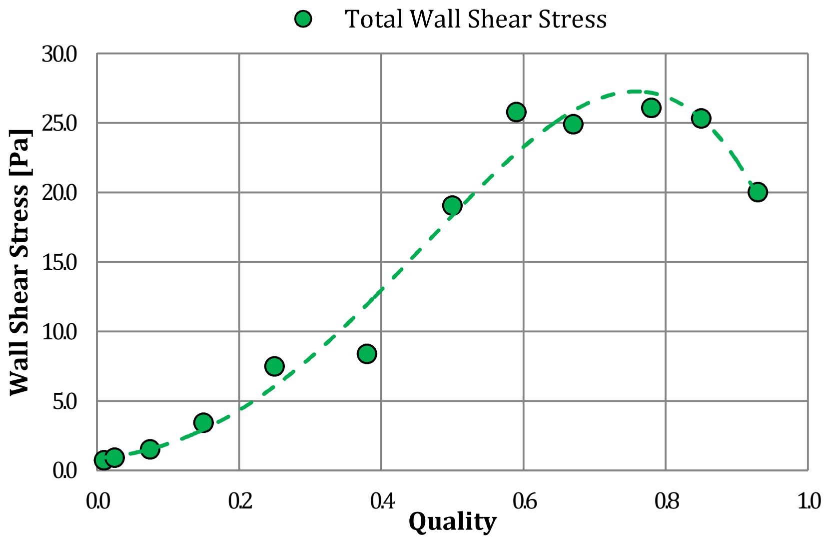

Figure 3.14 *Simulated values of total wall shear stress vs. quality*

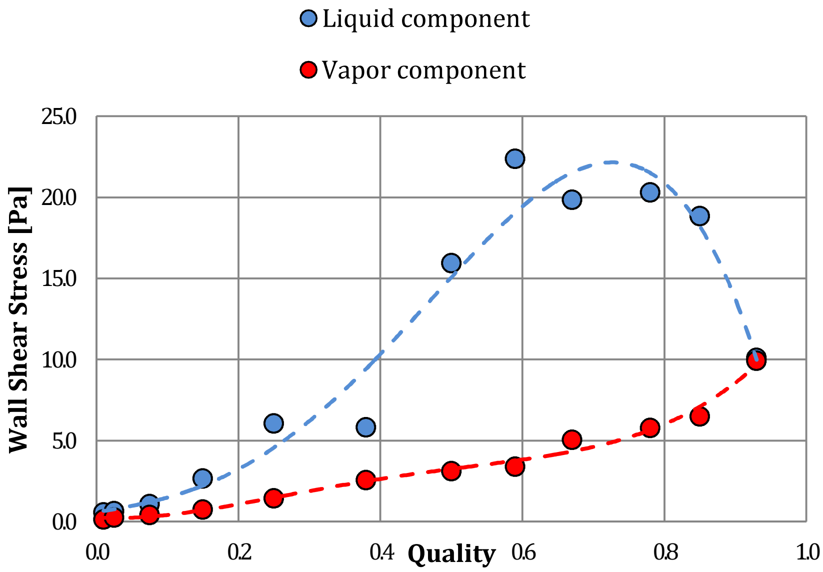

Figure 3.15 *Contribution of the two fictitious components*

In Figure 3.15 the different trend of the liquid and vapor fictitious components is shown. As expected, looking at the numerical results it is noticeable that the shear stress due to the liquid phase is the main responsible of friction in almost all the spectrum of quality. Only in the final part of Zone 3, i.e. when dispersed flow regime is established, the two contributions tend to be equal.

The verified concordance between pressure drop and wall shear stress guarantees the consistence of the numerical results. Since pressure drop profiles have been validated with experimental data, one can assume the reliability of wall shears stress values. Nevertheless, there is no way to validate the angular dependence discussed in next paragraph, thus, only a qualitative consistency of the profiles can be assumed.

3.6.3 Angular dependence

The analytical expression of τ_w is given by:

$$\tau_w = -\mu \left(\frac{\partial u}{\partial r}\right)_{r=r_0} \tag{1.37}$$

where μ is the dynamic viscosity of the flowing fluid. The wall shear stress is then strictly correlated to the axial velocity gradient at the surface. Hence, one would expect that wall shear stress, and in consequence pressure drop, becomes greater as the velocity of the flow increases, since a condition of zero-slip at the surface is plausible, and in a single-phase flow this condition is effectively verified. However, it has been widely argued in this work that experimental pressure drop profile of two-phase steam-water flow under adiabatic conditions in vertical straight tubes sometimes shows a hint of a change in its slope in the final part of the boiling process (see Figure 2.1 and Figure 2.2), depending on operative conditions: in general, a high mass flux tends to hide this phenomenon[9]. Instead, in helically coiled tubes pressure drop profile presents a clearly visible maximum when the quality reaches approximately the value 0.8 and then decreases (Figure 2.3 through 2.5). This remarks guide to formulate the hypothesis that the main responsible of the non-monotonic trend, i.e. the decrease of pressure drop in the final part of the quality spectrum, is the transition from annular to dispersed flow regime in two phases. Then, the effects of gravity and centrifugal force break the equilibrium of the flow and also the symmetry of the wall shear stress, amplifying the effects of the changing of flow regime. In other words:

- liquid stuck to the surface, compared to vapor, is expected to generate a greater stress, and the increasing quality, causing also an increase of the velocity of the flow, leads to a consequent growth of the wall shear stress from the beginning of the boiling process until annular flow regime is stable;
- the drying of the liquid film covering the inner surface produces a relaxation of the wall shear stress;

---

[9] The reasons that explain this fact are not investigated in present work.

- the asymmetric force field introduced by body forces renders this phenomenon more evident, thus two-phase flow in helically coiled tubes present a maximum in pressure drop profile at *x≈0.8*.

In order to verify this theory, it is necessary to investigate the variation of wall shear stress along the tube surface, since the asymmetry certainly generates a non uniform distribution of it. The graphics in Figure 3.16 show the behavior of wall shear stress on the perimeter of Surface 3 of the fine mesh after the fifth series of numerical simulation: τ_w is plotted as a function of the angle θ, where the value 0° represents the inner side of the tube, 180° the outer side, and counter-clockwise convention is adopted. Notice the change of scale between Simulation 06 and Simulation 07: two different scales are used to let appreciate also the differences among the numerical simulation at low quality. When the software manage to resolve the presence of only one phase in the near wall cells, i.e. presence of the liquid film or dry-out, the other lays to the zero, while if both liquid and vapor are recognized close to the surface, they show non zero values.

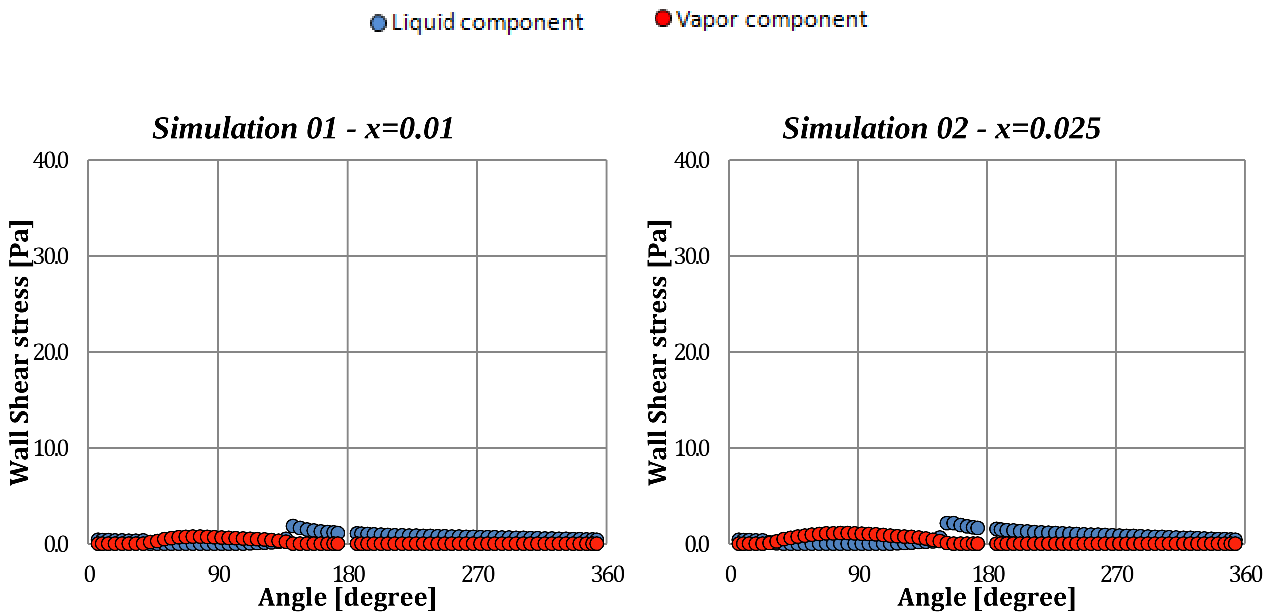

Simulation 01 - x=0.01

Simulation 02 - x=0.025

Simulation 03 - x=0.075

Simulation 04 - x=0.15

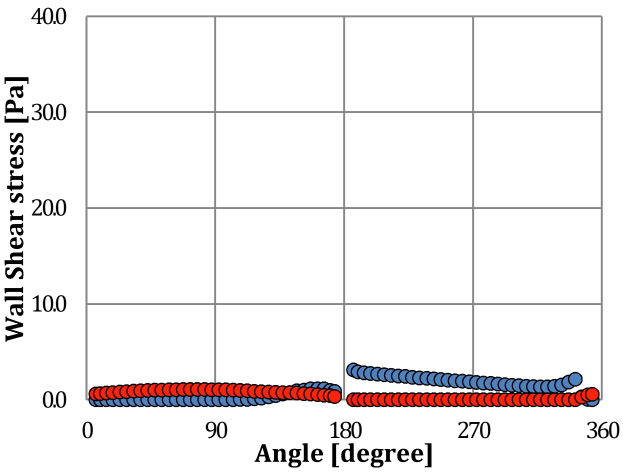
Wall Shear stress [Pa]
40.0
30.0
20.0
10.0
0.0
0
90
180
270
360
Angle [degree]

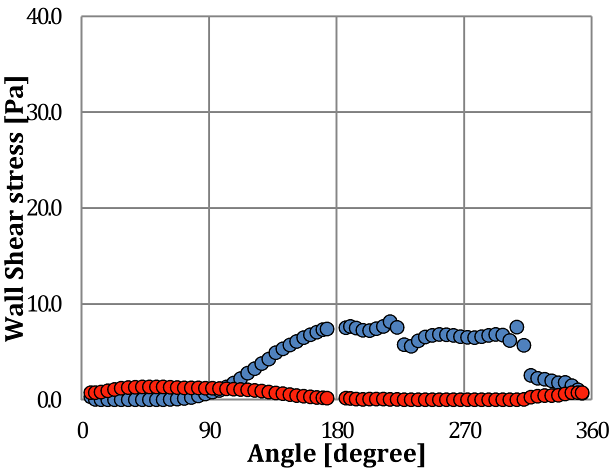
Wall Shear stress [Pa]
40.0
30.0
20.0
10.0
0.0
0
90
180
270
360
Angle [degree]

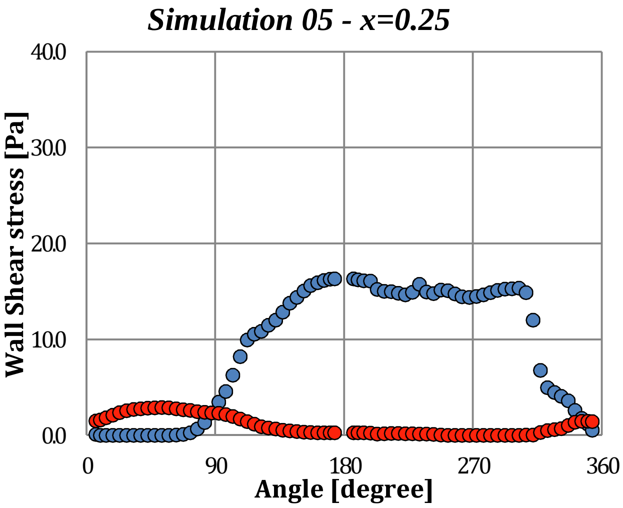
Simulation 05 - x=0.25
Wall Shear stress [Pa]
40.0
30.0
20.0
10.0
0.0
0
90
180
270
360
Angle [degree]

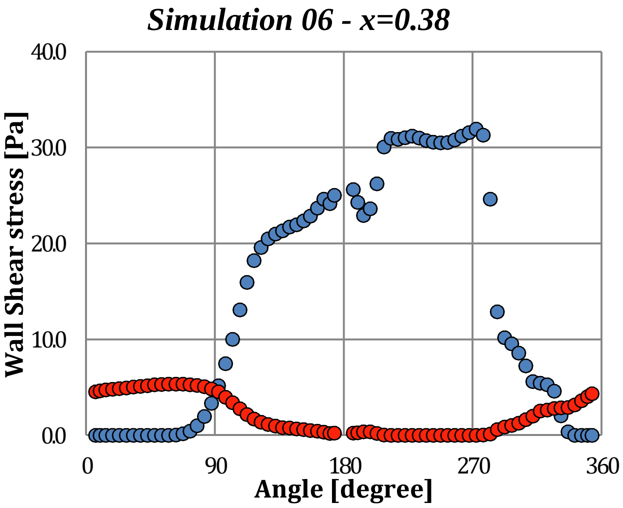
Simulation 06 - x=0.38
Wall Shear stress [Pa]
40.0
30.0
20.0
10.0
0.0
0
90
180
270
360
Angle [degree]

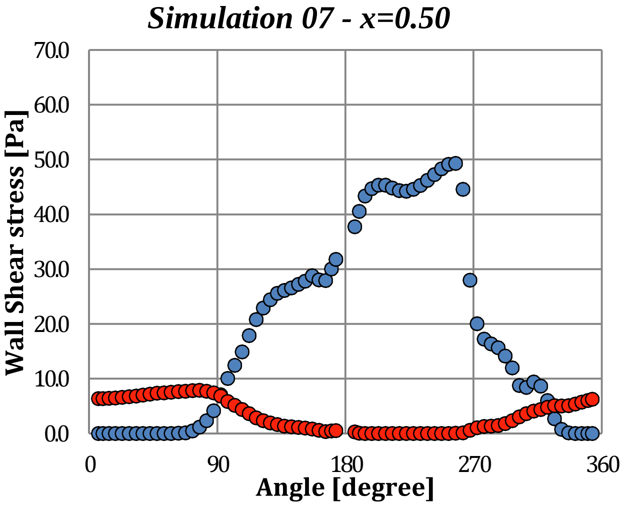
Simulation 07 - x=0.50
Wall Shear stress [Pa]
70.0
60.0
50.0
40.0
30.0
20.0
10.0
0.0
0
90
180
270
360
Angle [degree]

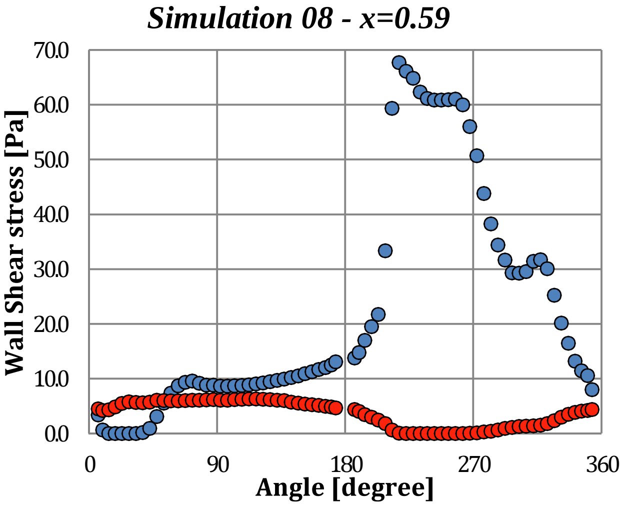
Simulation 08 - x=0.59
Wall Shear stress [Pa]
70.0
60.0
50.0
40.0
30.0
20.0
10.0
0.0
0
90
180
270
360
Angle [degree]

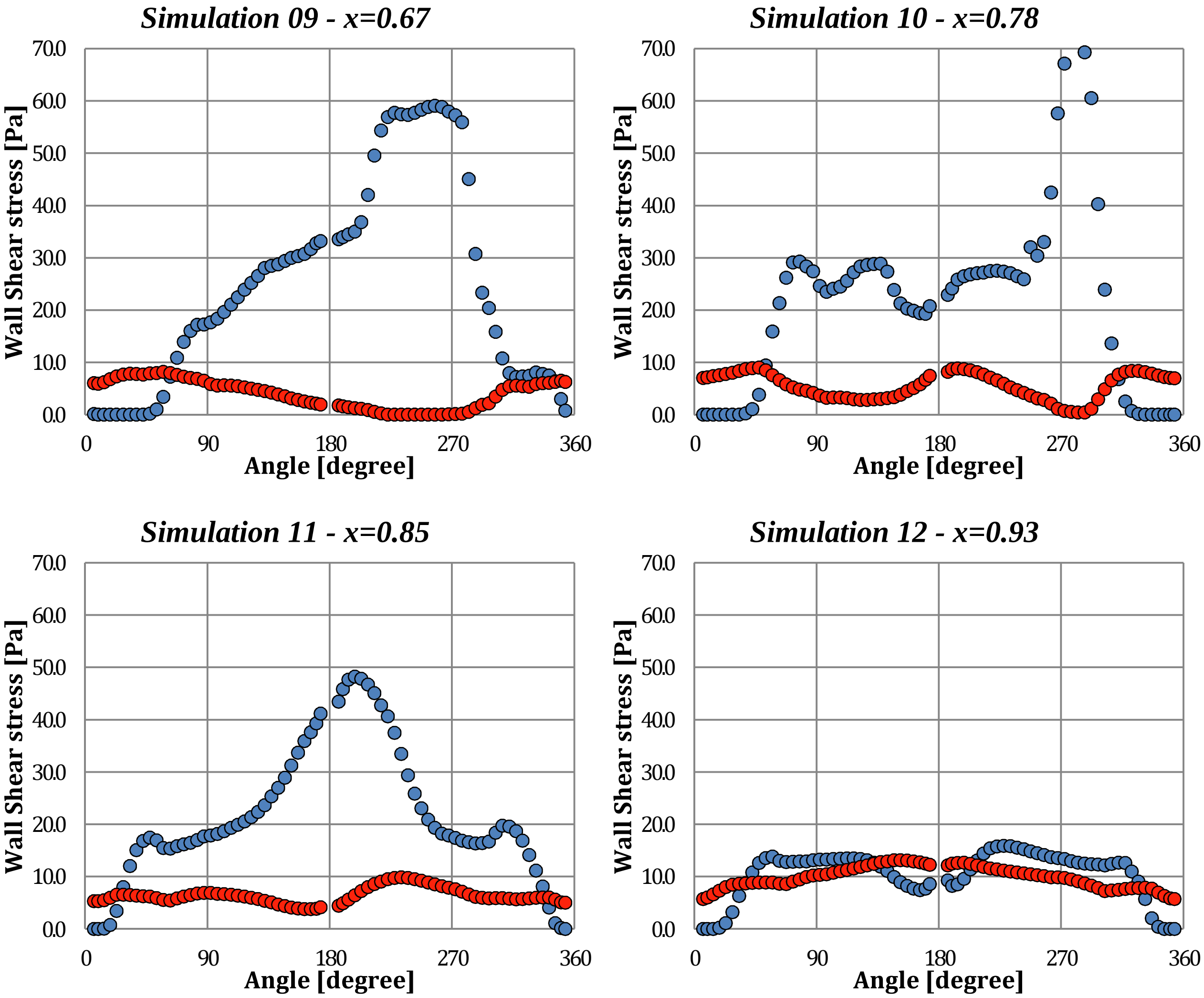

Figure 3.16 *Numerical wall shear stress profiles on Surf 3 obtained with the Fine Mesh (5th run).*

The sum of the two curves gives the profile total wall shear stress, which, for the sake of clearness, is not reported. Integrating those curves, values similar[10] to those reported in Figure 3.15 are obtainable.

The most important feature that is noticeable in these graphics is the position of the peak of the liquid component: for the simulations of Zone 1 and Zone 2 it is settled between 180° and 270°, that is to say the down outer side of the tube surface. This means that the liquid buildup, which appears as a consequence of gravity and centrifugal force, is the main responsible of the wall

---

[10] In Figure 3.19 the numerical values have been computed averaging on the entire inner surface of the fine mesh, not only on the perimeter of Surface 3.

shear stress, the taller the peak the greater the quality and in consequence the velocity of the flow. The plateau formed at the summit of the peak represents the size of the accumulation of liquid: it begins to be visible since Simulation 03, then it reduces as the curve increases in height, and finally it collapses. Simulation 10 marks the transition between annular and dispersed flow regime: actually in this case the liquid buildup reaches the smallest size, but the elevated velocity of the flow generates a high velocity gradient at the surface, making this little portion of tube experience the greater local wall shear stress. Then, the drying of the liquid layer relaxes the stress on the wall: without the accumulation of liquid on the surface, the wall shear stress is globally less intense; consequently, a decrease of frictional pressure drop is observable. Substantially, the departure from annular flow regime produces a general reduction of the forces exercised by the flow on the surface; since the presence of body forces tends to accentuate the consequences of the accumulation of liquid on that zone of the wall corresponding to the resulting of their direction, in some particular geometry that allows the exhibition of the related effects, like the helically coiled tube, frictional pressure drop profile as function of quality shows a non-monotonic behavior. Even though the fine mesh does not resolve a complete annular flow regime, it allows a good definition of the part of the inner surface that gives the greater contribution to wall shear stress. Therefore, the employ of the fine mesh for this purpose is fundamental, because the coarse mesh is not able to provide a qualitative correct resolution of the angular profiles of the wall shear stress. An example is reported (Simulation 07, *x=0.50*): the plateau representing the liquid buildup is not visible in this case, the shape of the profile cannot be physically interpreted and the sum of the integral of the two curve would lead to an incorrect estimation of the wall shear stress.

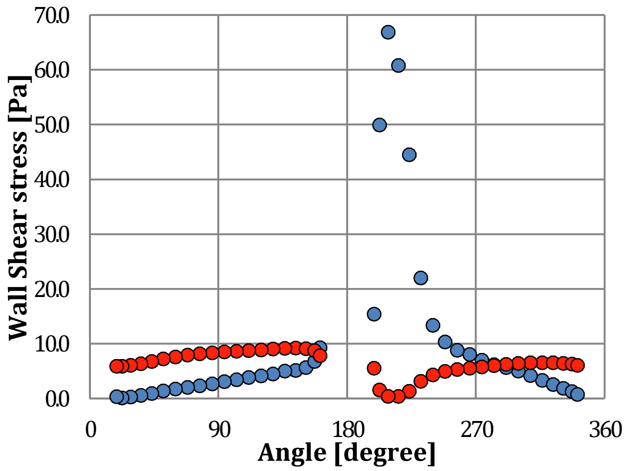

Figure 3.17 *Angular profile of wall shear stress obtained with the coarse mesh (Simulation 07)*

3.6.4 Consequences of the analysis of the wall shear stress

The above explained achievement is of fundamental importance: the finding of a direct connection between the distribution of the shear stress on the surface and the transition of flow regime suggests the idea that an approach based on the wall shear stress may be preferable in order to investigate pressure drop in helically coiled tubes and to create a correlation for a two-phase flow. Actually, correlations available in literature are often based on the Lockhart – Martinelli's multipliers methods and on fittings of experimental data, then providing predictions that strongly depend upon the geometry and the operative conditions used in the empirical study; in fact, up to now there is not an equation that guarantees high accurate predictions of two-phase flow pressure drop in a wide range of helicoidal geometries and operative conditions. Instead, by directly analyzing the cause of frictional pressure drop, a different method, not based only on experimental data but more linked to the physical description of the problem, can be employed.

Thanks to a numerical model that allow obtaining reliable results on pressure drop and qualitatively good profiles of void fraction and wall shear stress, a great advantage is achieved: the opportunity to investigate the interaction between the steam-water two-phase flow and the wall under adiabatic conditions in various situations. It is then possible to study the effects of the geometric parameters, i.e. tube diameter, coil diameter, coil pitch, on the hydrodynamic behavior by performing various numerical simulations and then examining the relationship between the geometry of a helical tube and the average wall shear stress (and qualitatively also on the angular dependence of wall shear stress). Similarly, it is possible also to analyze the consequences induced by pressure and mass flux. Hence, it is possible to directly observe how the physic of the problem is influenced by the most critical parameters of the design. A correlation obtained by following this approach would be suitable for a great amount of situations, providing more reliable predictions than other formulas available in literature. The results would not be anymore linked to experimental data, which would be used only to validate the correlations, since CFD simulations allow resolving the governing equations of the two-phase flow and then generating a very large amount of data.

3.3 Conclusion

The CDF investigation of a steam-water two-phase flow in helically coiled tubes conducted in this work allows the following conclusion.

- A physical explanation for the maximum in pressure drop profiles at $x \approx 0.8$ evidenced by experimental data is provided. The drying of the liquid film covering the inner surface and, in particular, of the liquid buildup in the down-outer side of the tube, causes a relaxation of the wall shear stress: therefore, frictional pressure drop decreases when the dry-out occurs. This result may imply important consequences, suggesting a new approach in the determination of a correlation for pressure drop in two-phase flow.
- The modeling method chosen, i.e. realizable k-ε model for modeling turbulence, with Enhanced Wall Treatment for the handling of the near-wall region, and Eulerian model for boundary conditions at the interface, with Universal Drag Law for modeling the momentum transfer between the phases, allows obtaining acceptable estimates of pressure drop and void fraction profiles. Certainly, turbulence model can be improved and an optimization of the parameter used in the governing equations, i.e. bubbles / droplets diameter, can be made.
- The employ of a grid adequately fine and including a boundary layer is of fundamental importance in order to achieve an exact resolution of the hydrodynamic behavior of the two-phase flow: otherwise, the mesh is not fine enough to correctly resolve the liquid buildup, which is the main responsible of pressure drop.
- The homogeneous model is not adequate for a CFD study of a two-phase flow. Nevertheless, the pressure drop results of the numerical simulations performed with this approach, which substantially models an equivalent single-phase flow, are in great accordance with Ito's equation for turbulent flow. This fact indicates that CFD can accurately predict pressure drop of a single-phase flow.

3.4 REFERENCES

[1] S. Ghorai, K.D.P. Nigam (2005) "CFD modeling of flow profiles and interfacial phenomena in two-phase flow in pipes" © *2005 Elsevier B.V. Chemical Engineering and Processing 45 (2006) 55–65*

[2] H. Gao, H.Y. Gu, L.J. Guo (2002) "Numerical study of stratified oil–water two-phase turbulent flow in a horizontal tube" *©2002 Elsevier Science Ltd. International Journal of Heat and Mass Transfer 46 (2003) 749–754*

[3] S. Vashisth, K.D.P. Nigam (2007) "Prediction of flow profiles and interfacial phenomena for two-phase flow in coiled tubes" *© 2008 Elsevier B.V. Chemical Engineering and Processing 48 (2009) 452–463*

[4] T. K. Bandyopadhyay, A. B. Biswas and S. K. Das (2010) "Gas-Non-Newtonian liquid flow through helical coils –pressure drop and CFD analysis" *AIP Conference Proceedings 1298, 98 (2010); doi: 10.1063/1.3516433*

[5] M. R. Rahimi, A. Askari, M. Ghanbari (2011) "Simulation of Two Phase Flow and Heat Transfer in Helical Pipes" *2nd International Conference on Chemistry and Chemical Engineering IPCBEE vol.14 (2011) © (2011) IACSIT Press, Singapore*

[6] J. S. Jayakumar (2012) "Helically Coiled Heat Exchangers, Heat Exchangers - Basics Design Applications" *Dr. Jovan Mitrovic (Ed.), ISBN: 978-953-51-0278-6, InTech*

[7] J.S. Jayakumar, S.M. Mahajani, J.C. Mandal, Kannan N. Iyer, P.K. Vijayan (2010) "Thermal hydraulic characteristics of air–water two-phase flows in helical pipes" © *2009 The Institution of Chemical Engineers. Published by Elsevier B.V. chemical engineering research and design 88 (2010) 501–512*

[8] V. Kumar, S. Saini, M. Sharma, K.D.P. Nigam (2006) "Pressure drop and heat transfer study in tube-in-tube helical heat exchanger" © *2006 Elsevier Ltd, Chemical Engineering Science 61 (2006) 4403 – 4416*

[9] B.E. Launder, D.B. Spalding (1972) "Mathematical Models of Turbulence" *Academic Press, London*

[10] S.V. Patankar, V.S. Pratap, D.B. Spalding (1975) "Prediction of turbulent flow in curved pipes" *Journal of Fluid Mechanics 67, 583–595*

[11] FLUENT Users Guide – FLUENT Theory Guide, Release 14.0 *ANSYS, Inc. Southpointe 275 Technology Drive © 2011 SAS IP, Inc.*

[12] M. Wolfshtein (1969) "The Velocity and Temperature Distribution of One-Dimensional Flow with Turbulence Augmentation and Pressure Gradient" *Int. J. Heat Mass Transfer. 12. 301–318. 1969.*

[13] N. I. Kolev (2005) "Multiphase Flow Dynamics 2: Thermal and Mechanical Interactions" *Springer, Berlin, Germany, 2nd edition. 2005*

[14] S. V. Patankar (1980) "Numerical Heat Transfer and Fluid Flow" *Hemisphere,Washington, DC. 1980.*

[15] IAEA-TECDOC-1203 (2001) "Thermo-hydraulic relationships for advanced water cooled reactors" *Nuclear Power Technology Development Section International Atomic Energy Agency, Vienna, Austria*

[16] R.W. Lockhart, R.C. Martinelli, (1949) "Proposed correlation of data for isothermal two-phase, two-component flow pipes" *Chem. Eng. Prog. 45(1) (1949) 39 48.*

[17]R. C. Xin, A. Awwad, Z. F. Dong, M. A. Ebadian (1995) "An investigation and comparative study of the pressure drop in air-water two-phase flow in vertical helicoidal pipes" © *1995 Elsevier Science Ltd Int. J. Heat Mass Transfer. Vol. 39, No. 4, pp. 735 743, 1996*

[18]R. C. Xin, A. Awwad, Z. F. Dong, M. A. Ebadian (1997) "An experimental study of single-phase and two-phase flow pressure drop in annular helicoidal pipes" © *19975 Elsevier Science Ltd Int. J. Heat and Fluid Flow 18: 482-488, 1997*

[19] S. Banerjeé, E. Rhodes, D.S. Scott (1969) "Studies on Cocurrent GasHLiquid Flow in Helically Coiled Tubes" *The Canadian Journal of Chemical Engineering, Vol. 47, October, 1969*

[20]A. Armand, G.G. Treschechev, (1959) "Investigation of the resistance during the movement of steam-water mixtures in a heated boiled pipe at high pressure" *Izv. Vses. Teplotekhn. Inst. 4 (1947) 1e5 AERE Libr. Trans. 1959;816.*

[21] Z. Stomma (1980) "Void fraction, pressure drop and critical heat flux correlations in cylindrical, annular and multirod boiling channels" *Energ. Nucl. 27(10) (1980) 335 348.*

[22]S. N. Mandal, S. K. Das (2003) "Gas-Liquid Flow through Helical Coils in Vertical Orientation" © *2003 American Chemical Society Ind. Eng. Chem. Res. 2003, 42, 3487-3494*
[23] Z. Rouhani, E. Axelsson, (1970) "Calculation of void volume fraction in the subcooled and quality boiling regions", *Int. J. Heat Mass Transfer 13 (1970) 383–393.*
[24] J. El Hajal, J.R. Thome, A. Cavallini, (2003) "Condensation in horizontal tubes. Part 1: two-phase flow pattern map", © *2003 Elsevier Science Ltd Int. J. Heat Mass Transfer 46 (2003) 3349e3363.*

4 Nomenclature

a = Coriolis coefficient
A = section of the tube
D_{coil} = diameter of the coil
De = Dean number
dp = pressure drop
d_{tube} = diameter of the tube
e = roughness
e = specific kinetic energy
f = friction factor
F_{CF} = centrifugal force
F_{VM} = virtual mass forces
g = gravitational constant
G = mass flux
h = specific entalpy
H= height of the tube
k = turbulent kinetik energy
L = length of the tube
P = perimeter of the section of the tube
p = pitch of the coil
p = relative pressure
q'' = thermal flux
Q = thermal power
r = radius of the tube
Re = Reynolds number
s = slip ratio
T = Temperature
t = time step
u = axial velocity
u = maximum axial velocity on the section
U = specific internal energy
v = specific volume
$\overrightarrow{V_{lv}}\ \overrightarrow{V_{vl}}$= inter-phase velocities
W = mechanic power
X = Martinelli's parameter
x = quality
y^+ - y^* = non dimensional wall distance
z = coordinate along the axis of the tube

Greek symbols

α_v = vapor volume fraction
β = torsion parameter
Γ = mass flow rate
γ = slope of the tube
δ = coil curvature
Δp = pressure drop
ε = turbulence dissipation rate
μ = dynamic viscosity
ρ = density
τ = coil torsion
τ_w = wall shear stress
$\bar{\bar{\tau}}$ = stress-strain tensor
Φ = Lockhart - Martinelli multiplier

Subscripts

a = adiabatic
c = cell
c = coil
CF = Centrifugal Force
$crit$ = critical
d = diabatic
f = fluid
g = gas
hom = homogeneous
l = liquid
lo = liquid only
ls = saturated liquid
lv = liquid to vapor
m = mixture
s = straight
vl = vapor to liquid
VM = Virtual Mass
vs = saturated vapor
w = wall

CURRICULUM SCIENTIFICO DEL GRUPPO DI RICERCA

Il gruppo di lavoro impegnato nell’attività è costituito da un professore ordinario di Impianti Nucleari del Politecnico di Milano (Dipartimento Energia), Marco Enrico Ricotti, da un ricercatore dello stesso Dipartimento, Antonio Cammi, e da un assegnista di ricerca, Marco Santinello.

Il prof. Ricotti e il prof. Cammi svolgono attività di ricerca da oltre 15 anni al Politecnico nel campo della Ingegneria Nucleare, con particolare riferimento alla termoidraulica, alla sicurezza, agli aspetti economici dell’energia nucleare ed hanno svolto o coordinato ricerche teorico-modellistiche e sperimentali nel gruppo Reattori Nucleari del Dipartimento di Energia del Politecnico di Milano, pubblicando i risultati su rivista e in atti di Congresso, quasi esclusivamente internazionali. Sono autori di diversi rapporti nell'ambito dei PAR trascorsi.

L’ing. Santinello è assegnista di ricerca del Politecnico di Milano e svolge ricerche sulle tematiche teorico-modellistiche e sperimentali che sono oggetto del presente rapporto.

Maggiori dettagli sulle attività di ricerca nonché l’elenco delle pubblicazioni più recenti si possono trovare sul sito Web del gruppo di ricerca del Politecnico di Milano (http://www.nuclearenergy.polimi.it).